Islamic University of Gaza
Deanery of Graduate Studies
Faculty of Science
Physics Department

ELECTRICAL AND OPTICAL PROPERTIES OF ORGANIC DIODES

By

Ahed Mohammed El-Afghani

Supervised By

Dr. Taher El-Agez
Associate Prof. of Physics

Dr Sofyan A. Taya
Assistant Professor of Physics

Thesis

Submitted to the Faculty of Science as Partial Fulfillment of the Master of Science (M.Sc.) in Physics

Palestine, Gaza
Aug. 2012

CONTENTS

Contents……ii
Acknowledgements…..…….……v
Abstract (English)……... …….....vi
Abstract (Arabic)……..…vii
List of Symbols and Abbreviation…….…....viii
List of Tables……..…....xi
List of Figures..……...…xii

CHAPTER ONE
INTRODUCTION TO POLYMER

1.1 Basic Concepts of Polymer Sciences..……1
1.2 Homopolymers……2
1.2.1 Linear Homopolymers…..…….2
1.2.2 Branched Homopolymers……...…….....3
1.2.3 Crosslinked homopolymers...……...4
1.3 Copolymers…….5
1.3.1 Linear Copolymers……...5
1.3.2 Branched (Graft) Copolymers……..7
1.3.3 Crosslinked Copolymer……7
1.4 Thermoplastic Polymers……..8
1.5 Thermoset Polymers……8
1.6 Elastomers Polymers……...9
1.7 Conducting Polymers……..9
1.8 Electronic Properties of Conducting Polymers…….10
1.9 Electronic States of Polymers……...12
1.10 Physical Properties of the Polymers……...……14
1.10.1 Glass Transition Temperature…….……..14
1.10.2 Relaxation Processes…….15
1.11 Poly N-Vinylcarbazole……...……15
1.11.1 Carbazole..……..……..15

1.11.2 Poly (9-Vinylcarbazole)……...16

CHAPTER TWO

ELECTRICAL CONDUCTION MECHANISIM AND LUMINESCENCE

2.1 Introduction……....18
2.2 Electrical Conduction……18
2.2.2 Ionic Conduction……19
2.2.2 Electronic Conduction……...……19
2.3 Electrical Transport……...20
2.3.1 Electrical Transport by Tunneling……...……..20
2.3.2 Electrical Transport by Hopping……21
2.4 Mechanisms of Charge Carrier Injection Through a Metal/Polymer Interface……23
2.4.1 Thermionic Rmission……23
2.4.2 Field Emission……...……24
2.4.3 Transition from Field to Thermal Emission Limited Characteristics……26
2.5 Ohmic Contact……...……...27
2.6 Space-Charge Effect……...……..28
2.7 An Exciton……...……30
2.7.1 Classification of Excitons……...……...30
2.8 Energy Transfer……31
2.8.1 Fŏster Transfer……...32
2.8.2 Dexter Transfer……...……...32
2.9 Luminescence……32
2.9.1 Fluorescence……...……...33
2.9.2 Phosphorescence……33

CHAPTER THREE

EXPERIMENTAL TECHNIQUES

3.1 Introduction……35
3.2 Equipments……...35
3.2.1 Spin coater device……..35
3.2.2 Inclined Casting Coating……..……..36

3.2.3 Dye Layer Preparation……36
3.3 Eutectic Gallium-Indium ……..….37
3.4 Rotating Polarizer Analyzer Ellipsometry ……..…….37
3.4.1 Mathematical treatment…….…….39
3.5 Measurement of the DC Electrical Conductivity ……..39

CHPTER FOUR

DOUBLE LAYER DEVICES

4.1 Introduction……41
4.2 Film Preparation……41
4.2.1 Substrate Cleaning……...……..41
4.2.2 Sample Structure……41
4.3 Thickness and Refractive Index Measurements...……..44
4.4 Experimental Procedure……49
4.5 Results and Discussion……..50
4.5.1 Current Density-Voltage Characteristic Curves...…….…….67
4.5.2 Relative Light Intensity with the Driving Voltage...…….…….67
4.5.3 Relative Light Intensity with Increasing the Current…….……68
4.5.4 Energy Band Diagram…..…...……..68
4.5.5 Conduction Mechanism……...……..68

CHAPTER FIVE

SINGLE LAYER DEVICES

5.1 Introduction……...70
5.2 Sample Structure……...70
5.3 Experimental Procedure….....73
5.4 Results and Discussions...……...……..73
5.4.1 Current Density-Voltage Characteristic Curves……106
5.4.2 Relative Light Intensity with Driving Voltage……..107
5.4.3 Relative Light Intensity with Increasing Current…….107
5.4.4 Conduction Mechanism……...…….107
CONCLUSIONS..……..110
RRFERENCE...……..114

ACKNOWLEDGMENTS

All gratitude and thanks to Allah to help me get this thesis, I have now come to the end of my journey and finally take this opportunity to express my gratitude to friends, colleagues, collaborators, etc who have contributed to the completion of this thesis .

I am principally quite grateful to my supervisors Dr. Taher El-Agez, Dr. Sofyan Taya, Dr. Ahmed El Tayyan and prof. Monzir Abdel-Latif for the excellent guidance, encouragement and help of all sorts. I have learnt a lot from their discussions.

Last but not least, quite special thanks goes to my family for the incredible support and care you gave me.

ABSTRACT

Two groups of samples have been prepared and some characteresations are studied. Every sample represents an organic diode. The first group is double layer device. Twelve samples with the structure ITO/PVK/dye/InGa have been prepared and studied. Three dyes were used namely Rhodamine B, Crystal violet, and Bromophenol blue. Four different thicknesses of the PVK layers hav been prepared. The thicknesses of thin films were measured using homemade spectroscopic ellipsometer. J-V characteristics curves for all samples have been measured and studied. The conduction mechanisms have been presented. The J-V characteristics show an exponential increase of current with the applied voltage, which is similar to a typical diode characteristics. The samples ITO/35.33nm PVK/50nm Rhodamine B /InGa device and ITO/44.3nm PVK/50nm Rhodamine B /InGa work as organic light emitting diodes (OLEDs). The threshold voltage is found to be 8 and 10 volt respectively.

The second group is single layer device. Sixteen samples with the structure ITO/blend of Poly(9-vinylcarbazole) (PVK) and dye/ InGa have been studied. Three dyes were used: Rhodamine B, Fluorescein, Bromophenol blue with concentrations 1%, 2%, 3%, 4% and 5% by weight. J-V characteristics curves have been carried out. The relative light intensity versus voltage and current have been plotted and fabricates samples work as OLED devices. The concentration dependence of electroluminescence have been studied.

الملخص بالعربي

تم تحضير ودراسة مجموعتين من العينات، كل عينة تمثل ثنائي عضوي. المجموعة الأولى تمثل جهاز من طبقتين طبقة PVK و طبقة صبغة dye، التركيب العام لهذه المجموعة هوITO/PVK/dye/InGa حيث تم تحضير اثنى عشر عينة من هذه المجموعة. و تم استخدام ثلاث اصباغ مختلفة في طبقة الصبغة وهي Rhodamine B، Crystal violet و Bromophenol blue. تم تحضير اربع قياسات لسمك طبقة ال PVK حيث تم قياس سمك الغشاء الرقيق لطبقة ال PVK باستخدام homemade spectroscopic ellipsometer.

تم قياس ودراسة خواص منحنيات J-V لكل العينات ودراسة ميكانيكة التوصيل. حيث وجد أن خواص منحنى J-V يظهر زيادة بشكل exponential مع الجهد المطبق وهو مشابه لمنحنى خواص الثنائي "diode".

العينتين ITO/35.33nm PVK/50nm Rhodamine B/InGa و ITO/44.3nm PVK/50nm Rhodamine B/InGa تمثلان ثنائي عضوي باعث للضوء (OLEDs) حيث تم ايجاد جهد العتبة threshold voltage للعينتين ولوحظ أن جهد العتبة للعينة الاولى 8 فولت بينما للعينة الثانية 10 فولت.

المجموعة الثانية تمثل جهاز من طبقة واحدة خليط من ال PVK والصبغة، التركيب العام لهذه المجموعة هو ITO/blend of PVK and dye/InGa حيث تم تحضير ستة عشر عينة من هذه المجموعة وتم استخدام ثلاث اصباغ مختلفة وهي Rhodamine B، Fluorescin و Bromophenol blue حيث طعمت مادة ال PVK من هذه الاصباغ بتركيز 1%، 2%، 3%، 4% و 5% بالنسبة للوزن. وتم رسم و دراسة منحنيات علاقة كثافة التيار كدالة في الجهد وكذلك علاقة شدة الإضاءة النسبية مع الجهد المطبق. وأيضا تغير الإضاءة النسبية مع تغير التيار والعلاقة بين اللوغارتيم الطبيعي لكثافة التيار مع اللوغاريتم الطبيعي للجهد. حيث وجد أن هذه العينات تمثل ثنائي عضوي باعث للضوء (OLEDs). كذلك تم دراسة تأثير زيادة التركيز على الإضاءة.

LIST OF SYMBOLES AND ABBREVIATIONS

PVC	Poly(vinyl chloride).
-co-	Random copolymers.
-alt-	Alternating copolymers.
-b-	Block copolymers.
SBS	Poly(styrene-b-butadiene-b-styrene)
-g-	Graft copolymers.
σ	Electrical conductivity.
HOMO	Highest occupied molecular orbital.
LUMO	Lowest unoccupied molecular orbital
SOMO	Occupied Molecular Orbital.
p_z	Unhybridized orbital.
Σ	Bonding orbitals.
Π	Bonding orbitals.
N	Nonbonding orbitals.
σ*	Antibonding orbitals.
π*	Antibonding orbitals.
T_g	Glass transition temperature.
PVK	Poly (9-Vinylcarbazole).
OLEDs	Organic light emitting diodes
THF	Tetrahydrofuran.
n_e	Concentration of electrons.
n_h	Concentration of holes.
q_e	Charge of electrons.
q_h	Charge of holes.
μ_e	Mobility of electrons.
μ_h	Mobility of holes.
k_B	Boltzmann constant.
E_σ	Activation energy.
T	Absolute temperature.
N_c	Effective densities of states in the conduction bands.
N_v	Effective densities of states in the conduction bands.

E_g	Energy band gap
H	Planck's constant
J_T	current density due to tunneling
E	Electric field
ϕ_m	Electrode work function.
m_e	Electronic mass.
A^0	Angstrom.
ϕ_B	Barrier height.
A^*	effective Richardson constant.
FN	Fowler- Nordheim tunneling.
FE	field emission
TFE	thermionic field emission
SCLC	Space charge limited current.
N	Drift velocity.
$\rho(x)$	Carrier density.
k	Dielectric constant.
ε_0	Permittivity of the free space.
D^*	Excited donor state.
A*	Excited acceptor state.
S_0	Ground state.
S_1	First excited singlet state.
T_1	First triplet excited state.
IC	Internal conversion.
ICS	Intersystem crossing,
VASE	Variable angle spectroscopic ellipsometer,
ITO	Indium tin oxide.
E_p	Parallel component of electrical field to the plane of incidence.
E_s	Perpendicular component of electrical field to the plane of incidence.
Δ	phase change between p- and s-polarized lights.
Ψ	The ratio of reflection coefficients.
δ_p	The phase changes for the p components of light.

δ_s	The phase changes for the *s* components of light.
r_p	Fresnel's reflection coefficient for P-component.
r_s	Fresnel's reflection coefficient for S-component.
Ω	Angular speed.
RAE	Rotating analyzer ellipsometer.
RPAE	Rotating polarizer and analyzer ellipsometer.
r_j	the Fresnel reflection coefficient.
T	Azimuth angle of the rotating polarizer.
Δ	Azimuth angle of the rotating analayzer.
a_0, a_n, and b_n	Fourier coefficients.
InGa	Indium gallium

LIST OF TABLES

Table 1.1	Some candidate polymers used in the formation of filled polymer systems	9
Table 4.1	Molecular formula, melting point, and molecular structure of the three dyes.	42
Table 4.2	The structure of double layer device.	49
Table 4.3	Different weights of the PVK polymer used to construct the PVK layer	50
Table 4.4	Experimental values of threshold voltage for G_1S_1 and G_2S_2.	67
Table 4.5	Experimental values of slope for each region of lnJ-lnV characteristic curves.	69
Table 5.1	Molecular formula, melting point, and molecular structure of Crystal violet, Fluorescein and Bromophenol blue.	71
Table 5.2	The structure of PVK-dye blend device.	71
Table 5.3	The threshold voltages for a single layer devices.	106
Table 5.4	Experimental values of slope for each region of lnJ-lnV characteristic curves.	108

LIST OF FIGURS

Figure 1.1	(a) Monomer "ethylene", (b) schematic representation of polyethylene.	2
Figure 1.2	An example of (a) a homopolymer (Polyethylene), (b) a linear polymer poly(vinyl chloride) (PVC).	3
Figure 1.3	Figure (1.3): (a) trifunctional monomer (glycerol), (b) Branched polymer.	4
Figure 1.4	Idealized structure of a cross-linked polymer.	4
Figure 1.5	(a) Idealized structure of a random copolymer, (b) poly(styrene-co-methyl methacrylate).	5
Figure 1.6	The structure of (a) an idealized alternating copolymer (b) poly (styrene-alt-maleic anhydride).	6
Figure 1.7	(a) Idealized structure of a block copolymer (b) poly(styrene-b-butadiene-b-styrene).	6
Figure 1.8	(a) Idealized structure of a branched copolymers (b) structure of a branched copolymers novolacs.	7
Figure 1.9	Structure of acrosslinked copolymer phenolics.	8
Figure 1.10	The range of conductivities of materials.	10
Figure 1.11	Bonding in conducting conjugated polymers. The sp2 hybrid orbitals are shown in light gray, and the unhybridized pz orbitals in white. Electrons are represented by the dots, the two sp2 hybrid orbitals on the side extend in and out of the plane of the page.	11
Figure 1.12	(a) Classification of molecular orbitals with respect to electron occupancy, (b) Molecular orbitals and electronic transitions induced by the absorption of a photon.	13
Figure 1.13	Specific volume of an amorphous polymer as function of the temperature.	14
Figure 1.14	The structure formulas of poly(N-vinylcarbazole), (a) Carbazole, (b) N-vinylcarbazole, and (c) Poly(N-vinylcarbazole).	17
Figure 2.1	Schematic illustration of ions polarized surrounding molecules or atoms.	20

Figure 2.2	Schematic illustration of an electron tunneling through a square potential barrier and an electron hopping across a square potential barrier.	22
Figure 2.3	Simple energy band diagrams illustrating the distributions of surface and bulk trapping states in energy and in space: (a) without an applied field and (b) with an applied field.	23
Figure 2.4	Energy band diagram showing thermionic emission of electrons over the barrier.	24
Figure 2.5	Energy band diagrams showing conduction mechanisms of (a) direct tunneling, (b) Fowler-Nordheim tunneling, (c) thermionic emission, (d) Frenkel-Poole emission.	26
Figure 2.6	Mechanisms of charge carrier injection through a metal/polymer interface, showing the three major current transport mechanisms: thermionic emission (TE), thermionic-field emission (TFE) and field-emission (FE).	27
Figure 2.7	Qualitative picture of the transition from Ohmic conduction to SCLC	30
Figure 2.8	The spatial discrimination of excitons (a) Wannier exciton, (b) Frenkel exciton.	31
Figure 2.9	Fõster Transfer (a) the intial state, (b) the final state.	32
Figure 2.10	Dexter Transfer (a) the intial state, (b) the final state.	33
Figure 2.11	Perrin-Jablonski diagram and illustration of the relative positions of absorption, fluorescence and phosphorescence spectra.	34
Figure 3.1	Schematic illustration of spin coater.	35
Figure 3.2	Photo image of a spin coater.	36
Figure 3.3	Simplified schematic diagram of the rotating polarizer analyzer ellipsometer, (1) unpolarized light, (2) linear polarizer, (3) sample, (4) linear analyzer, and (5) detector.	38
Figure 3.4	Photo image of an ellipsometer.	40
Figure 3.5	The experimental setup used in measurements.	40
Figure 4.1	(a) Schematic drawing of a double layer sample, (b) photo image of samples and, (c) photo image of experimental setup.	43
Figure 4.2	Figure 4.2: psi, delta and refractive index of PVK thin film on silicon wafer for S1 as a function of wavelength.	45

Figure 4.3	Psi, delta and refractive index of PVK thin film on silicon wafer for S2 as a function of wavelength.	46
Figure 4.4	Psi, delta and refractive index of PVK thin film on silicon wafer for S3 as a function of wavelength.	47
Figure 4.5	Psi, delta and refractive index of PVK thin film on silicon wafer for S4 as a function of wavelength.	48
Figure 4.6	Four characteristics curves of ITO/35.33nm PVK/50nm Rhodamine B /InGa device, (a) current density- voltage characteristics, (b) lnJ-lnV characteristics, (c) relative light intensity-voltage characteristics, and (d) relative light intensity-current characteristics.	52
Figure 4.7	Four characteristics curves of ITO/44.3nm PVK/50nm Rhodamine B /InGa device, (a) current density- voltage characteristics, (b) lnJ-lnV characteristics, (c) relative light intensity-voltage characteristics, and (d) relative light intensity-current characteristics.	54
Figure 4.8	Two characteristics curves of ITO/94.48nm PVK/50nm Rhodamine B /InGa device, (a) current density- voltage characteristics and, (b) lnJ-lnV characteristics.	55
Figure 4.9	Two characteristics curves of ITO/198nm PVK/50nm Rhodamine B /InGa device, (a) current density- voltage characteristics and, (b) lnJ-lnV characteristics.	56
Figure 4.10	Two characteristics curves of ITO/35.33nm PVK/50nm crystal violet /InGa device, (a) current density- voltage characteristics and, (b) lnJ-lnV characteristics.	57
Figure 4.11	Two characteristics curves of ITO/44.3nm PVK/50nm crystal violet /InGa device, (a) current density- voltage characteristics and, (b) lnJ-lnV characteristics	58
Figure 4.12	Two characteristics curves of ITO/94.48nm PVK/50nm crystal violet /InGa device, (a) current density- voltage characteristics and, (b) lnJ-lnV characteristics.	59
Figure 4.13	Two characteristics curves of ITO/198nm PVK/50nm crystal	60

violet /InGa device, (a) current density- voltage characteristics and, (b) lnJ-lnV characteristics.

Figure 4.14 Two characteristics curves of ITO/35.33nm PVK/50nm Bromophenol blue /InGa device, (a) current density- voltage characteristics and, (b) lnJ-lnV characteristics. 61

Figure 4.15 Two characteristics curves of ITO/44.3nm PVK/50nm Bromophenol blue /InGa device, (a) current density- voltage characteristics and, (b) lnJ-lnV characteristics. 62

Figure 4.16 Two characteristics curves of ITO/94.48nm PVK/50nm Bromophenol blue /InGa device, (a) current density- voltage characteristics and, (b) lnJ-lnV characteristics. 63

Figure 4.17 Two characteristics curves of ITO/198nm PVK/50nm Bromophenol blue /InGa device, (a) current density- voltage characteristics and, (b) lnJ-lnV characteristics. 64

Figure 4.18 4.18 J-V curves of all samples of ITO/PVK/50nm Rhodamine B/InGa. 65

Figure 4.19 J-V curves of all samples of ITO/PVK/50nm crystal violet/InGa. 65

Figure 4.20 4.20 J-V curves of all samples of ITO/PVK/50nm Bromophenol blue/InGa. 66

Figure 4.21 Relative light intensity-voltage characteristics of ITO/PVK/50nm Rhodamine B/InGa. 66

Figure 4.22 Mechanism of electroluminescence of a ITO/PVK /Rhodamine B/InGa device. 68

Figure 5.1 Schematic drawing of a single layer sample. 70

Figure 5.2 Four characteristics curves of ITO/44nm PVK /InGa device, (a) current density- voltage characteristics, (b) lnJ-lnV characteristics, (c) relative light intensity-voltage characteristics and, (d) relative light intensity-current characteristics. 75

Figure 5.3 Four characteristics curves of G_4S_1 (1% crystal violet-PVK blend), (a) current density- voltage characteristics, (b) lnJ-lnV characteristics, (c) relative light intensity-voltage characteristics and, (d) relative light intensity-current characteristics. 77

Figure 5.4 Four characteristics curves of G_4S_2 (2% crystal violet-PVK blend), (a) current density- voltage characteristics, (b) lnJ-lnV characteristics, (c) relative light intensity-voltage characteristics and, (d) relative light intensity-current characteristics. 79

Figure 5.5 Four characteristics curves of G_4S_3 (3%vrystal violet-PVK blend), (a) current density- voltage characteristics, (b) lnJ-lnV characteristics, (c) relative light intensity-voltage characteristics and, (d) relative light intensity-current characteristics. 81

Figure 5.6 Four characteristics curves of G_4S_4 (4% crystal violet-PVK blend), (a) current density- voltage characteristics, (b) lnJ-lnV characteristics (c) relative light intensity-voltage characteristics and, (d) relative light intensity-current characteristics. 83

Figure 5.7 Four characteristics curves of G_4S_5 (5% crystal violet-PVK blend), (a) current density- voltage characteristics, (b) lnJ-lnV characteristics, (c) relative light intensity-voltage characteristics and, (d) relative light intensity-current characteristics. 85

Figure 5.8 Four characteristics curves of G_5S_1 (1% Fluorescein-PVK blend), (a) current density- voltage characteristics, (b) lnJ-lnV characteristics, (c) relative light intensity-voltage characteristics and, (d) relative light intensity-current characteristics. 87

Figure 5.9 Four characteristics curves of G_5S_2 (2%Fluorescein-PVK blend), (a) current density- voltage characteristics, (b) lnJ-lnV characteristics, (c) relative light intensity-voltage characteristics and, (d) relative light intensity-current characteristics. 89

Figure 5.10 Two characteristics curves of G_5S_3, (3%Fluorescein-PVK blend), (a) current density- voltage characteristics, (b) lnJ-lnV characteristics. 90

Figure 5.11 Two characteristics curves of G_5S_4 (4%Fluorescein-PVK blend), (a) current density- voltage characteristics, (b) lnJ-lnV characteristics. 91

Figure 5.12 Figure 5.12 Two characteristics curves of G_5S_5 (5%Fluorescein-PVK blend), (a) current density- voltage characteristics, lnJ-lnV characteristics. 92

Figure 5.13 Four characteristics curves of G_6S_1 (1%Bromophenol blue-PVK blend) , (a) current density- voltage characteristics, (b) lnJ-lnV characteristics, (c) relative light intensity-voltage characteristics and, (d) relative light intensity-current characteristics. 94

Figure 5.14 Four characteristics curves of G_6S_2 (2%Bromophenol blue-PVK blend), (a) current density- voltage characteristics, (b) lnJ-lnV characteristics, (c) relative light intensity-voltage characteristics and, (d) relative light intensity-current characteristics. 96

Figure 5.15 Four characteristics curves of G_6S_3 3%Bromophenol blue-PVK blend), (a) current density- voltage characteristics, (b) lnJ-lnV characteristics, (c) relative light intensity-voltage characteristics, (d) relative light intensity-current characteristics. 98

Figure 5.16 Figure 5.16 Four characteristics curves of G_6S_4 (4%Bromophenol blue-PVK blend), (a) current density- voltage characteristics, (b) lnJ-lnV characteristics, (c) relative light intensity-voltage characteristics, and (d) relative light intensity-current characteristics. 100

Figure 5.17 Four characteristics curves of G_6S_5, (a) Current density- voltage characteristics, (b) Current lnJ-lnV characteristics, (c) Relative light intensity-voltage characteristics, (d) Relative light intensity-current characteristics. 102

Figure 5.18 Two characteristics curves of of ITO/1%, 2%, 3%, 4%, and 5%crystal violet-PVK blend /InGa**,** (a) current density- voltage characteristics and, (b) relative light intensity-voltage characteristics. 103

Figure 4.19 Two characteristics curves of of ITO/1%, 2%, 3%, 4%, and 5% Fluorescein -PVK blend /InGa**,** (a) current density- voltage characteristics and, (b) relative light intensity-voltage characteristics. 104

Figure 4.20 Two characteristics curves of of ITO/1%, 2%, 3%, 4%, and 5% Bromophenol blue -PVK blend /InGa**,** (a) current density-voltage characteristics and, (b) relative light intensity-voltage characteristics. 105

Figure 5.21 The energy band diagram for the polymer at neutral and different doping. 109

CHPTER ONE
INTRODUCTION TO POLYMER

1.1 Basic Concepts of Polymer Sciences

Polymer is a Greek word which can be divided into two parts poly (many) and mer (part). It means "many parts". The polymer is a large molecule constructed from the repetition of simple chemical units called monomers.The repeating units are connected together to form a chain which could be linear, branched, or three-dimensional networks [1,2].

The Chemical reaction of the monomer which constructs the polymer chain is called polymerization. This reaction is performed by using addition or condensation reaction. The number of repeating units which form the polymer is called the degree of polymerization, and the polymers with low degree of polymerization are called oligomers which is also a Greek term meaning a few part. An oligmer usually contains 1-10 mers. A polymer may contain monomers of identical or of different chemical structure. If the polymer contain one type of monomer then it is called homopolymer. If there are two or more types of monomer, the resulting is called copolymers [3-6].

Polymers can be classified in many ways, such as by source, method of synthesis, structural shape, thermal processing behavior, and end use of polymer. Thus, polymers have been classified as natural and synthetic according to source, as addition and condensation according to the mechanism of polymerization, and as linear, branched, and network according to the structural shape of polymer molecules. Acoording to the thermal processing behavior, polymers are classified as thermoplastics and thermosets, while according to the end use it is classified as plastics, fibers, and elastomers [1]. As an illustrative example, consider the single chemical monomer shown in Fig. 1.1 (a). This monomer is called *ethylene* (or *ethene*), which consists of two carbon atoms and four hydrogen atoms. The double lines between the carbon (C) atoms is a double covalent bond whereas the single line between the hydrogen (H) and carbon atoms represents a single covalent bond. The chemical structure of the ethylene monomer is written as C_2H_4 or $CH_2{=}CH_2$. Under specific conditions one of the double covalent bonds can be broken, which allows each of the two carbon atoms to form a new covalent bond with a carbon atom in a neighboring monomer and form a "new" molecule, which is three ethylene

monomers, whose atomic weight is three times as great as the initial monomer. If "*n*" ethylene monomers combine together, the chemical structure of the resulting molecule represented as $C_{2n}H_{4n}$, where *n* is a positive integer. In this way a "chain" of ethylene monomers combine together to form the polymer *polyethylene*, as shown in Fig. 1.1(b) [3].

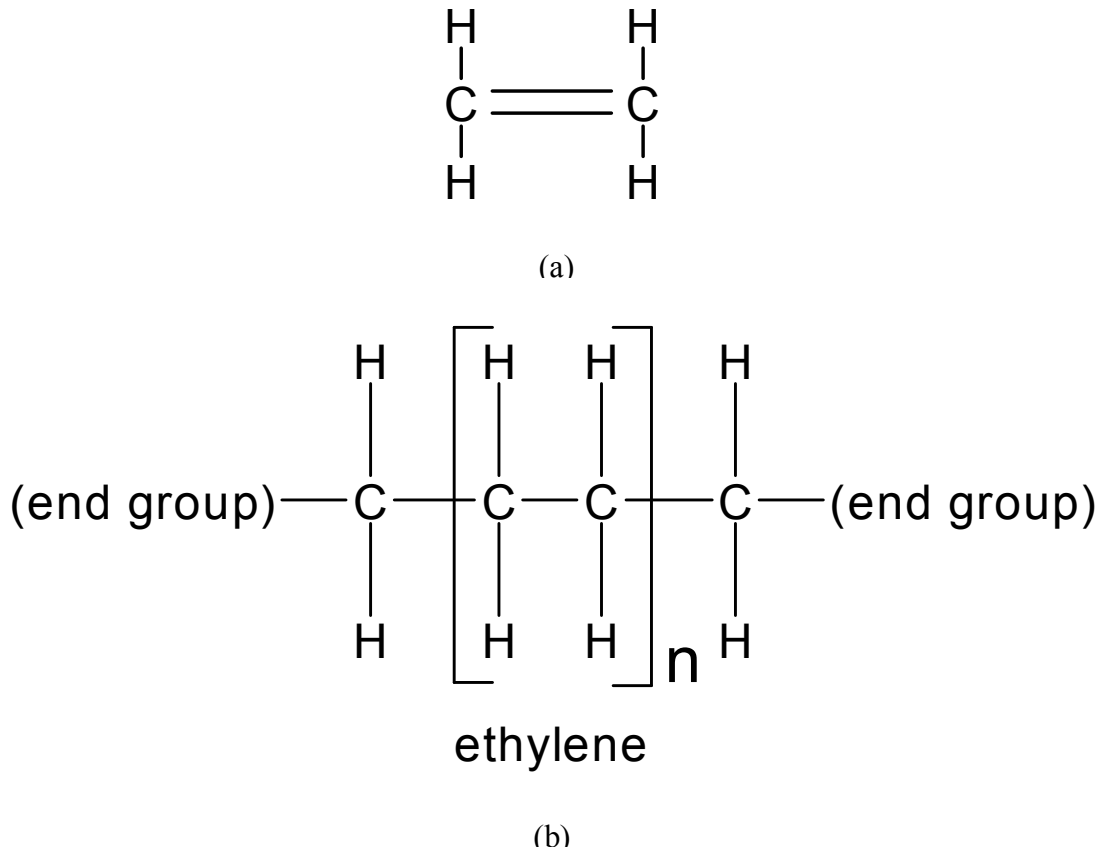

Figure 1.1 (a) Monomer "ethylene", (b) schematic representation of polyethylene.

1.2 Homopolymers

Homopolymers are polymers constructed from identical monomers. Polyethylene is an example of a homopolymer, which is constructed from a single repeating unit of ethylene as shown in fig. 1.1(b) The molecular structure of homopolymers can be classified according to how the atoms and chains are linked together in space as linear, branched, and crosslinked [4-7].

1.2.1 Linear Homopolymer

Linar polymer consist of a long chain with high degree of symmetry, which can be described as beads on a string. The length of these "strings" is huge, and the bead represents repeating the unit, such as poly(vinyl chloride) (PVC) as shown in fig. 1.2(b) [3,5].

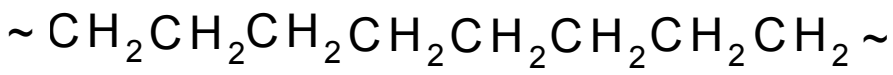

(a)

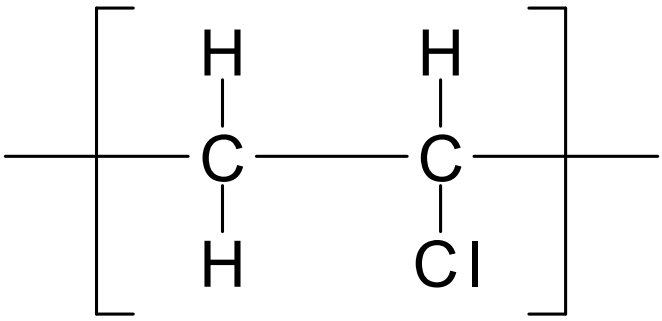

(b)

Figure 1.2 An example of (a) a homopolymer (Polyethylene), (b) a linear polymer (poly(vinyl chloride) (PVC).

1.2.2 Branched Homopolymers

Branched polymer consists of a long chain with side branches, also known as a two dimensional polymers. The monomers in this type can react with more than two molecules, so the monomers must be at least trifunctional. An example of a trifunctional monomer is glycerol, with three hydroxyl groups, as shown in Fig. 1.3 (a) the general shape of branched polymers is shown in Fig. 1.3 (b) [1,5,6].

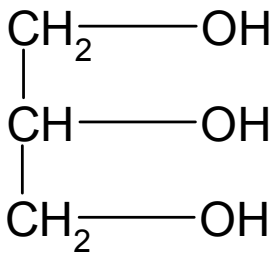

(a)

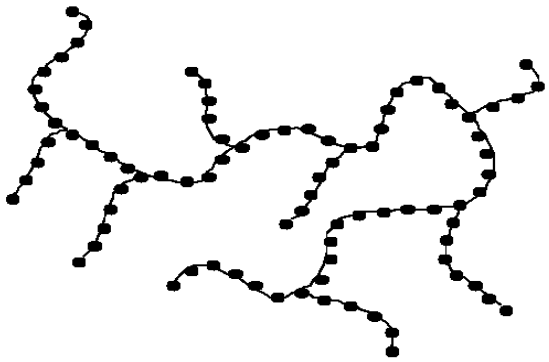

(b)

Figure 1.3 (a) trifunctional monomer (glycerol), (b) Branched polymer.

1.2.3 Crosslinked Homopolymers

A long chain connected into a three-dimensional network by chemical crosslinks is called crosslinked polymer and the individual molecular chains within a crosslinked polymer are themselves linked together by covalent bonds Fig. 1.4 shows an idealized structure of a cross-linked polymer. [5,6].

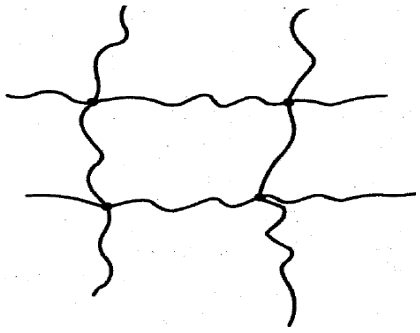

Figure 1.4 Idealized structure of a cross-linked polymer.

1.3 Copolymers

A copolymer is obtained from more than one type of monomers. When two different monomers are used in the polymerization process as A and B monomers, the result is a copolymer. Both the repeating units A and B exist in the polymerized product and their varying configurations give different types of copolymers as linear, branched, and crosslinked copolymers [1,4]

1.3.1 Linear Copolymers

Linear copolymers appear in three different forms: random, alternating, and block copolymers . When the distribution of repeating units is irregular in its structure, this is referred to as a random copolymer. The name of random copolymers includes the names of the monomers separated by the interfix -co- such as poly(styrene-co-methyl methacrylate) as shown in Fig. 1.5 [1,4].

—A–A–B–A–A–A–B–B–A–B–B–B—

(a)

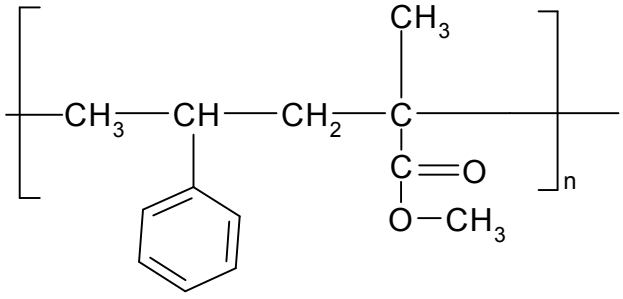

(b)

Figure 1.5 (a) Idealized structure of a random copolymer, (b) poly(styrene-co-methyl methacrylate).

In the alternating copolymer, the two mers alternate in a regular shape along the polymer chain. The interfix -alt- is used, for example poly (styrene-alt-maleic anhydride) as shown in Fig. 1.6 [1].

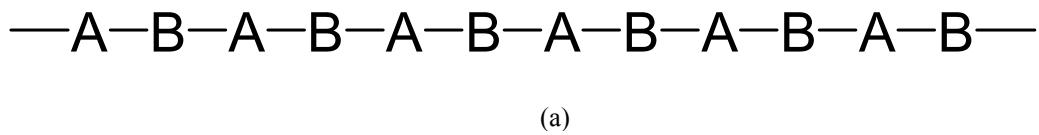

(a)

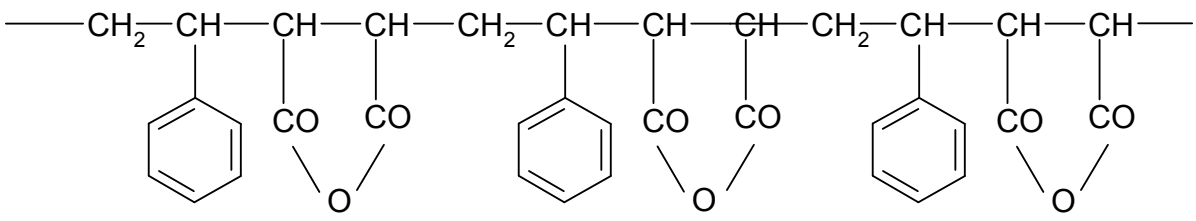

(b)

Figure 1.6 The structure of (a) an idealized alternating copolymer (b) poly (styrene-alt-maleic anhydride).

A block copolymer is a linear polymer with one or more long continuous sequences of each mer in the chain. Block copolymers may have different number of blocks in the molecule. Thus, A_xB_y, $A_xB_yA_x$, $A_xB_yA_xB_y$, $(A_xB_y)_n$ are referred to as diblock, triblock, tetrablock and multiblock copolymers, respectively, x and y as well as n represent average values, in the nomenclature of block copolymers, b or block. Block copolymers of A and B monomers are named poly(A-b-B), poly(A-b-B-b-A) and block copolymer of A, B and C is named poly(A-b-B-b-C), and so on, such as triblock polymer poly(styrene-b-butadiene-b-styrene) also called (SBS) block copolymer as shown in fig. 1.7 [1].

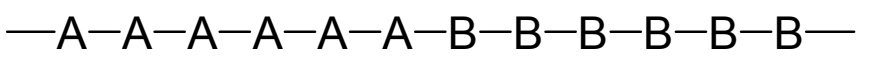

(a)

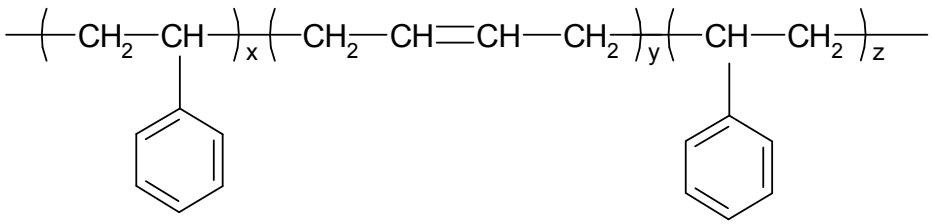

(b)

Figure 1.7 (a) Idealized structure of a block copolymer (b) poly(styrene-b-butadiene-b-styrene)

1.3.2 Branched (Graft) Copolymers

A branched copolymers has a long chain of monomers of one kind in their main backbone and monomers of another type in their side branches. In the nomenclature of graft copolymers, (g) for example, poly(A-g-B) with the backbone polymer $-(A)_n-$ [1,5]. The structures of branched copolymers are shown in Fig. 1.8.

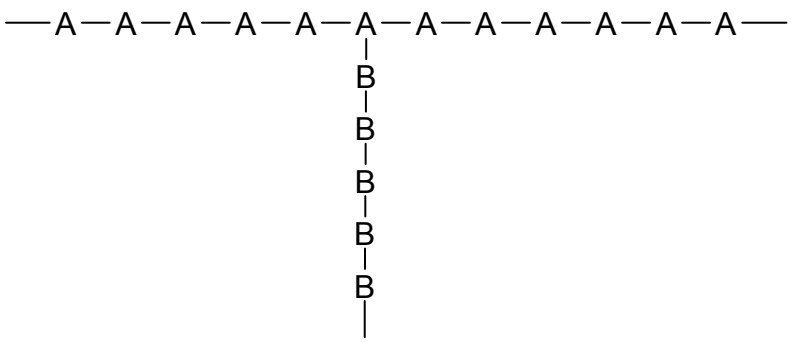

(a)

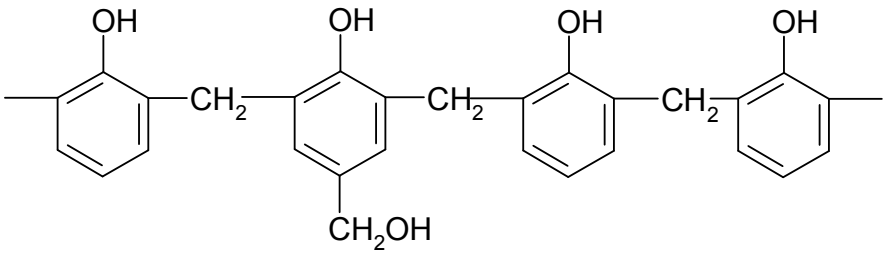

(b)

Figure 1.8 (a) Idealized structure of a branched copolymers (b) structure of a branched copolymers novolacs.

1.3.3 Crosslinked Copolymer

Crosslinked copolymer is also called network copolymer. As an example of the crosslinked copolymer is phenolics see Fig. 1.9. It should be noted that the structure of phenolics is much more random than that shown in Fig. 1.9. This figure is simplified in order to clarify the three-dimensional network [4].

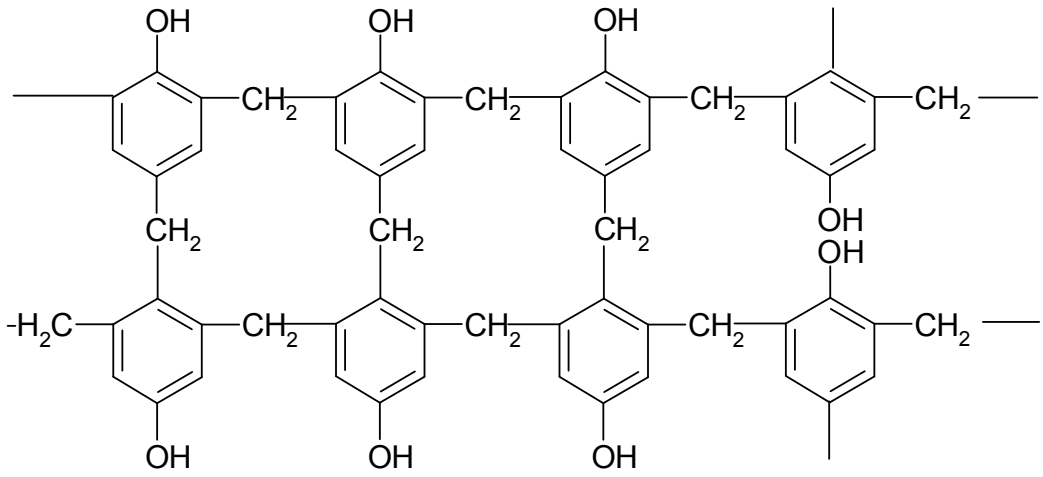

Figure 1.9 structure of a crosslinked copolymer phenolics

1.4 Thermoplastic Polymers

Thermoplastic polymer is a soften polymer and its shape is changed with the application of heat and pressure. The average distance between individual molecular chains is increased as temperature is increased. This results in an increase in the molecular mobility and a decrease in the secondary bonding forces. Both linear and branched polymers are thermoplastics and can be re-melted and reprocessed. Thermoplastics can be sub-divided into those which crystallize on cooling and those which do not crystallize on cooling. The ability of polymers to crystallize depends upon many factors such as the degree of branching and the regularity of molecules [1,4,6].

1.5 Thermoset Polymers

Thermosets are network polymers with heavily cross-linked. The crosslinked structure of thermosets are stable to heat. When the temperature is increased the distance between individual segments of the molecular network are increased, but not enough to allowing the free motion between chain segment and the crosslink which limit of the molecular motion, so the crosslinked polymer cannot be melted . At high temperature, the covalent bonds that form the crosslinks are broken and the polymer is destroyed. Thermosets polymers are usually stiff [4,6,9].

1.6 Elastomers Polymers

Elastomers are network polymers with lightly crosslinked molecular networks. Elastomers are also called rubbers. When we apply pressure on the rubber, its shape will deform and when we remove the applied pressure the rubber will return to its original shape. Rubbers are available as natural or synthetic. Rubbers become glassy on cooling or become partially crystallize and can't be melted on heating, that mean they cannot flow, because of the cross-links [4,9]. Some of the candidate polymers from the above three categories which are used in the formation of filled polymer systems are given in Table 1.1.

Table 1.1 Some candidate polymers used in the formation of filled polymer systems

Thermplastics	Thermosets	Elastomers
Nylons	Epoxies	Neoprenes
Polypropylene	Phenolics	Nitriles
Polystyrene	Unsaturated polyesters	Styrene butadienes

1.7. Conducting Polymers

An insulator has conductivities in the range of 10^{-18} to 10^{-5} S/cm. A semiconductor is in the range of 10^{-7} to 10^{-3} S/cm, and a conductor is usually given as 10^{-3} to 10^{6} S/cm. Conjugated organic polymers are classified as insulators in their pure state. Polystyrene, polyethylene and nylon are insulators [8].

Fig.1.10 shows the range of conductivities that can be achieved with polymers compares with other materials. There are three mechanisms where a polymer may exhibit electrical conductivity.

(i) conducting particles as dyes or metalic materials may be inserted into non conducting polymer.

(ii) the polymer may contain impurities from polymerization process which have ions.

(iii) the polymer may show electronic conductivity from the motion of electrons along the polymer chains.

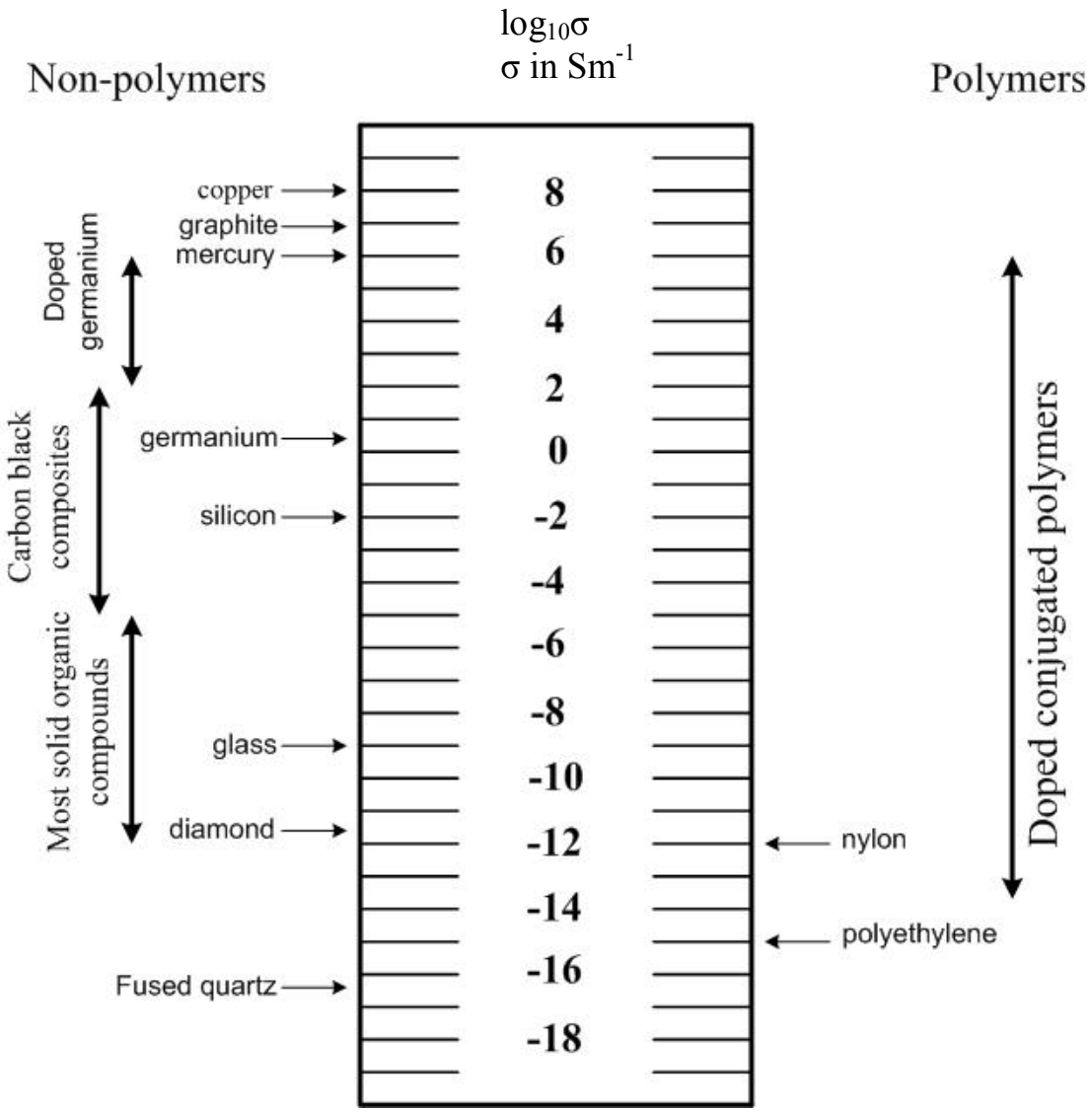

Figure 1.10 The range of conductivities of materials.

In the first mechanism, the polymer does not take role in the conduction process and acts as a support for the conducting material. In the second and the third mechanisms the conduction takes place through the polymer itself. Conduction and dielectric properties are not the only electrical properties that polymers can exhibit. Some polymers, in common with certain other types of materials, can exhibit ferroelectric properties or photoconductive properties [8].

1.8. Electronic Properties of Conducting Polymers

The characteristic electronic properties of conductivity, electrochromism, electroluminescence and electroactivity of the polymer is caused by the particular bonding arrangement of the carbon atoms in the polymer backbone. Fig. 1.11

illustrates the presence of double bonds alternating with single bonds along the polymer chain, mean conjugated bonds. The electron configuration of the six electrons in a carbon atom (in its ground state) is $1s^2\ 2s^2\ 2p^2$. The electrons in the core orbitals do not contribute to the chemical bonding since the 2s shell is filled. In conjugated polymers, one 2s orbital pairs with the two 2p orbitals to form 3 sp^2 hybrid orbitals, leaving one p orbital unhybridized. Two of the sp^2 orbitals on each carbon atom form covalent bonds with neighboring carbons. The third generally forms a covalent bond with a hydrogen or side group. This is called a σ-bond. The unhybridized p_z orbital overlaps with the unhybridized p_z orbital on the neighboring carbon. This is called a π-bond [10].

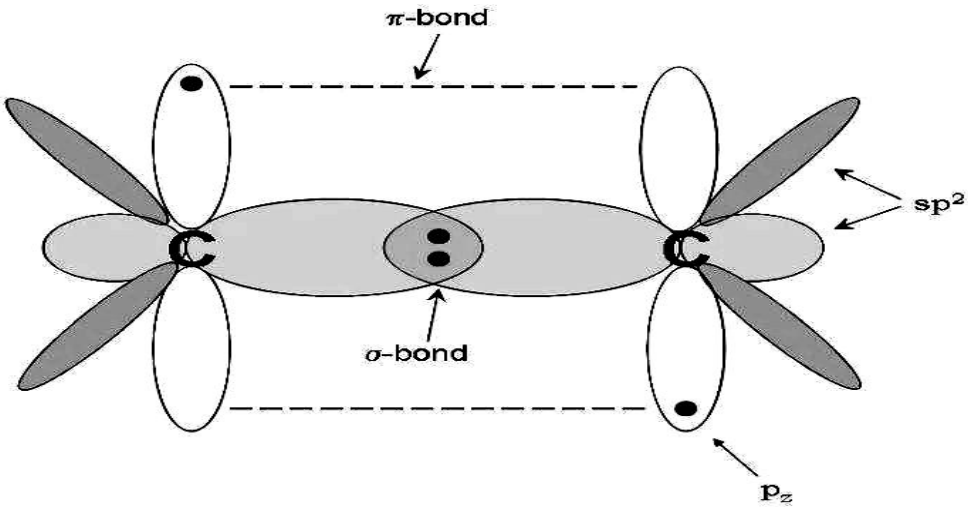

Figure 1.11 Bonding in conducting conjugated polymers. The sp^2 hybrid orbitals are shown in light gray, and the unhybridized p_z orbitals in white. Electrons are represented by the dots, the two sp^2 hybrid orbitals on the side extend in and out of the plane of the page.

The electrons in the π-bonds are weakly bound, and thus they are relatively easily delocalized. These delocalized π electrons are the conduction electrons in these materials [10].

1.9. Electronic States of Polymers

For polymers, we can imagine the band model such as, each monomer molecule having electronic states which consists of the molecular orbitals of the molecule. The molecular orbitals are degenerate on each monomer and overlap to form a series of

extended electronic states. Bonding and antibonding molecular unit orbitals lead to polymer valence and conduction bands. The linear combination of the valence shell orbitals of the atoms forms the molecular orbitals which link together in the molecule. The combination of two adjacent single orbitals results in two molecular orbitals , one of lower and the other of higher energy than before combination. The low-energy orbital is called bonding orbital and is occupied by a pair of electrons of antiparallel spin. The high-energy molecular orbital, denoted as antibonding orbital, is unoccupied in the ground state but may be occupied at electronic excitation of the molecule. The difference between the highest occupied state (molecular orbital), HOMO, and the lowest unoccupied state (molecular orbital), LUMO is called the band gap as shown in Fig. 1.12 (a). Therefore, excitation of electrons from HOMO to LUMO states is possible [11-13].

Another term has to be mentiond here which is SOMO that stands for Singly Occupied Molecular Orbital. However, There are different kinds of molecular orbitals: bonding σ and π orbitals, nonbonding n orbitals, and antibonding σ^* and π^* orbitals. When a molecule in its ground state absorbs a photon, an electron occupying a σ, π or n orbital is promoted to a higher-energy σ^* or π^* orbital. In principle, the following transitions are possible: $\sigma \rightarrow \sigma^*$, $\pi \rightarrow \pi^*$, $n \rightarrow \pi^*$, and $n \rightarrow \sigma^*$. Photon absorption initiates transitions of n or π electrons rather than those of σ electrons. As shown in Fig. 1.12 (b) [11-13].

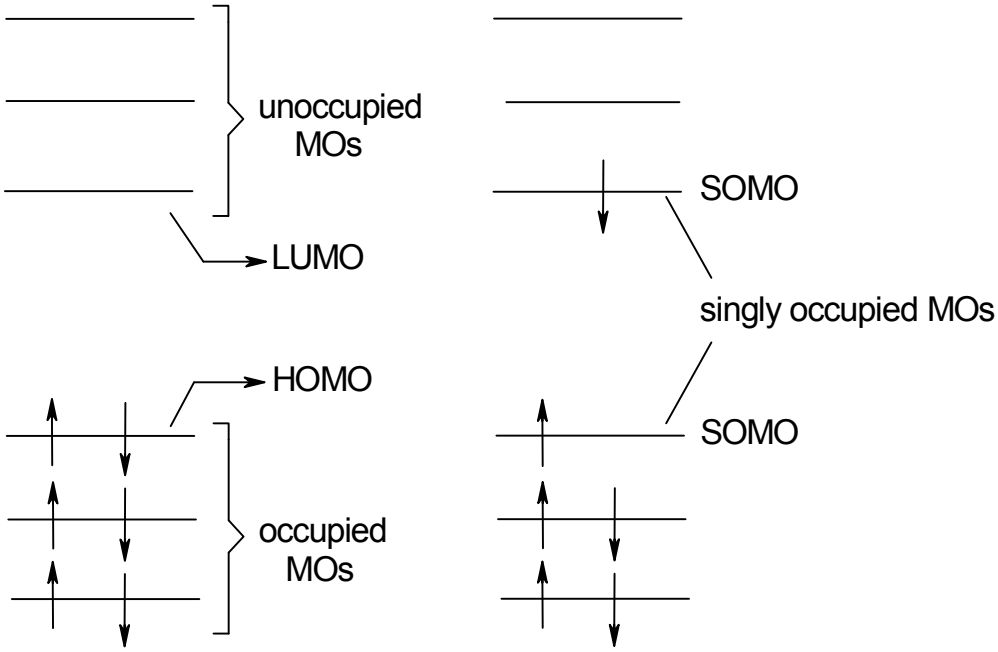

(a)

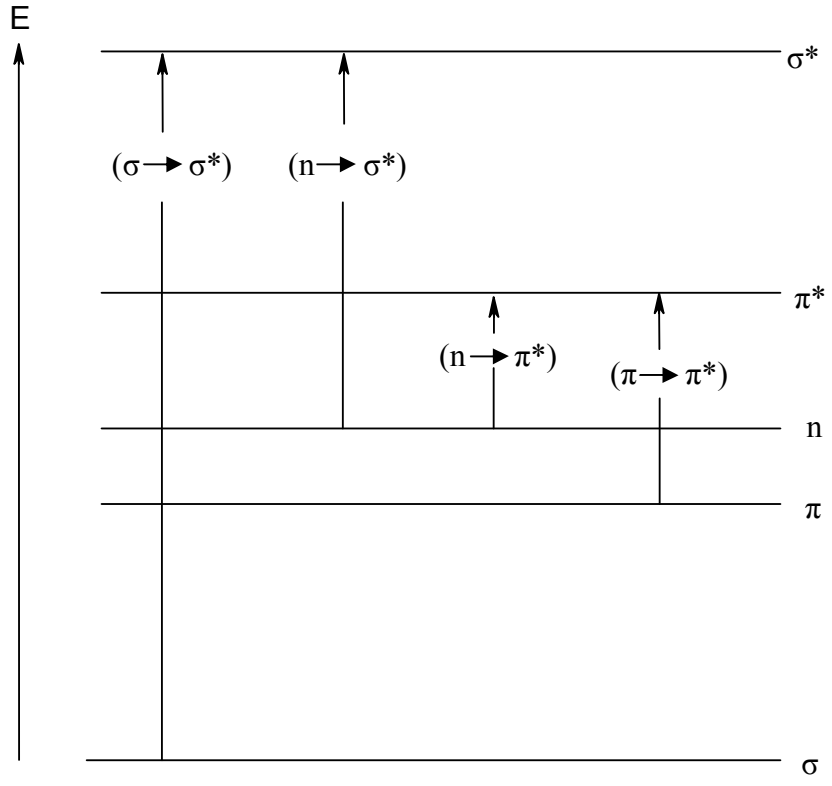

(b)

Figure 1.12 (a) Classification of molecular orbitals with respect to electron occupancy, (b) Molecular orbitals and electronic transitions induced by the absorption of photons.

1.10. Physical Properties of the Polymers

1.10.1 Glass Transition Temperature

The temperature at which the polymer is transformed from a relatively glassy to a relatively rubbery is called the transition temperature T_g. An increase in temperature increases the energy of molecules and widen the bonds between the chains. The temperature affects the stiffness of both thermoplastic and thermoset polymers. We need to know about specific volume which is the reciprocal of the density to understand the glass transition temperature. Fig. 1.13 shows the dependence of the specific volume on the temperature for an amorphous polymer. We can explain the elasticity of rubbers by using molecular theory which is based on the freedom of the chain to take all the conformations allowed by rotations around single bonds, that take place if there is a free space available for molecular segments to move into and the conformational changes of the backbone are done . As shown in Fig. 1.13, the curve of the specific volume has a kink at the glass transition temperature and the specific volume grows more strongly with temperature than before. This additional volume is called free volume. The free volume comes from the growth of the distance between the molecular chains at high temperatures, which is due to thermal activation that allows to overcome intermolecular bonds and increase the mobility of the molecules. Thermal activation allows to break and re-form these bonds frequently enough for the atoms to be able to move freely past each other. Increasing the temperature, and thus the kinetic energy, also increases the distance between the molecules strongly. The mobility of the chain molecules is much larger than below the glass transition temperature [6,9,14].

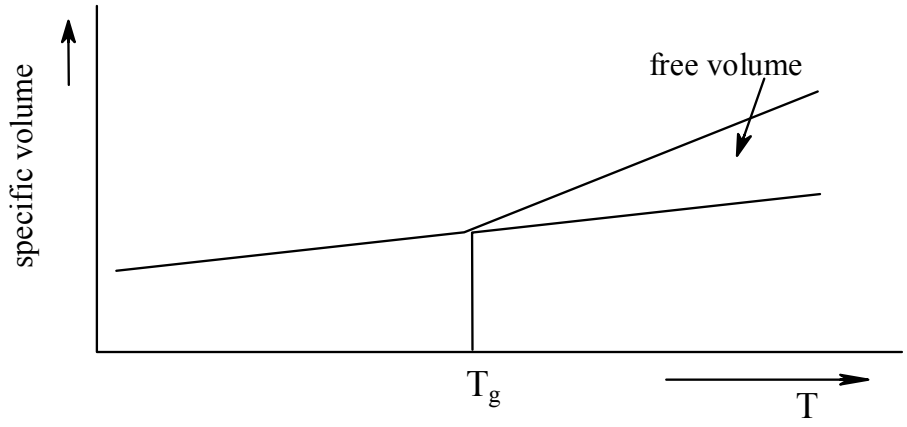

Figure 1.13 Specific volume of an amorphous polymer as function of the temperature.

At temperatures significantly below T_g, the polymer is in a "glassy" state and exhibits a high stiffness and a lower ductility. The polymer molecules are tightly bonded by secondary bonding forces and cannot easily slide past each other. Conversely, at temperatures significantly above the T_g, the polymer is in a rubbery state and exhibits a lower stiffness and higher ductility. The polymer molecules are less bonded by secondary bonding forces and can more readily slide past each other [6,9,14].

1.10.2 Relaxation Processes

Amorphous thermoplastics consist of covalently bonded chain molecules bonded to each other by intermolecular interactions. At low temperatures, the chain molecules are fixed in their positions and the intermolecular bonds are strained. At high temperatures, the rearrangements and movements within and between the chains can occur. These processes can be reversible and called relaxation processes. The name relaxation processes is due to the lowering of applied stresses. A simple example of a relaxation process is a rotation along the axis of a molecular chain as in polyethylene. Although a single C-C bond can rotate freely, this is not true for the bond along the molecular chain because the attached hydrogen atoms and the chain itself impede the rotation [9,14].

1.11 Poly N-Vinylcarbazole

1.11.1 Carbazole

Carbazole is an aromatic tricyclic compound which was discovered in 1872 by Graebe and Glaser from the coal tar. The chemical structure of carbazole is illustrated in Fig. 1.14(a). Pure carbazole is a white crystalline organic material which has a melting point of 246^0C, and 167.2 g/mole molecular weight. Carbazole has a high boiling point compared with many organic materials . It is an electroluminescent material. Carbazole emits strong fluorescence and long phosphorescence by exciting with enough energy (ultraviolet). It is readily soluble in acetone, slightly soluble in ether and ethanol, and barely soluble in acetic acid, carbon tetrachloride, and carbon disulfide. Carbazole is also used to synthesize the monomer N-vinylcarbazole, which can be polymerized to form poly(N-vinylcarbazole) [5,6].

1.11.2 Poly (9-Vinylcarbazole)

Poly(N-vinylcarbazole) (PVK) can be polymerized by both free radical and cationic polymerization. The propagating chain end stabilizes electron deficient centers by resonance, involving the nonbonding electron pair on the nitrogen of the Carbazole ring. N-Vinyl Carbazole has not been successfully polymerized by anionic means. The number 9 in Poly(9-vinylcarbazole) indicates that the vinyl group is attached to the nitrogen in the Carbazole molecule. The structural formula of poly(9-vinylcarbazole) is shown in Fig. 1.14(b). We can categorize poly (9-vinylcarbazole) as an organic homopolymer since it consists of only one type of constitutional repeating units, also, it is a heterochain polymer since its main chain made up of different kind of atoms . Poly(9-vinylcarbazole) (PVK) is a transparent thermoplastic material, with a good thermal and chemical stability. The softening point of PVK is nearly a 175 ^{0}C and its glass transition temperature (T_g) is at 211^{0}C. The solubility of PVK is very strong in alcohol, ether and tetrahydrofuran (THF). Usually PVK films are deposited by spin coating [5,6].

PVK has good optical properties. It has strong photoconductive and electroluminescence properties. It has a high refractive index ~1.69 in the visible region. Electrically, PVK is an insulator in dark but under the ultraviolet radiation, it exhibits electro-conductivity. Commercially PVK is used as a paper capacitor, in organic light emitting diodes (OLEDs), data storage, sensors and transistors. In OLEDs, PVK is used as a hole transport material [5,6].

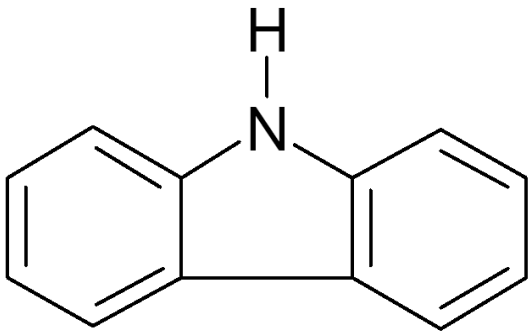

(a)

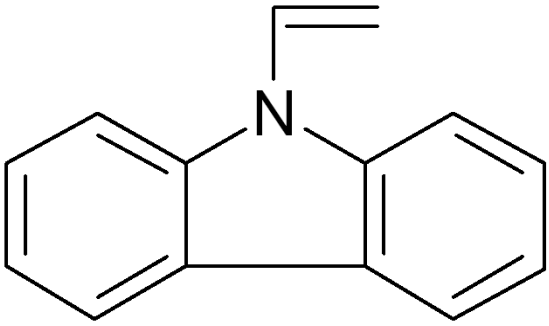

(b)

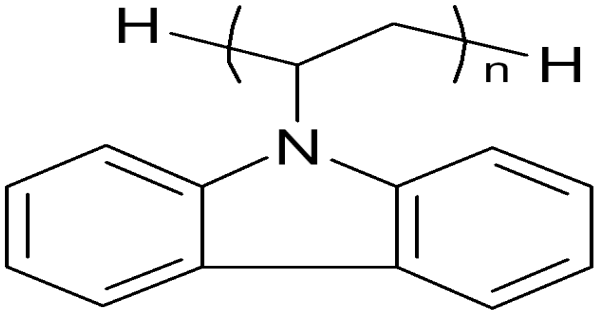

(c)

Figure 1.14 The structure formulas of poly(N-vinylcarbazole), (a) Carbazole, (b) N-vinylcarbazole, and (c) Poly(N-vinylcarbazole).

CHAPTER TWO
ELECTRICAL CONDUCTION MECHANISM AND LUMINESCENCE

2.1 Introduction

Electrical conduction essentially depends on the charge carriers and their transport in a material. It also depends on the energy band gap which is the difference between valence and conduction band levels. Energy gap determines the characteristic of the material if its metal, semiconductor, or insulator. In metals, there are no energy gap and the charge carriers are electrons which can move freely inside the materials and give good conductivity. In semiconductors, the energy gap exists and the charge carriers are both holes and electrons. On the other hand, in an insulator the energy gap is larger than in semiconductor thus its conductivity is poor. We can enhance the conductivity by doping process which can add or remove electron from the atoms of the material. In this section, we shall discuss the features of various types of conduction, manner of electrical transports and the different mechanisms that explain the flow of carriers through metal-polymer junction.

2.2 Electrical Conduction

Electrical conductivity of a material is defined as the ability of the charge carriers to move across the material. Electrical conduction may involve electronic and ionic conduction. In metals, electrical conduction is due to the mobility of electrons, whereas in ionic materials, conduction results from the net movement of charged particles in addition to electrons motion. Electrons and holes represent the charge carriers in semiconductors and in doped conductive polymers. The electrical conductivity denoted as σ can be written for metals, semiconductors, and ionic materials as [15-17]

$$\sigma = n_e q_e \mu_e \text{, (metals)} \tag{2.1}$$

$$\sigma = n_e q_e \mu_e + n_h q_h \mu_h \text{, (semiconductors.)} \tag{2.2}$$

$$\sigma_{totl} = \sigma_{electronic} + \sigma_{ionic} \text{, (ionic materials.)} \tag{2.3}$$

Where n_e, n_h, q_e, q_h, μ_e, and μ_h are the concentrations of charges, charges and mobility where *e* and *h* indicate to electrons and holes respectively. When the conduction arises from charge carriers of the pure material it is called intrinsic conduction. The charge carriers density can be increased by adding impurities. This addition is called doping and gives extrinsic conduction. Doping a polymer by oxidation or reduction agent increases its conductivity. The most common dopants are iodine, bromine, ferric chloride and arsenic pentafluoride, which are all p-type dopants. Alkali metals are used as n-type dopants [15-17].

2.2.1 Ionic Conduction

Ionic conduction involves the transport of ions. An ion (anions or cations) will polarize its surrounding from atoms or molecules as shown in Fig. 2.1. The polarization reduces the electrostatic energy of this ion. This effect traps the ion and hinders its motion. This is equivalent to a potential barrier and the ion requires an activation energy to surmount the potential barrier in order to move. The variation of ions involving an energy k_BT can cause ions and vacancies to exchange sites. Vacant lattice sites must be present for ionic movement. In intrinsic ionic conduction, the charge carriers are vacancies and the crystal has thermally created vacant sites in the lattice. The activation energy E_σ for intrinsic ionic conduction consists of the energy required for the creation vacancies and that required for the movement of the vacancies. The vacancies might also be introduced into the crystal by dopants, in nonionic solids, ionic conduction is extrinsic. Insulating materials such as polymers may contain ions and other impurities introduced into the polymer during fabrication processes. For example, insulating polymers such as PVC may contain H_3O^+, Na^+, K^+, OH^-, Br^- [15].

2.2.2 Electronic Conduction

Electronic conduction involves the transport of electrons and holes. Consider a semiconductor crystal such as silicon, the intrinsic concentrations of electrons *n* and of holes *p* are equal and is given by [15]

$$n = p = n_i = \left(N_c N_v\right)^{1/2} \exp\left(-E_g / 2k_B T\right), \tag{2.4}$$

where N_c and N_v are the effective densities of states in the conduction and the valence bands, respectively, E_g is the energy band gap, and k_B and T are the Boltzmann constant and the absolute temperature, respectively. From the above equation we can see that, when E_g is increasing (with no change in other parameters) n_i will be reduced, also the conductivity will be reduced. This means that the intrinsic conductivity of insulating materials would be negligibly small, and the conductivity is extrinsic or injection from metallic electrodes [15].

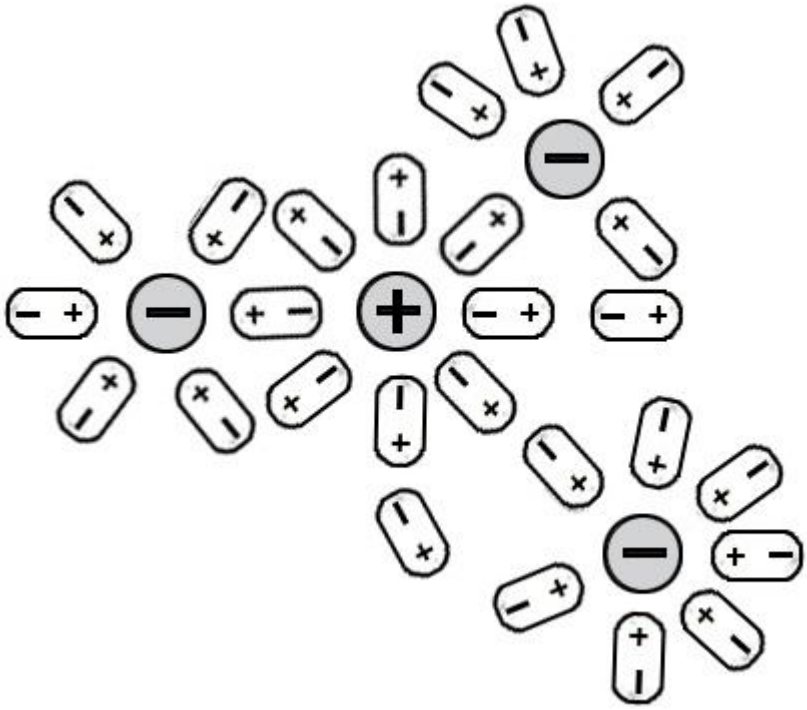

Figure 2.1 Schematic illustration of ions polarizing surrounding molecules or atoms.

2.3 Electrical Transport

Charge carriers can move by tunneling process from one site through the barrier to the next, or by hopping process from one site across a potential barrier to a neighboring site. Both mechanisms depend on the profile of the potential barrier and thermal energy.

2.3.1 Electrical Transport by Tunneling

Tunneling is a quantum mechanical effect. An electron in a molecule when excited can tunnel to a neighboring molecule with energy conservation, or return to its ground

state. For metal-semiconductor interface, with high enough doping in the semiconductor, if the width of the depletion region at the metal-semiconductor interface is very thin, the wave function of an electron in the metal electrode extends into the semiconductor; thus there is some probability that the electron can exist there. The current density due to tunneling formula is given by [6,17]

$$J_T = \frac{e^2 E^2}{8\pi h \phi_m} \exp\left(-\frac{8\pi\sqrt{2m_e}}{3heE} (e\phi_m)^{3/2} \right), \tag{2.5}$$

where h is Planck's constant, ϕ_m is the electrode work function, m_e is the electronic mass and E is the electric field. For metal polymer interface electrons can tunnel from metallic electrode to surface state of the polymer which exists in the energy band gap of the polymer. Then electrons move to conduction band by thermal activation without applying voltage as shown in Fig. 2.2. For sufficiently thin insulator film, electron may tunnel from one electrode to the other without involving the movement of carriers in the conduction band or in the valance band of the insulator. This tunneling depends on the thickness of the insulating film [6,17].

2.3.2 Electrical Transport by Hopping

The charge carriers move from one molecule to another by hopping process if they gain the energy required to overcome the potential barrier. Electrons and ions can move by hopping if the distance between two adjacent molecules is larger than 10 A^0. Electrons hopping process occur rather than tunneling process. Fig. 2.3 shows the tunneling and hopping process [17].

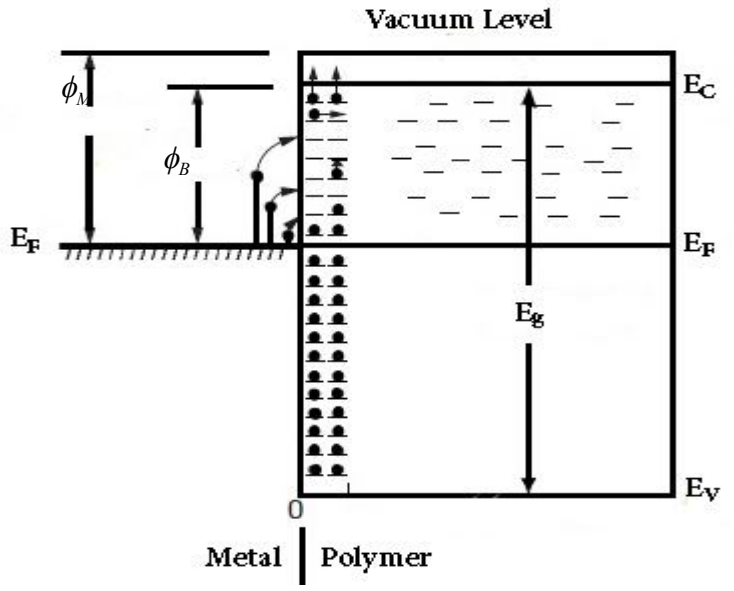

(a)

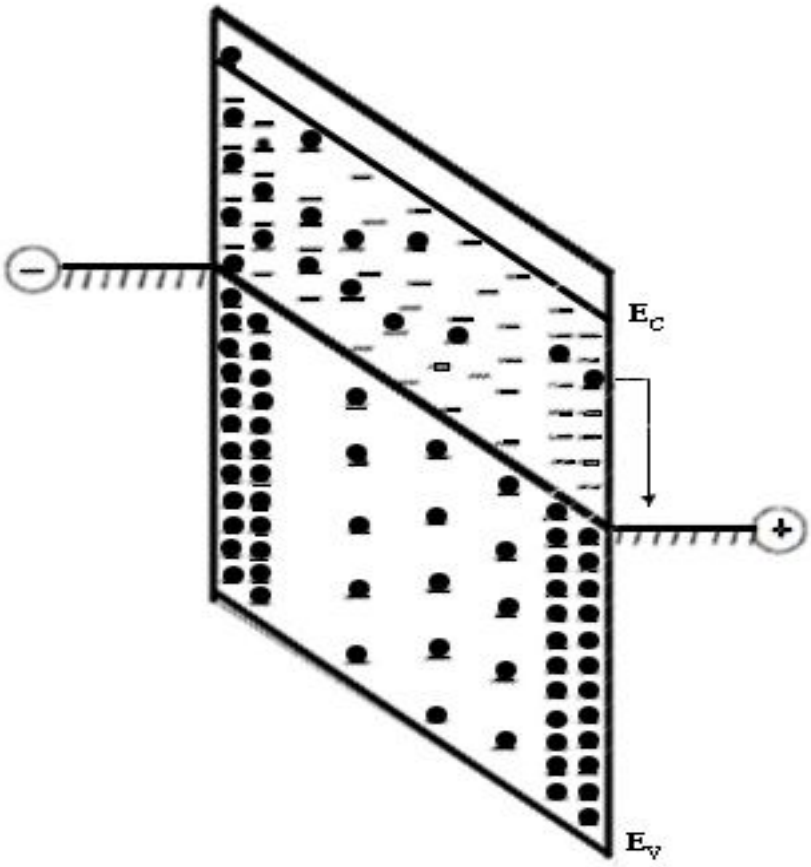

(b)

Figure 2.2 Simple energy band diagrams illustrating the distributions of surface and bulk trapping states in energy and in space: (a) without an applied field and (b) with an applied field.

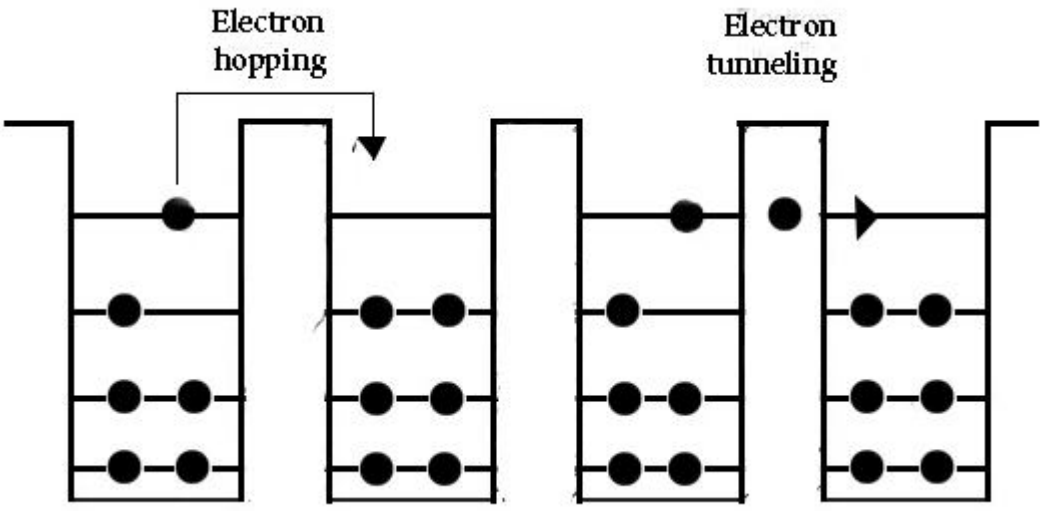

Figure 2.3 Schematic illustration of an electron tunneling through a square potential barrier and an electron hopping across a square potential barrier.

2.4 Mechanisms of Charge Carrier Injection Through A Metal/Polymer Interface

2.4.1 Thermionic Emission

The assumption of thermionic emission means that an electron emitted from the metallic electrode can be injected into the polymer if it gains a sufficient thermal energy to overcome the potential barrier that results from the superposition of the external and the image charge potential as shown in Fig. 2.4. At lower fields and higher temperatures, the charge injection is due to thermionic emission model and most injected carriers will backflow into the electrode. It should be noted that the critical parameter is the barrier height and not the shape of the barrier. At higher fields, the metal electrode work function for thermionic emission is reduced, thus lowering the Schottky barrier height (image force lowering) [18-20]. The total electron current over the barrier is given by

$$J = A^{*}T^{2}\exp\left(-\frac{q\phi_{B}}{k_{B}T}\right), \tag{2.6}$$

The Schottky equation, taking into account the image force lowering, may be written as [21]

$$J = A^* T^2 \exp\left(-\frac{\phi_B}{k_B T}\right) \exp\left[\left(\frac{q^3 V}{4\pi\varepsilon_0 \varepsilon_r d}\right)^{1/2} \Big/ k_B T\right], \tag{2.7}$$

where ϕ_B, d, ε_0, and ε_r are the interface potential barrier height, film thickness, vacuum permittivity, and optical dielectric constant, respectively. A^* is called the effective Richardson constant and is a function of the effective mass and is given by [18,19]

$$A^* = \frac{4\pi q m^* k^2}{h^3}, \tag{2.8}$$

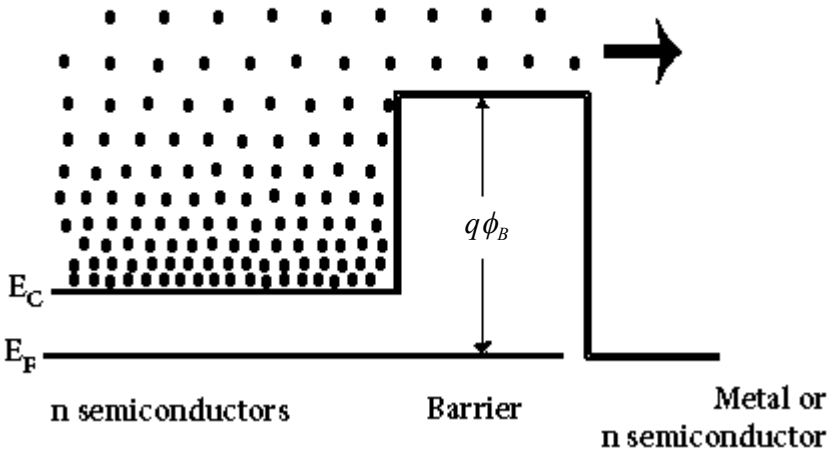

Figure 2.4 Energy band diagram showing thermionic emission of electrons over the barrier.

2.4.2 Field Emission

Field emission is tunneling of electrons through the potential barrier from metal to insulator or semiconductor in the presence of a strong electric field and low temperature. Most electrons tunnel at the Fermi level of the metal. When the barrier is triangular, the tunneling is called Fowler- Nordheim (FN) tunneling [15,20]. Fig. 2.5 shows different mechanisms of conduction. The field emission cancels image charge

effects and invokes tunneling process. When the field emission dominates, the J-V characteristics are described by

$$J = AE^2 \exp\left(-\frac{8\pi\sqrt{2m^*}\phi_B^{3/2}}{3hqE}\right), \tag{2.9}$$

where m^* is the effective charge carrier mass, E is the applied electric field, and A [in A/V^2] is a rate coefficient that contains a tunneling prefactor and the rate of current back-flow. It can be deduced from the treatment by Kao and Huang that A is given by [21]

$$A = \frac{q^3}{8\pi h\phi_B}. \tag{2.10}$$

Equation (2.9) can also be written as

$$J = AE^2 \exp\left(-\frac{k}{E}\right), \tag{2.11}$$

where

$$k = \frac{8\pi\sqrt{2m^*}\phi_B^{3/2}}{3qh} = constant. \tag{2.12}$$

If the value of k is known, then the barrier height between the electrode and the film may be estimated from Eq. (2.12) as

$$\phi_B = \left[\frac{3kqh}{8\pi\sqrt{2m^*}}\right]^{2/3}. \tag{2.13}$$

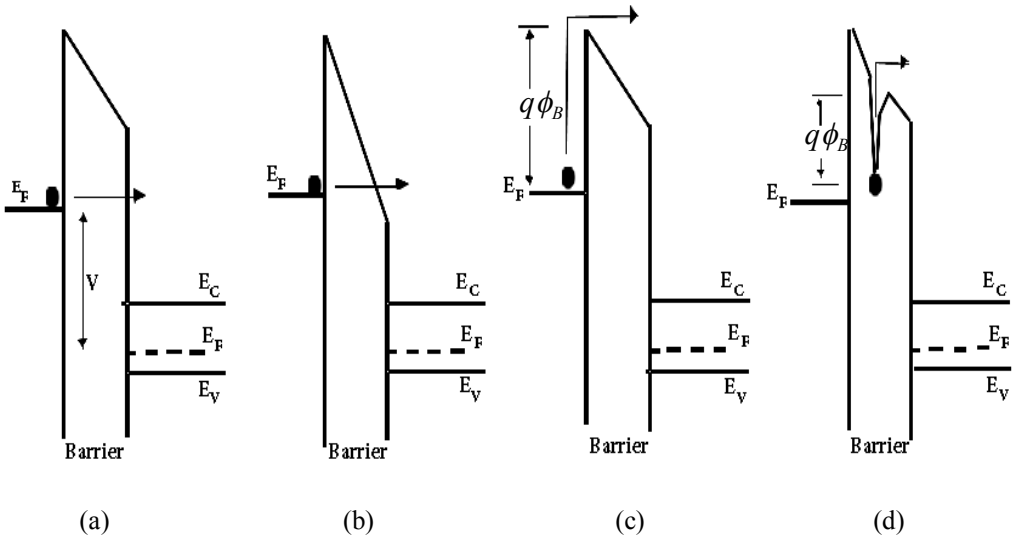

Figure 2.5 Energy band diagrams showing conduction mechanisms of (a) direct tunneling, (b) Fowler-Nordheim tunneling, (c) thermionic emission, (d) Frenkel-Poole emission.

2.4.3 Transition from Field to Thermal Emission Limited Characteristics

This emission is a hybrid model of thermionic and field emission. An increase in electric field causes barrier lowering due to image charge, and the charge carriers can move over the barrier. This model is called field assisted thermionic emission. Moreover, an increase in temperature makes the barrier thinner and hence increases the probability of tunneling. The most electrons above Fermi level of the metal can tunnel. This model is called thermally assisted field emission [15,21]. For $k_BT/q\phi_B$ << 1, field emission (FE) dominates, or carrier tunneling through the entire barrier and the contact is ohmic. For $k_BT/q\phi_B$ >> 1, thermionic emission (TE) dominates and the contact is rectifying, while for $k_BT/q\phi_B$ ≈ 1, the hybrid model thermionic field emission (TFE) dominates, tunneling of hot carriers through the top of the barrier or hopping of carriers over the barrier [22]. Figure. 2.6 shows the three major current transport mechanisms.

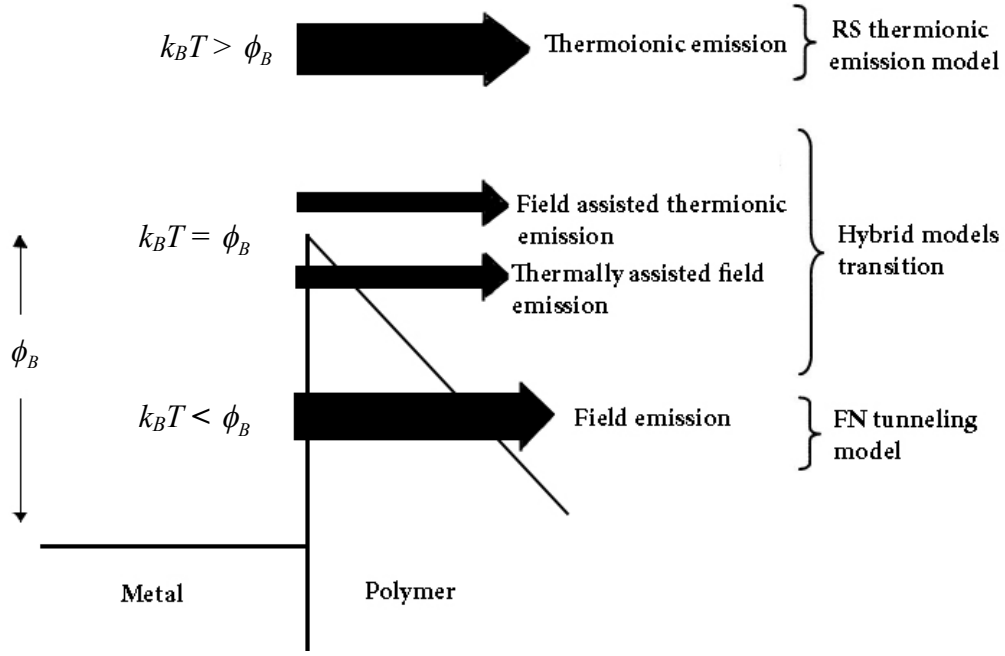

Figure 2.6 Mechanisms of charge carrier injection through a metal/polymer interface, showing the three major current transport mechanisms: thermionic emission (TE), thermionic-field emission (TFE) and field-emission (FE).

2.5 Ohmic Contact

The ohmic contact refers to metal-semiconductor contact with very low junction resistance and is independent of applied voltage. It has a linear *I-V* characteristic curve in both directions. The charge carrier density at and near the contact is too high. To obtain an ohmic contact, the semiconductor surface has to be doped to create a Sckottky barrier at the interface between the metal and the semiconductor. This barrier is so thin and the charge carriers can tunnel through it. Ohm's law can be written as [15,18,19,22,23].

$$J_{ohm} = qn\mu\frac{V}{d}, \tag{2.14}$$

where q is the electronic charge, n is the charge carrier density, μ the carrier mobility, V is the applied voltage, and d is the thickness of the sample.

2.6 Space-Charge Effect

Space charge effect occurs when the charge carriers injected under bias are larger than their value in equilibrium before charge injection. This will form space charge cloud near electrodes. In general, the DC current of a device can be divided into two main regimes, ohmic regime and space charge regime. In the ohmic regime, the current is linearly proportional to the electric field according to the following relation

$$J\alpha\ E. \tag{2.15}$$

In the second regime, the current density is proportional to the square of the electric field

$$J\alpha\ E^2 \tag{2.16}$$

This regime is called space charge limited current (SCLC). The space-charge effect is more common in lightly doped materials and it can occur outside the depletion region [5,18,19]. If the injected charge changes the electric field configuration inside the polymer that screens the source-drain field, the transport becomes space-charge limited. The screening due to these "space charges" produces nonlinear *I-V* characteristics. The space charge effect emerges in a material such as an organic semiconductor, where the mobility of the charge carrier is poor. To obtain a current-voltage relation for samples operating in the space-charge limited currents regime, we can use the current density and Poisson's equation given by [12]

$$J = \mu\rho(x)E(x), \tag{2.17}$$

and

$$-\frac{d^2\phi}{dx^2} = \frac{J}{\varepsilon\mu E(x)}. \tag{2.18}$$

where μ is the mobility defined as the constant of proportionality in the relationship between the applied electric field, E, and the drift velocity of the carriers, v, given by

$v = \mu E$, $\rho(x)$ is the local carrier density, and ε is the permittivity of the medium .The electric field is the derivative of the potential, $E(x) = -d\phi/dx$. Using this relation and moving both derivatives to the left hand side leads to

$$\frac{d\phi}{dx}\frac{d^2\phi}{dx^2} = \frac{J}{\varepsilon\mu}. \tag{2.19}$$

Now for a trick on the lefthand side of Equation (2.19). It is equivalent to

$$\frac{1}{2}\frac{d}{dx}\left(\frac{d\phi}{dx}\right)^2 = \frac{J}{\varepsilon\mu}. \tag{2.20}$$

Reorganizing Equation (2.20) and integrating from x = 0 to a distance x, we have

$$\int_0^x d\left(\frac{d\phi}{dx}\right)^2 = \frac{2J}{\varepsilon\mu}\int_0^x dx, \tag{2.21}$$

which evaluates to

$$\left(\frac{d\phi}{dx^2}\right)_{x=x}^2 - \left(\frac{d\phi}{dx}\right)_{x=0}^2 = \frac{2Jx}{\varepsilon\mu}. \tag{2.22}$$

Using a boundary condition, E(0)=0, simplifies the expression to give form of the electric field, E(x),

$$\left(\frac{d\phi}{dx^2}\right)^2 = \frac{2Jx}{\varepsilon\mu} \rightarrow E(x) = -\frac{d\phi}{dx} = -\left(\frac{2J}{\varepsilon\mu}\right)^{1/2} x^{1/2}, \tag{2.23}$$

which we can rearrange to be

$$d\phi = \left(\frac{2J}{\varepsilon\mu}\right)^{1/2} x^{1/2} dx. \tag{2.24}$$

Integrating the lefthand side from $\phi = 0$ to $\phi = \phi(x)$ and the right hand side from $x = 0$ to $x = x$, gives

$$\int_0^{\phi(x)} d\phi = \left(\frac{2J}{\varepsilon\mu}\right)^{1/2} \int_0^x x^{1/2} dx. \tag{2.25}$$

This leads to the functional form of the potential,

$$\phi(x) = \left(\frac{2J}{\varepsilon\mu}\right)^{1/2} \frac{2}{3} x^{3/2}. \tag{2.26}$$

Applying a boundary condition, $\phi(d) = V$, and solving for J to obtain the space charge limited current,

$$J_{SCL} = \frac{9}{8} \mu\varepsilon \frac{V^2}{d^3}. \tag{2.27}$$

Eq. (2.27) shows that the current rises quadratically with voltage in the space-charge regime. This relationship is called the Child's law and it holds for materials where the presence of traps and defect states are low [12,13]. Figure 2.7 shows the transition from ohmic conduction to SCLC conduction.

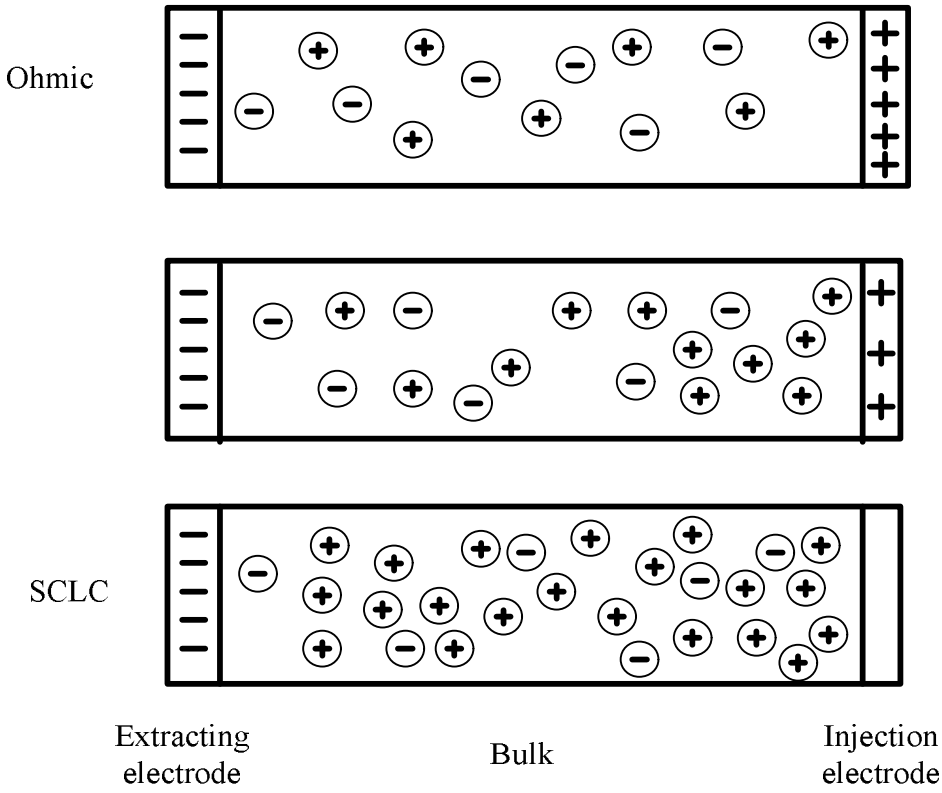

Figure 2.7 Qualitative picture of the transition from ohmic conduction to SCLC

2.7 An Exciton

The combination of an electron and a hole under a columbic force is called an exciton. This combination form excited states such as singlet exciton, triplet exciton and different mechanisms of charge transfer which decay and may release emission . The exciton is classified into two main types, Wannier and Frenkel excitons.

2.7.1 Classification of Excitons

The first type of exciton is Wannier exciton which occurs when the exciton extends over molecular units as shown in Fig. 2.8 (a) The Wannier exciton radius (distance between hole and electron) is larger than the lattice constant that will reduce the binding energy. Wannier exciton occurs in crystals and in organic semiconductors. The second type of exciton called Frenkel exciton which occurs when the exciton is localized on one molecular unit, that make the Frenkel exciton smaller than Wannier and has a higher binding energy as shown in Fig. 2.8(b) [20,23-25].

2.8 Energy Transfer

A donor can transfer its energy to an acceptor due to dipole dipole coupling between two molecules. There are two types of energy transfer, fõster and dexter transfer, where both of them are non radiative [5,20,24]

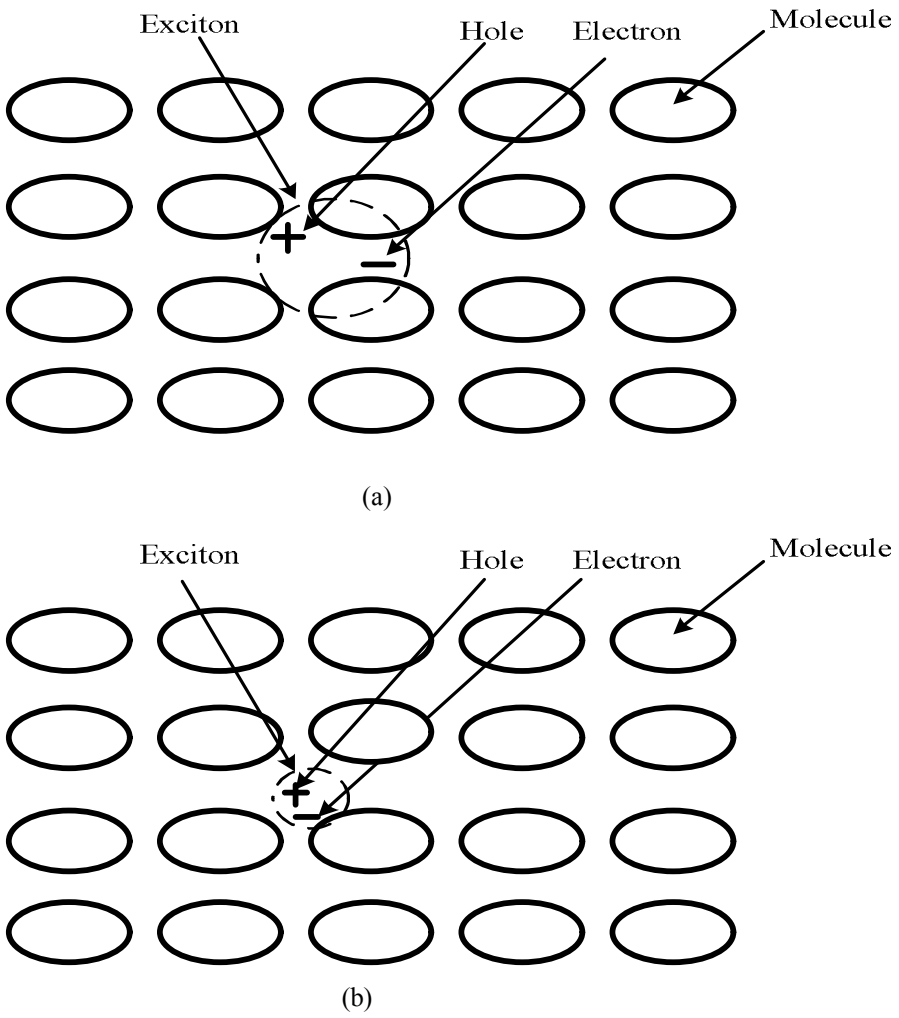

Figure 2.8 The spatial discrimination of excitons (a) Wannier exciton, (b) Frenkel exciton.

2.8.1 Fŏster Transfer

Fŏster Transfer is a non radiative transfer process that means there is no emission of light from the donor molecule. Fŏster Transfer is singlet-singlet transfer energy which occurs in a very short time less than 10^{-9} sec. The mechanism of Fŏster Transfer is that the electron in the excited donor state D^* loses its energy and becomes in the ground state. The electron in the ground state of the acceptor molecule A gains the lost energy and becomes excited in the excited acceptor state A* as shown in fig. 2.9 [24,26,27].

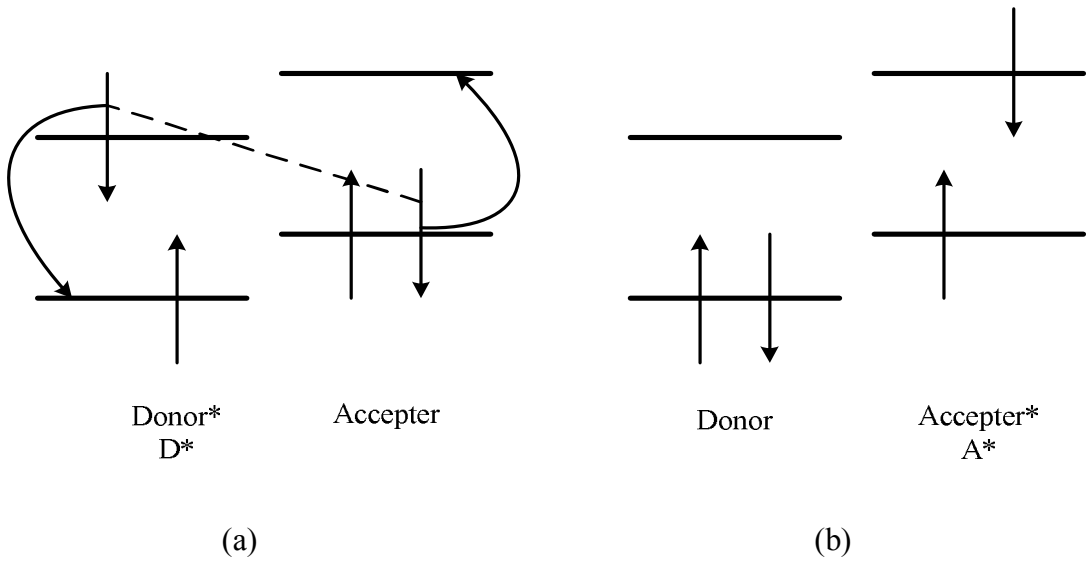

Figure 2.9 Fŏster transfer (a) the intial state, (b) the final state.

2.8.2 Dexter Transfer

The Dexter transfer is singlet-singlet or triplet-triplet transfer which is strongly bound. The electron hole pair are localized on a single molecule, the mechanism of this transfer is that the electron in the excited state of the donor D* jumps to the excited state of the acceptor A* and the electron in the ground state of the acceptor A jump to the ground state of the donor D as shown in fig. 2.10. In Dexter transfer singlet-singlet or triplet-triplet transitions are allowed. About 25% of the formed excitons will be singlets and 75% will be triplets [24,26,27].

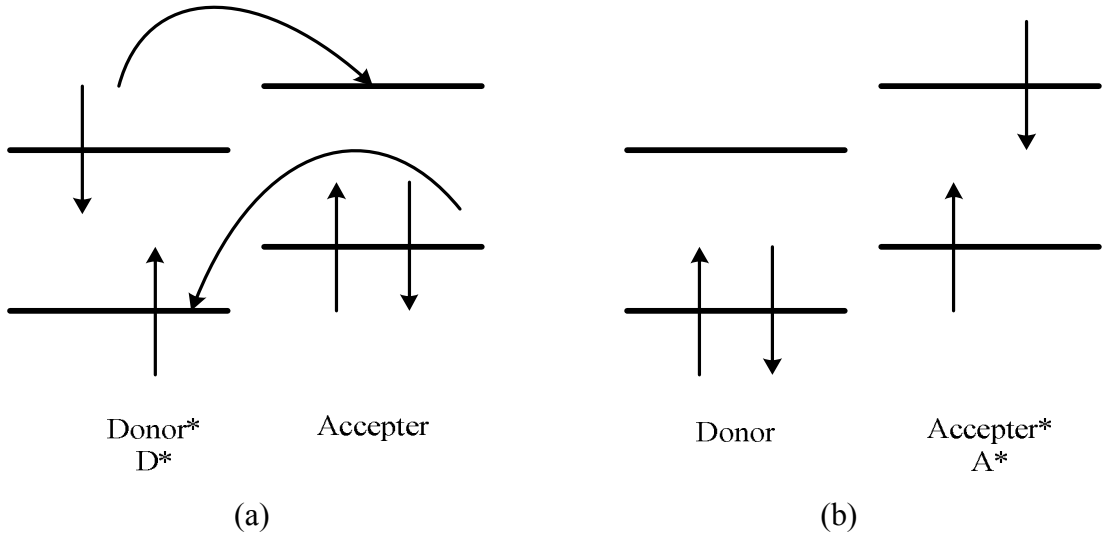

Figure 2.10 Dexter transfer (a) the intial state, (b) the final state.

2.9 Luminescence

Luminescence is the emission of light which occurs from electronically excited state. Luminescence is divided into two types: Fluorescence and Phosphorescence, which resulting from the return of the electron from first excited singlet state S_1, or from the first triplet excited state T_1 to the ground state S_0, respectively [15,20].

2.9.1 Fluorescence

Fluorescence is the emission of light from singlet excited state. Singlet excited state can be generated by the absorption of a photon. The electron in the excited state has opposite spin as the electron in the ground state S_0. The transition of electron from S_1 to S_0 is allowed which causes fluorescence. The life time of electron in S_1 lies between 10^{-9} to 10^{-7} sec. which is very short time. The amount of radiation emitted as fluorescence is lower than the average amount absorbed by a molecule because part of the energy is used in making vibrations and relaxations of electrons to main electronic level [5,15].

2.9.2 Phosphorescence

Phosphorescence is the emission of light from triplet excited state. The electron in excited state has the same spin as the ground state. The transition from the triplet to the ground state is forbidden. Spin orientation is needed for the transition to occur. The electron in the first singlet excited state S_1 can be transferred to the first triplet

state T_1. The electron orients its spin and returns to the ground state S_0 with phosphorescence. This transition is called singlet-triplet transition. The phosphorescence life time is about $1\text{-}10^{-3}$ sec. The emission of light continues after the end of excitation. In general, the transition between energy states with the same multiplicity is allowed and exhibits radiation but the transition is not allowed when the transition between energy states has different multiplicity. Phosphorescence dyes possess strong probability of transition from the excited singlet state to the triplet state (S_1 to T_1). Little or no fluorescence is observed in these materials. The processes, which occur between the absorption and emission of light, are usually illustrated by Jablonski diagram. As shown in Fig. 2.11 the transitions between states with the same spin is referred to internal conversion (IC), where the transitions between the states with different spin is referred to intersystem crossing (ICS). A typical Jablonski diagram is shown in Fig. 2.11 [5,15,20].

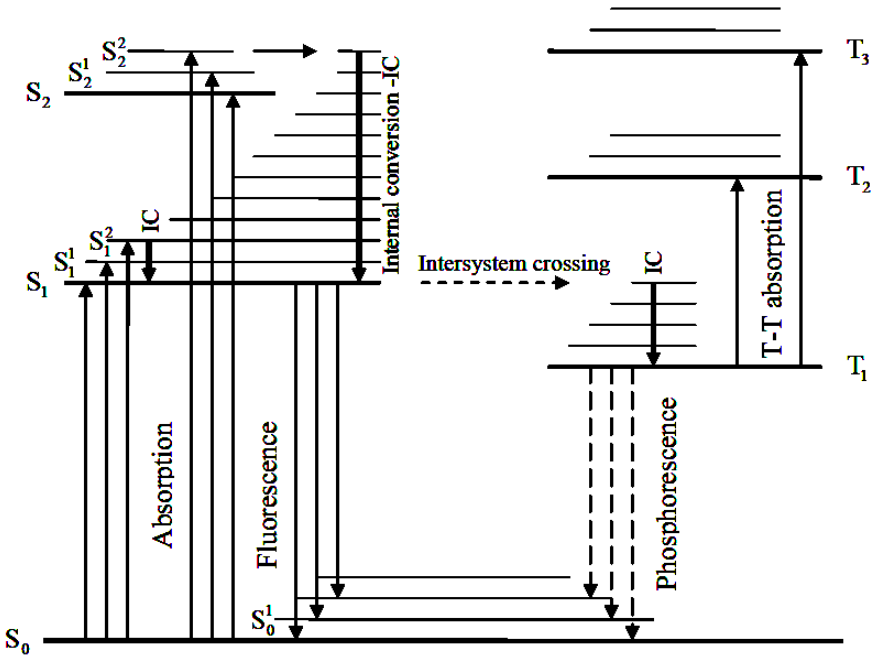

Figure 2.11 Perrin-Jablonski diagram and illustration of the relative positions of absorption, fluorescence and phosphorescence spectra.

CHAPTER THREE
EXPERIMENTAL TECHNIQUES

3.1 Introduction

In this chapter, we shall describe the equipment and techniques used in this thesis. Those equipments were used for the preparation of double layer and single layer films by inclined casting coating and spin coating techniques. Moreover, the homemade variable angle spectroscopic ellipsometer (VASE) is used to measure the thickness and the refractive index of the organic film. The experimental setup used for electrical conductivity measurements will also be described.

3.2 Equipments

3.2.1 Spin Coater

The spin coating process is a commonly used technique to deposit a thin films on substrates using a spin coater. A spin coater consist of a circular table connected to fast a motor with different angular speeds as shown in fig. 3.1. The angular speed is controlled by varying the applied voltage. A cleaned substrate is fixed on the table. Few drops of the desired solution are placed on the substrate and spun at different speeds for 60 second to form different film thicknesses. The solution will spread on a substrate by centrifugal force and a thin film is created. Finally, the samples are placed in an oven at 60 ^{0}C for a several hours to remove the remaining solvent. The film thickness is controlled by using different concentrations of the solution and different angular speeds. Low concentration and high angular speed for a long time give thinner films [5,28].

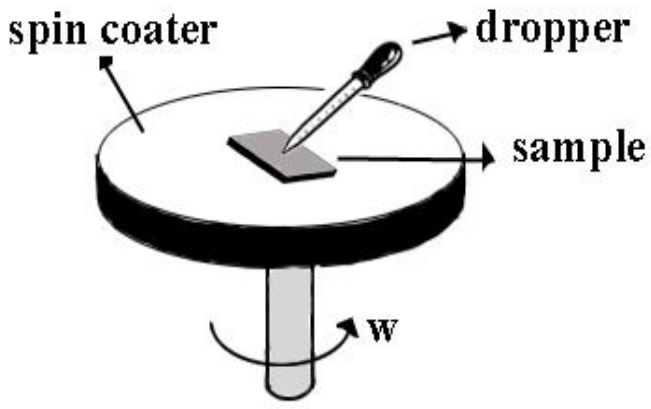

Figure 3.1 Schematic illustration of a spin coater.

Figure 3.2 Photo image of a spin coater.

3.2.2 Inclined Casting Coating

Thin films of soluble polymer can be prepared by a simple technique. A small amount of the desired solution is placed on the substrate and the substrate is then inclined at an angle of 45^0 for several minutes. The solution spreads on the surface of the substrate due to gravity forming a thin film on the surface. The sample is then placed in an oven at 60^0C. The thickness can be increased by increasing the concentration of the polymer in the solution and vice versa. This process is sensitive to the variations in temperature due to different evaporation rates.

3.2.3 Dye Layer Preparation

A known amount of the required dye is weighted and is dissolved in a known amount of methyl alcohol to make a solution of certain concentration. A calculated volume V is drawn with a micropipette and is spun with a spin coater.

The area of found thin film is calculated and the thickness is found using the following relation

$$\rho = \frac{m}{Ad}, \tag{3.1}$$

where ρ is the density of the dye, A is the area of the film, d is the film thickness and m is the mass of the film.

The mass of the film can be obtained using

$$m = CV, \tag{3.2}$$

where C is the concentration of the dye and V is the volume drawn with the micropipette.

3.3 Eutectic Gallium-Indium

Eutectic Gallium-Indium (EGaIn is a mixture of gallium (Ga) and indium (In), typically 75% Ga, 25% In by weight. The melting point is 15.5 ^{0}C, EGaIn is electrically conductive. The resistivity of EGaIn is ~24.4×10^{-6} Ω-cm;[4,5] this property allows EGaIn to be used as a contact electrode for the electrical characterization of thinfilm organic and semiconductor devices. The work function is about (4.1- 4.2)eV [29,30].

3.4 Rotating Polarizer Analyzer Ellipsometry

Ellipsometry is a well known accurate technique used to determine the optical properties of materials such as refractive index and thickness of a thin film. An ellipsometer usually consists of a source of light, polarizer, analyzer and detector as shown in Fig. 3.3 and Fig 3.4. Ellipsometry is a technique that measures the change in the state of light polarization upon reflected/transmitted from a sample. The mechanism of ellipsometry is that, incident unpolarized light passes through a polarizer, that linearly polarizes the light with two electrical field components E_p and E_s parallel and perpendicular to the plane of incidence respectively. The light then impinges a sample. The reflected light changes its polarization and becomes elliptically polarized, and then the light passes through an analyzer and becomes linearly polarized again.

An ellipsometric measurement allows one to quantify the phase difference between $\mathbf{E}_p$ and $\mathbf{E}_s$, and Δ, the change in the ratio of their amplitudes given by $\tan\psi$. For a reflecting surface, the forms of Δ and ψ are

$$\Delta = \delta_p - \delta_s \text{ and } \tan\psi = \frac{|r_p|}{|r_s|}, \tag{3.3}$$

where δ_p and δ_s are the phase changes for the *p* and *s* components of light and r_p and r_s are the complex Fresnel reflection coefficients for the *p* and *s* components which may be written as [5]

$$\left.\begin{aligned} r_p &= \rho_p e^{i\delta_p} \\ r_s &= \rho_s e^{i\delta_s} \end{aligned}\right\}. \tag{3.4}$$

Ellipsometry allows for the determination of the complex reflectance ratio ρ of a surface. This quantity is defined as the ratio of *p* and *s* reflection coefficients, r_p and r_s respectively. Commonly, the reflectance ratio is expressed in terms of ψ and Δ as [5]

$$\rho = \frac{r_p}{r_s} = \tan(\psi) e^{i\Delta}, \tag{3.5}$$

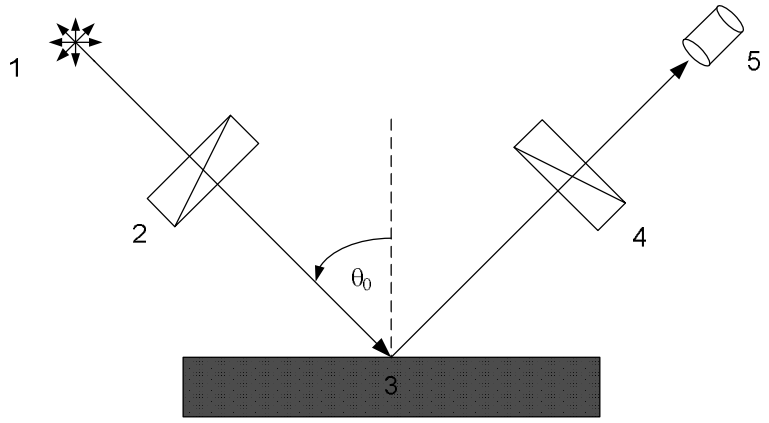

Figure 3.3 A simplified schematic diagram of the rotating polarizer analyzer ellipsometer, (1) unpolarized light, (2) linear polarizer, (3) sample, (4) linear analyzer, and (5) detector.

A homemade rotating polarizer and analyzer spectroscopic is used to characterize some samples. In this system, the polarizer and the analyzer rotate in same directions with the same angular speed. The transmission axes of the two elements are rotated using microstepping motors. Commercial software for thin film analysis (TFCompanion-optical metrology software) obtained from Semiconsoft,Inc is used to

analyze the experimental results. The results reveal a high accuracy device for thin film characterization.

3.4.1 Mathematical treatment

A well-collimated beam of monochromatic unpolarized light is assumed to emerge through a fixed polarizer, a rotating polarizer, then is reflected from a sample, and finally is collected by a detector through the projection of a rotating analyzer. The intensity received by the detector can be written as [31,32]

$$I(t) = I_0[1 + a_1 \cos 2\omega t + a_2 \cos 4\omega t + a_3 \cos 6\omega t], \tag{3.6}$$

where I_0 is the average irradiance and ω is the mechanical angular speed of the rotating elements. The coefficients a_1, a_2, a_3, are the Fourier coefficients. The ellipsometric parameters ψ and Δ can be obtained using the Fourier coefficients as follows

$$\tan\psi = \frac{\sqrt{a_1 + a_3}}{\sqrt{a_1 - 4a_2 + 9a_3}}, \tag{3.7}$$

$$\cos\Delta = \frac{-3a_3 + a_1 - 2a_2}{\sqrt{(a_1 + a_3)(a_1 - 4a_2 + 9a_3)}}. \tag{3.8}$$

3.5 Measurement of the DC Electrical Conductivity

The voltage-current signals were applied and recorded through NI USB-6251 data acquisition card, which is a high speed, multifunction analog/digital I/O expansion board that turns a host computer into accurate data-acquisition and signa1-analysis instrument. This card is used to control and measure the voltage across the sample, and the current passing through it as well as to record the photocurrent. The output from the card was amplified in order to extend the range of applied potential from -30 to 30 volt. Figure 3.5 shows the experimental setup used in the measurements.

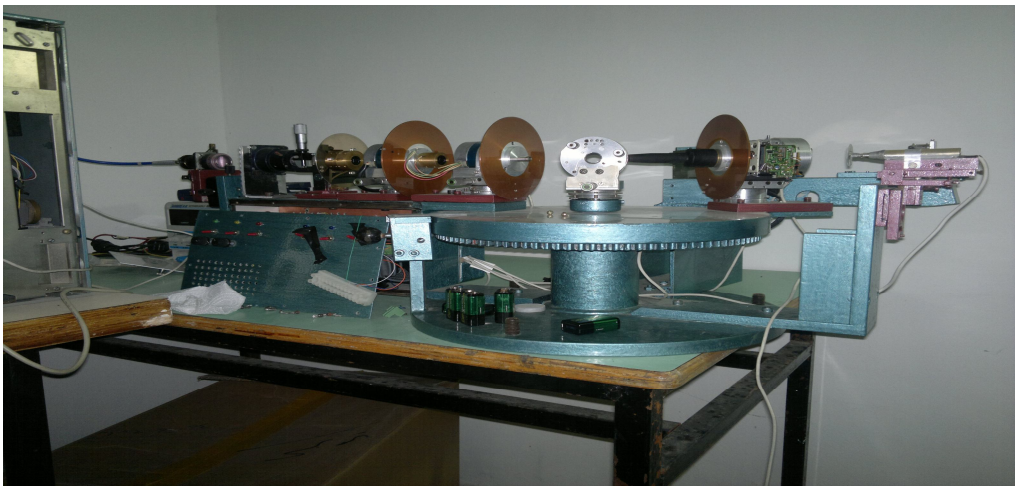

Figure 3.4 Photo image of an ellipsometry.

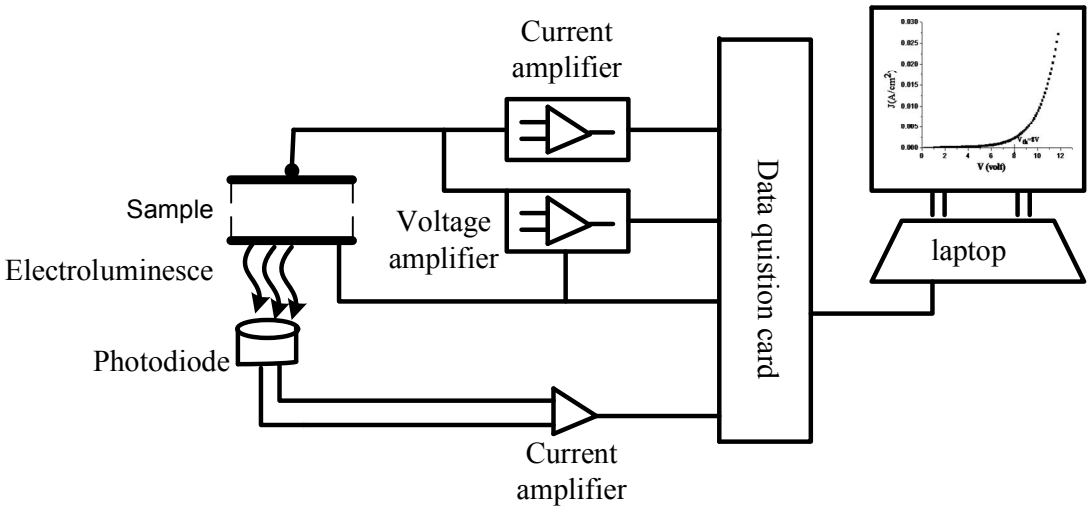

Figure 3.5 The experimental setup used in measurements

CHPTER FOUR
DOUBLE LAYER DEVICES

4.1 Introduction

In this chapter, the procedure of preparing double layer devices and the measurements done on them will be described. The device under consideration has the structure ITO/PVK/dye/InGa. Devices with different thicknesses of PVK layers and different dyes will be studied. The J-V characteristic curves will be investigated. Electroluminesce will be studied with the applied voltage. Morever, conduction mechanisms are also investigated and explained. The results were taken at room temperature and analyzed and plotted by using Origin 8.0 program. Finally, ellipsometry measurements that extract the optical parameters of thin films and their thickness will be reported.

4.2 Film Preparation

4.2.1 Substrate Cleaning

The substrate is indium tin oxide (ITO) coated glass sheet with dimension 7.5cm × 2.5 cm. Each sheet was cut by diamond scribe to smaller pieces of dimensions 2.5 cm × 2.5 cm. The ITO substrates were cleaned drops of acetone on the surface of the sample and then wiping with lens paper. The ITO substrate then rinsed by isoprobanol alcohol and dried in an oven at a temperature of 60 ^{0}C.

4.2.2 Sample Structure

The first group of samples were prepared in this study is double layer samples with the general structure ITO/ PVK/dye/ InGa as shown in Fig. 4.1. Three dyes were used namely Rhodamine B, crystal violet, and Bromophenol blue. Table 4.1 shows molecular formula, melting point, and molecular structure of each dye. Each dye was deposited on four different thicknesses of PVK layers. All samples are listed in table 4.2.

Table 4.1 Molecular formula, melting point, and molecular structure of the three dyes.

Deys	Molecular formula	Melting point	Molecular structures
Rhodamine B	$C_{28}H_{31}ClN_2O_3$	210 - 211 °C	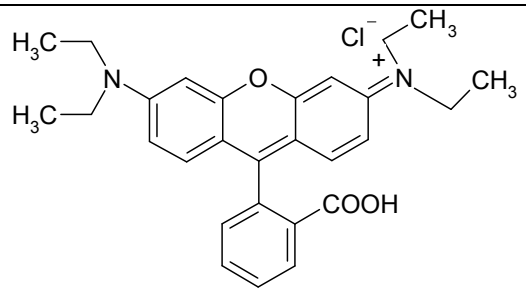
Crystal violet	$C_{25}N_3H_{30}Cl$	205 °C	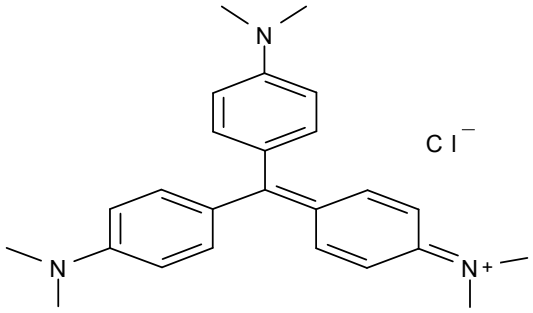
Bromophenol blue	$C_{19}H_{10}Br_4O_5S$	272 - 273 °C	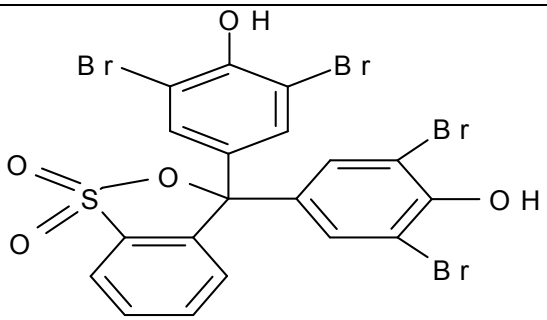

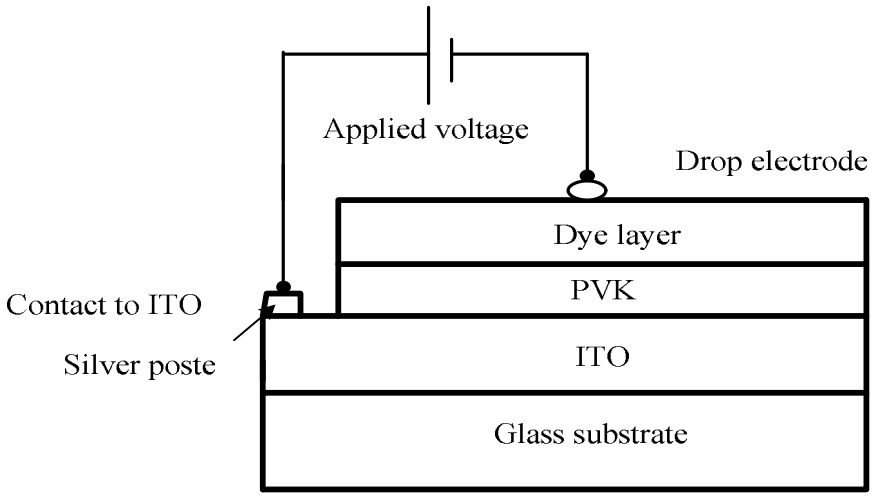

(a)

(b)

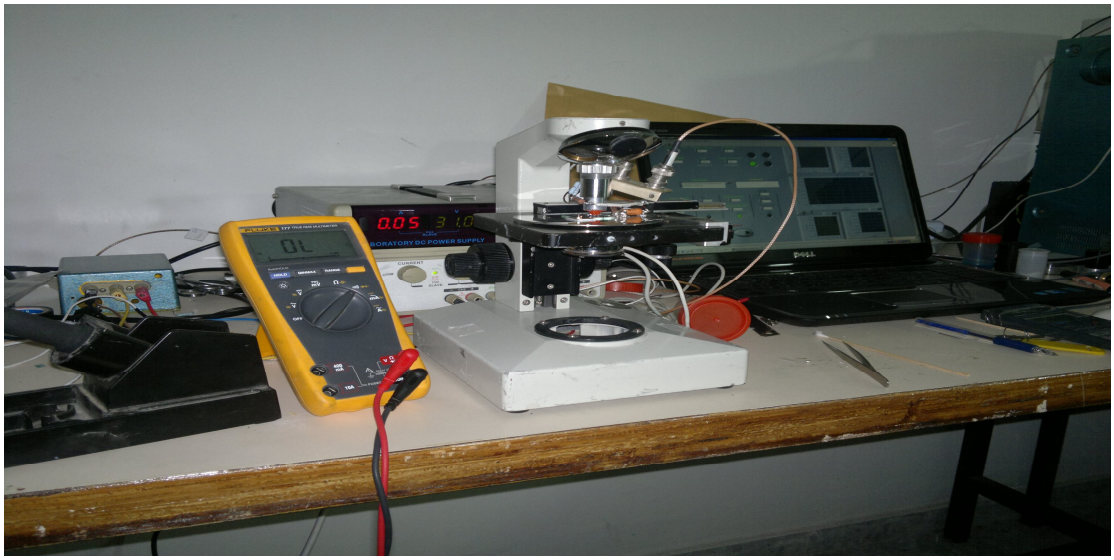

(c)

Figure 4.1 (a) Schematic drawing of a double layer sample, (b) photo image of samples and, (c) photo image of the experimental setup.

4.3 Thickness and Rfractive Index Mesurments

The thickness and refractive index were measured using a homemade variableangle ellipsometr. The data were taken at room temperature with an angle of incidence equal to 70 °. The data were analyzed and plotted by using TFCompanion program. TFCompanion is a powerful software for thin film analysis and metrology applications. Four samples have been studied. The samples are thin PVK films deposited on Silicon (Si) substrate which is illustrated in table 4.2. Fig. 4.2 through Fig. 4.5 show the ellipsometry spectra obtained with the ellipsometer for S1,S2,S3 and S4. Discrete Fourier analysis was performed to deduce the normalized Fourier coefficients for each photon energy and then the ellipsometric parameters (ψ and Δ) were obtained using Eqs. (3.7) and (3.8). Thickness and the refractive index of the samples were extracted using TFCompanion software. Solid lines in Figs. 4.2 (a,b)-4.5 (a,b) represent the calculated ellipsometric parameters using Eqs. (3.7) and (3.8) whereas circles represent the experimental data in the range 300 nm to 800 nm. The measured thickness obtained from TFCompanion software was 35.33±0.00068 nm for S1, 44.3±0.444 nm for S2, 94.48±0.745 nm for S3 and 198±4.091 nm for S4. Moreover, the spectroscopic measurements of the refractive index of the PVK films in the spectral range 300 nm to 800 nm are shown in Figs. 4.2. (c)-4.5 (c) for S1, S2,S3 and S4, respectively. As can be seen from the figures, at λ_{20}^{D} =589.3 nm, the measured index was 1.71 with percent error1.1% for S1, 1.674 with percent error of 0.9% for S2, 1.683 with a percent error of 0. 5% for S3 and 1.673 with a percent error of 0. 4% for S4 [5,32].

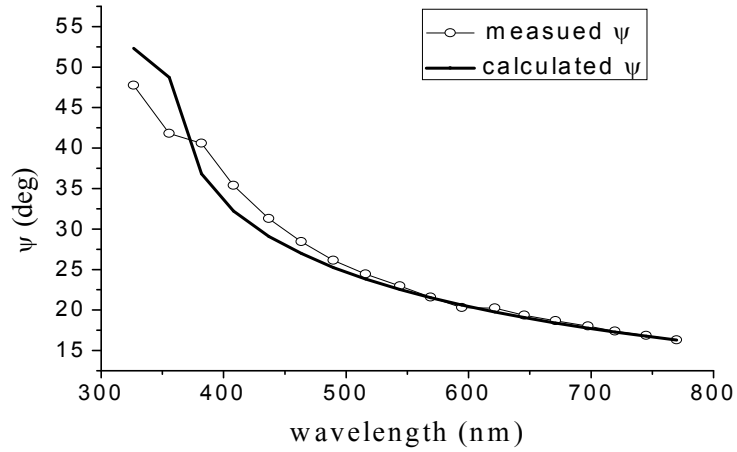

(a)

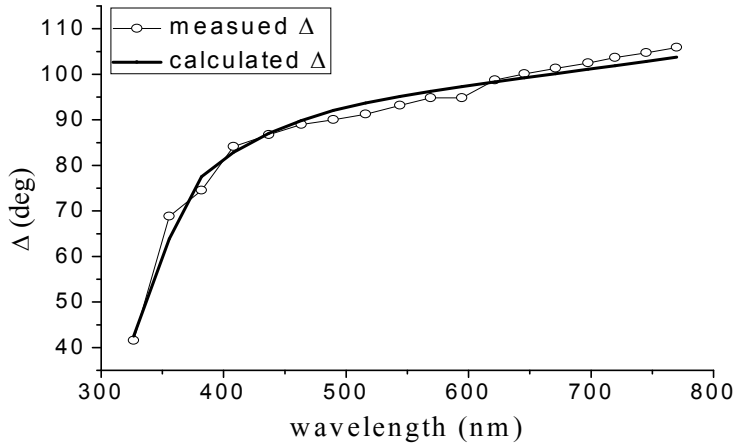

(b)

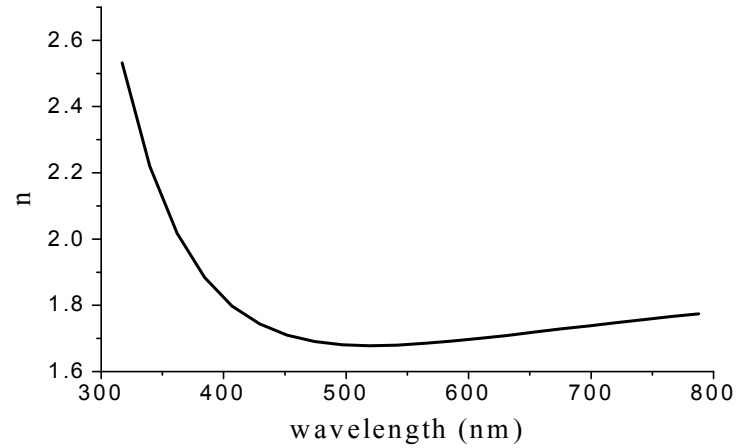

(c)

Figure 4.2 Psi, delta, and refractive index of PVK thin film on silicon wafer for S1 as a function of wavelength.

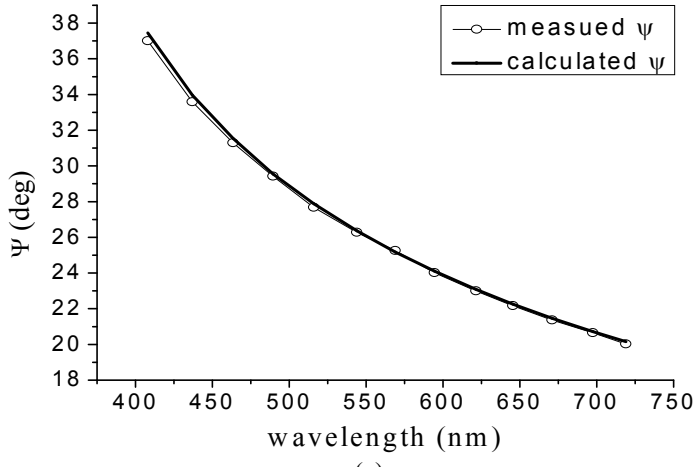

(a)

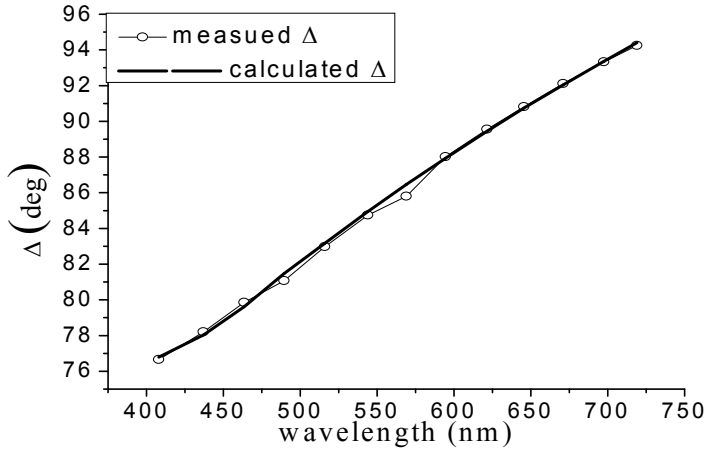

(b)

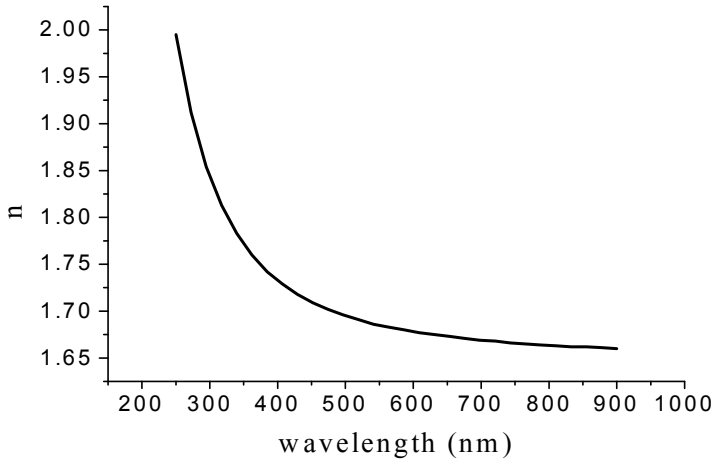

(c)

Figure 4.3 Psi, delta, and refractive index of PVK thin film on silicon wafer for S2 as a function of wavelength.

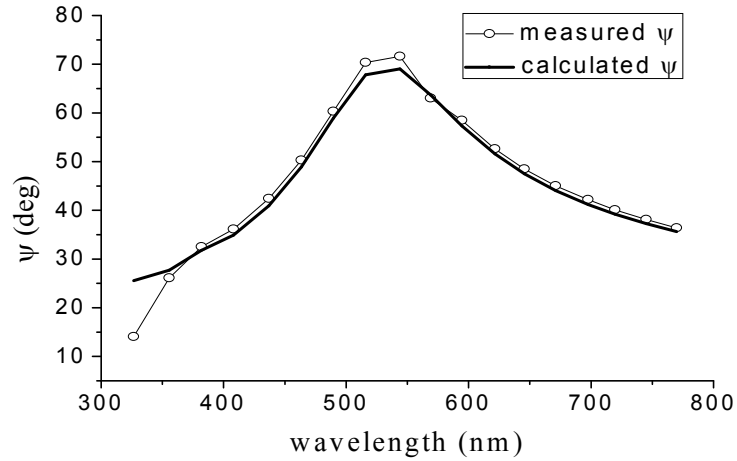

(a)

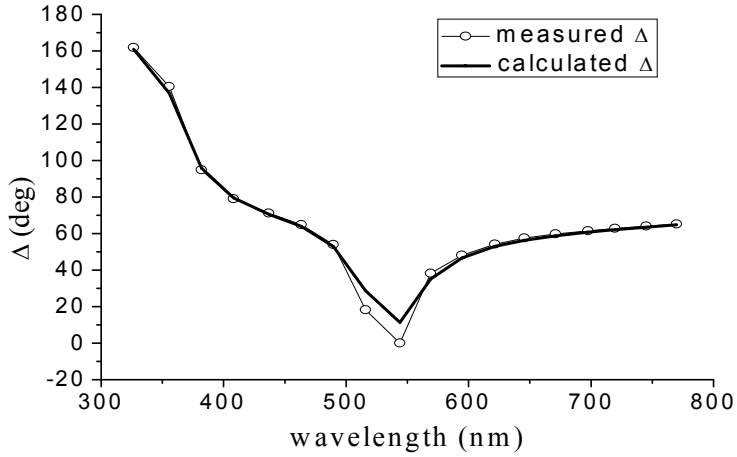

(b)

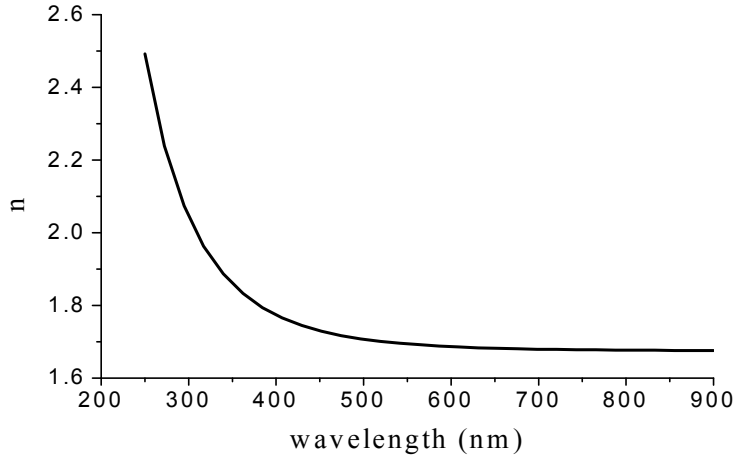

(c)

Figure 4.4 Psi, Delta and Refractive index of PVK thin film on silicon wafer for S3 as a function of wavelength.

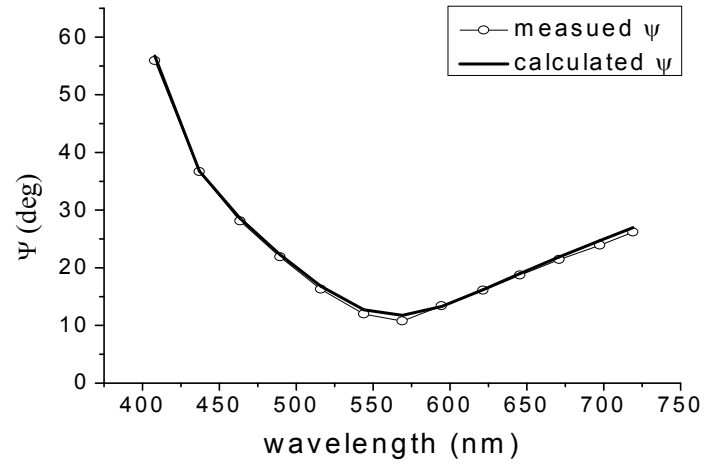

(a)

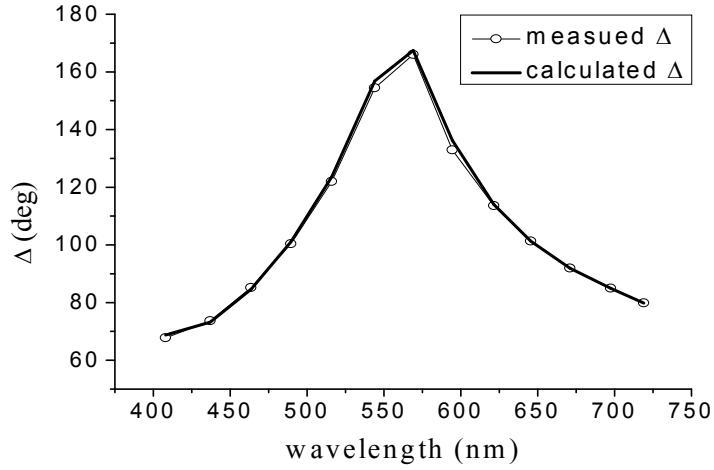

(b)

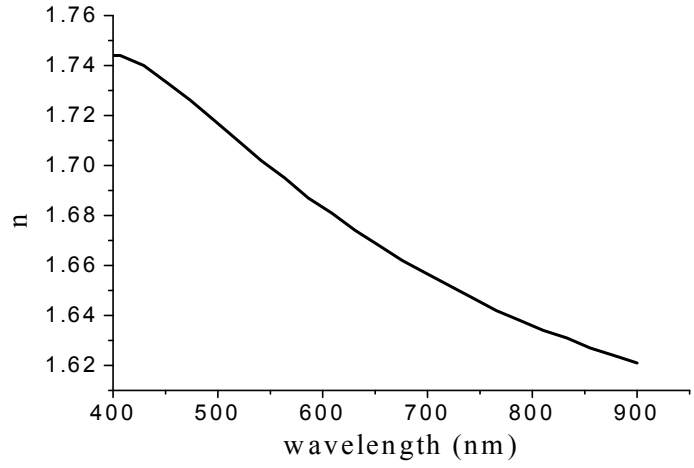

(c)

Figure 4.5 Psi, delta and refractive index of PVK thin film on silicon wafer for S4 as a function of wavelength.

Table 4.2 The structure of double layer device.

Group No.	Structure	Sample No.	Thickness of PVK (nm)	Thickness of dye (nm)
G_1	ITO/PVK/Rhodamine B /InGa	G_1S_1 G_1S_2 G_1S_3 G_1S_4	35.33 44.30 94.48 198	50
G_2	ITO/PVK/crystal violet/InGa	G_2S_1 G_2S_2 G_2S_3 G_2S_4	35.33 44.30 94.48 198	50
G_3	ITO/PVK/ Bromophenol blue/ InGa	G_3S_1 G_3S_2 G_3S_3 G_3S_4	35.33 44.30 94.48 198	50

4.4 Experimental Procedure

As mentioned above, the double layer device has the structure ITO/PVK/Dye/InGa. The PVK powder with an average molecular weight of 11×10^5 was weighted using a sensitive electrical balance (ESJ182-4) with a resolution of 10^{-4} gm. The PVK was dissolved in a proper amount of mixed solvents such as toluene and tetrahydrofuran THF as shown in table 4.3. A homogenous solution was then obtained. To construct a single layer of PVK thin film, a known amount of the solution was placed on the cleaned ITO substrate. Inclined coating method was used to form the film. The film thickness was increased by increasing the concentration of the PVK. A proper amount of dye was weighted and dissolved in methyl alcohol. The 50nm thickness of dye is then deposited on the PVK layer by spin coating technique by dropping few drops of the dye solution and operating the spin coater spun at 2000 rpm for one minute. Then, the sample was placed in an oven and heated at 60 ^{0}C. A drop of InGa was used as cathode.

Table 4.3: Different weights of the PVK polymer used to construct the PVK layer.

Sample No.	polymer	Weight	Solvents	Thickness(nm)
S1	PVK	10 mg	5 ml THF+1 ml toluene	35.33
S2	PVK	15 mg	5 ml THF+1 ml toluene	44.30
S3	PVK	20 mg	5 ml THF+1 ml toluene	94.48
S4	PVK	30 mg	5 ml THF+1 ml toluene	198

4.5 Results and Discussions

In this section, the expremintal results obtained for all fabricated devices are presented. These results include the current-voltage characteristics, current-voltage relation in logarithmic scale, and relative light intensity with the applied voltage and the current. Twelve samples have been studied. The InGa electrode was negatively biased whereas the transparent electrode ITO was positivley biased. All samples are biased over the range of voltages from 0 to 16 volt. Electrical measurment were carried out at room teperature. The driving voltage and the resulting current were obtained and measured using NI USB-6251 data acquisition card interfaced with a laptop. The relative intensity was measured using a photodiode. The output of the photodiode was amplified and the collected by the same data acquistion card. Fig. 4.6 through 4.17 show the various characterstics of the fabricated twelve samples.

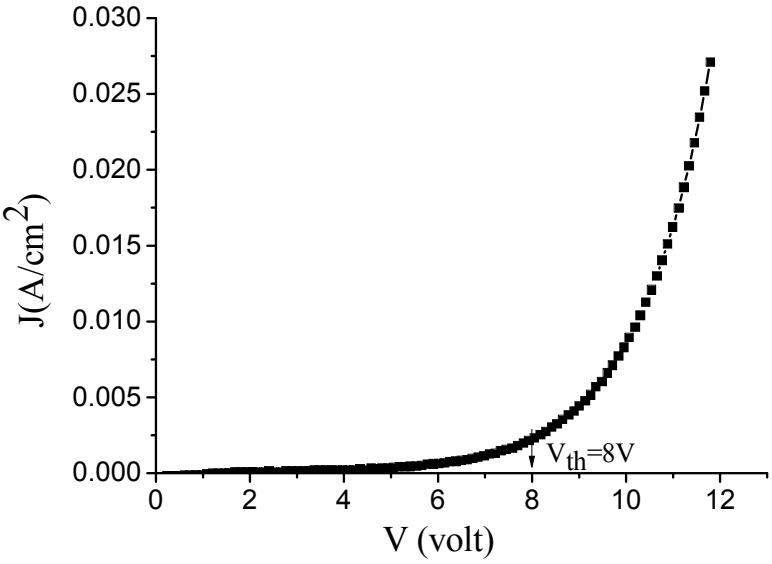
0.030
0.025
0.020
0.015
0.010
0.005
0.000
J(A/cm2)
0
2
4
6
8
10
12
V (volt)
Vth=8V

(a)

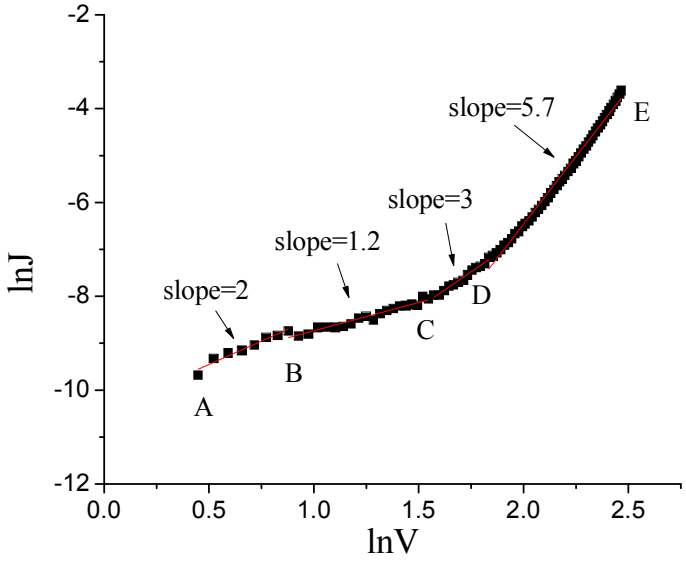
-2
-4
-6
-8
-10
-12
lnJ
0.0
0.5
1.0
1.5
2.0
2.5
lnV
slope=2
slope=1.2
slope=3
slope=5.7
A
B
C
D
E

(b)

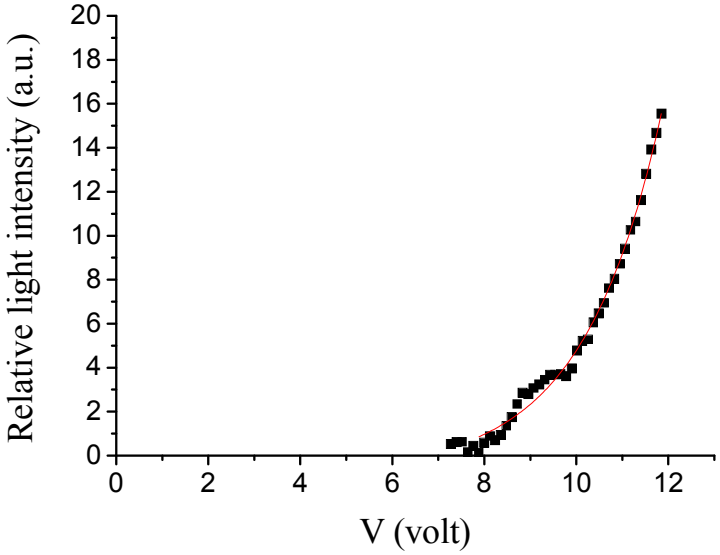

(c)

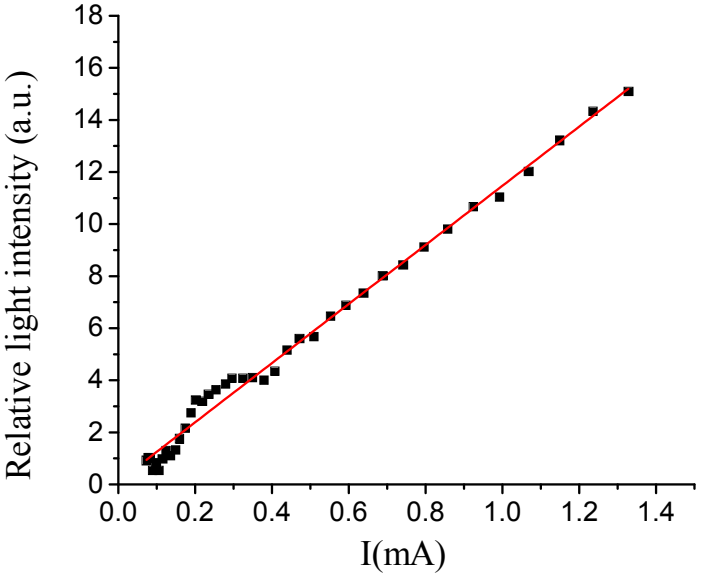

(d)

Figure 4.6 Four characteristics curves of ITO/35.33nm PVK/50nm Rhodamine B /InGa device, (a) current density- voltage characteristics, (b) lnJ-lnV characteristics, (c) relative light intensity-voltage characteristics, and (d) relative light intensity-current characteristics.

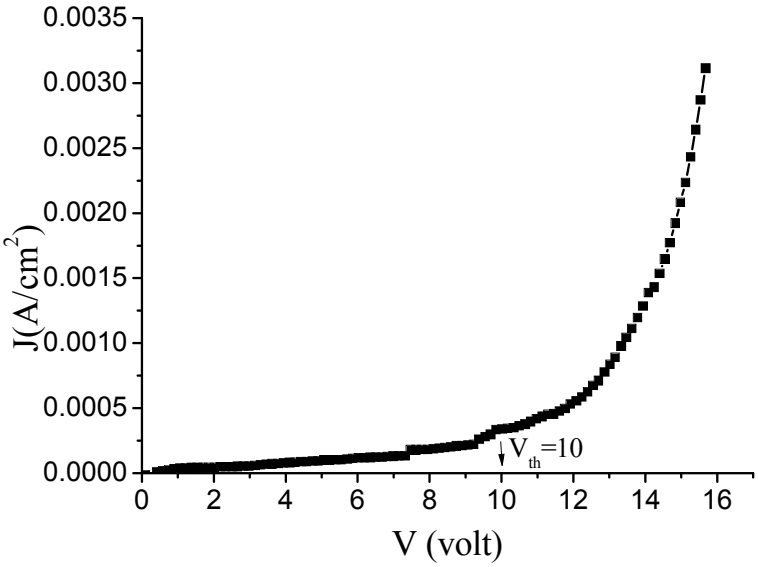
0.0035
0.0030
0.0025
0.0020
0.0015
0.0010
0.0005
0.0000
J(A/cm2)
Vth=10
0
2
4
6
8
10
12
14
16
V (volt)

(a)

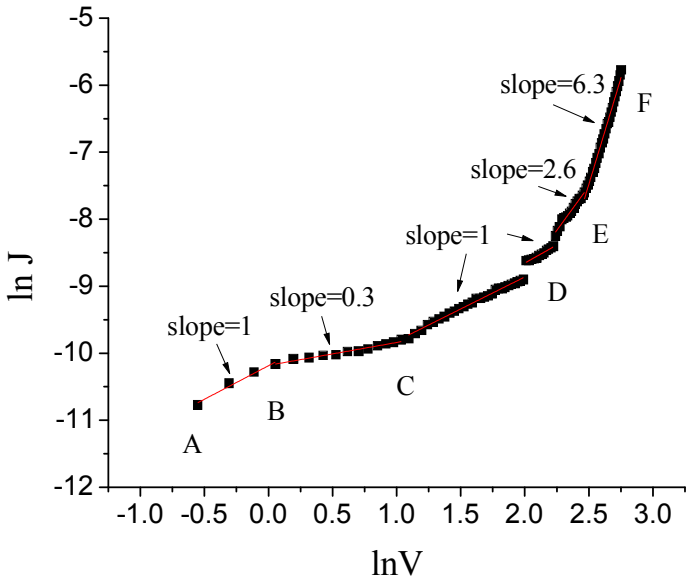
-5
-6
-7
-8
-9
-10
-11
-12
ln J
slope=6.3
F
slope=2.6
slope=1
E
D
slope=0.3
slope=1
C
B
A
-1.0
-0.5
0.0
0.5
1.0
1.5
2.0
2.5
3.0
lnV

(b)

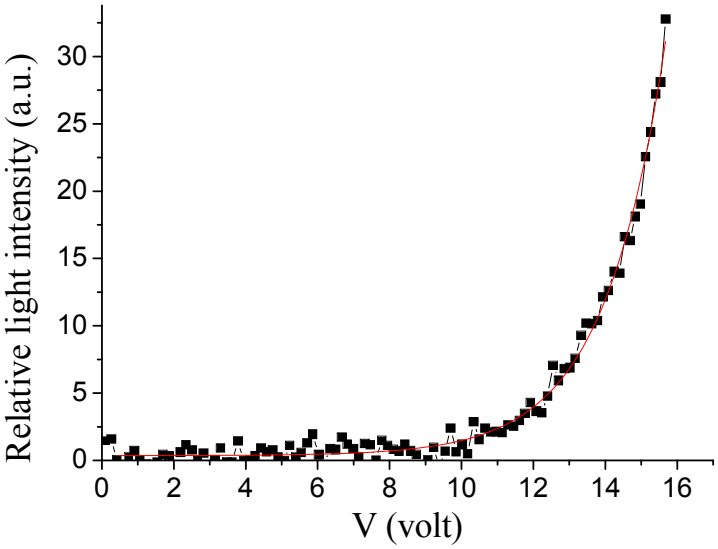

(c)

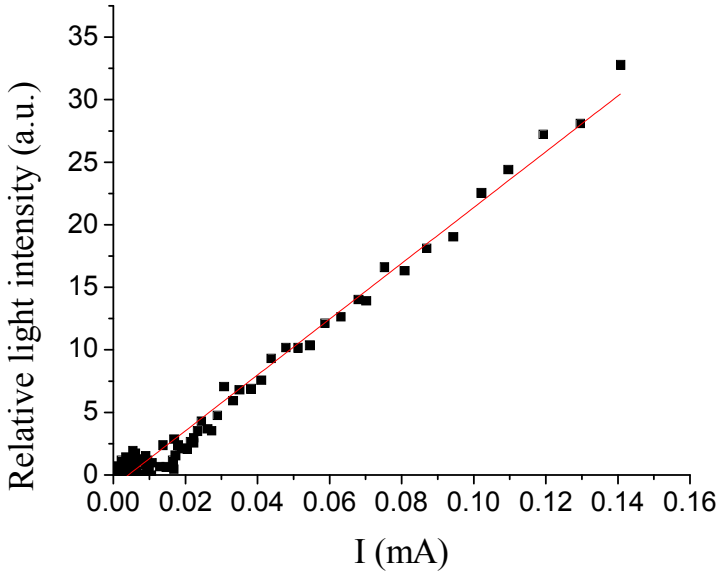

(d)

Figure 4.7 Four characteristics curves of ITO/44.3nm PVK/50nm Rhodamine B /InGa device, (a) current density- voltage characteristics, (b) lnJ-lnV characteristics, (c) relative light intensity-voltage characteristics, and (d) relative light intensity-current characteristics.

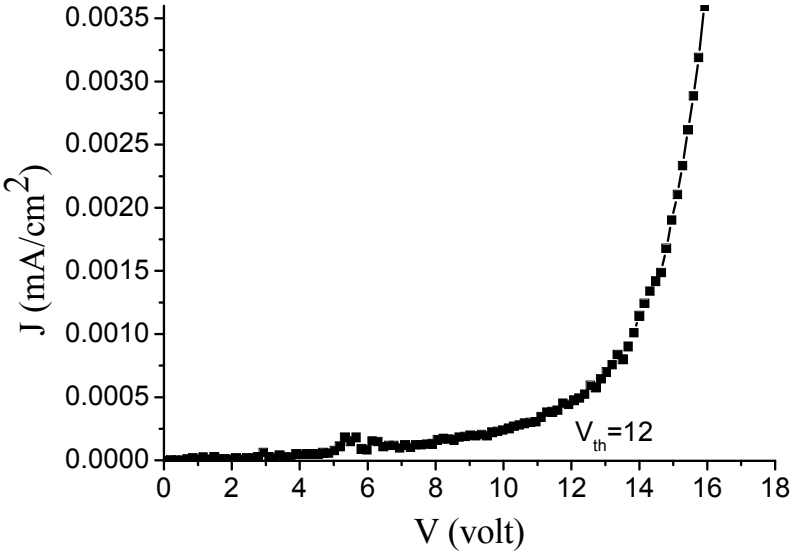

(a)

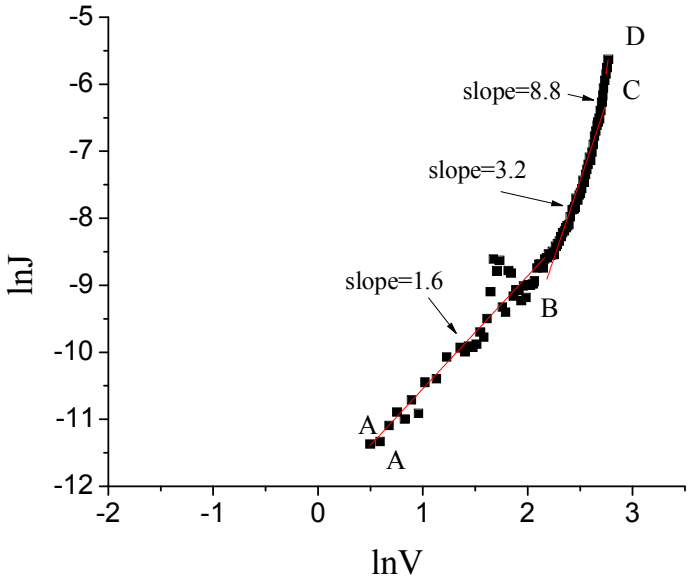

(b)

Figure 4.8 Two characteristics curves of ITO/94.48nm PVK/50nm Rhodamine B /InGa device, (a) current density- voltage characteristics and, (b) lnJ-lnV characteristics.

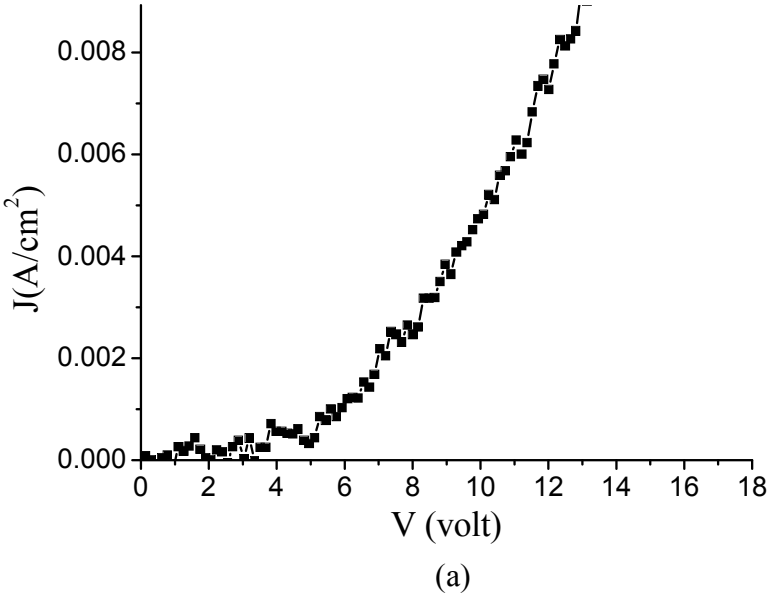

(a)

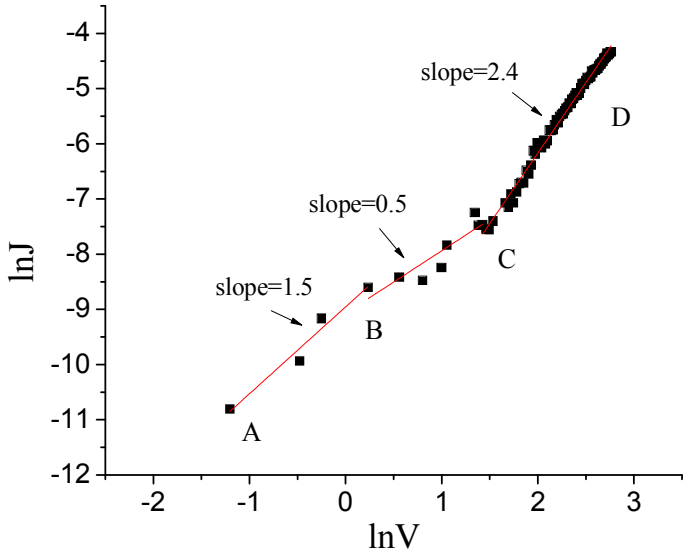

Figure 4.9 Two characteristics curves of ITO/198nm PVK/50nm Rhodamine B /InGa device, (a) current density- voltage characteristics and, (b) lnJ-lnV characteristics.

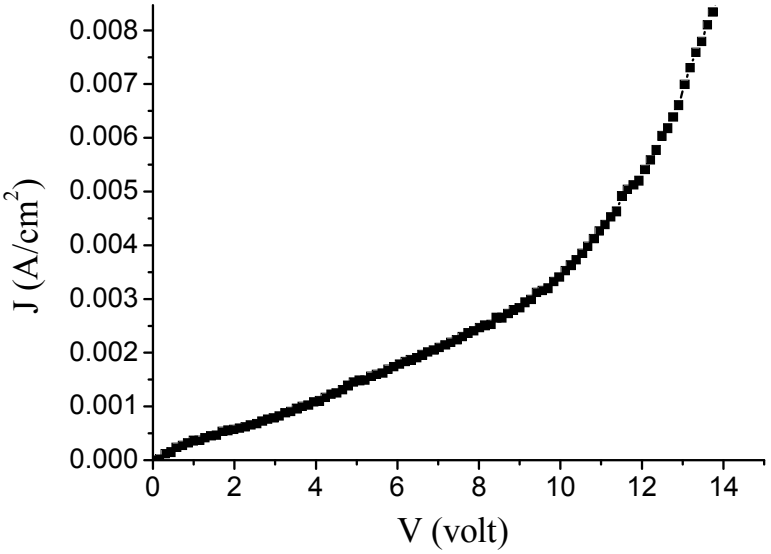

(a)

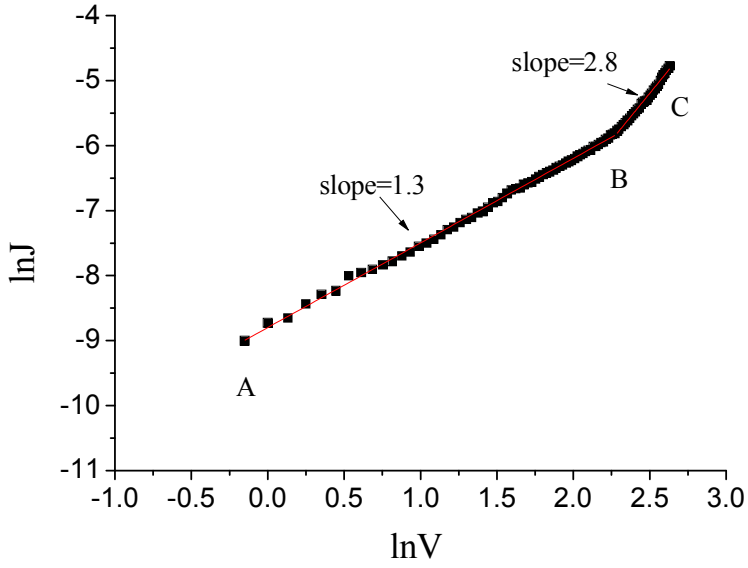

(b)

Figure 4.10 Two characteristics curves of ITO/35.33nm PVK/50nm crystal violet /InGa device, (a) current density- voltage characteristics and, (b) lnJ-lnV characteristics.

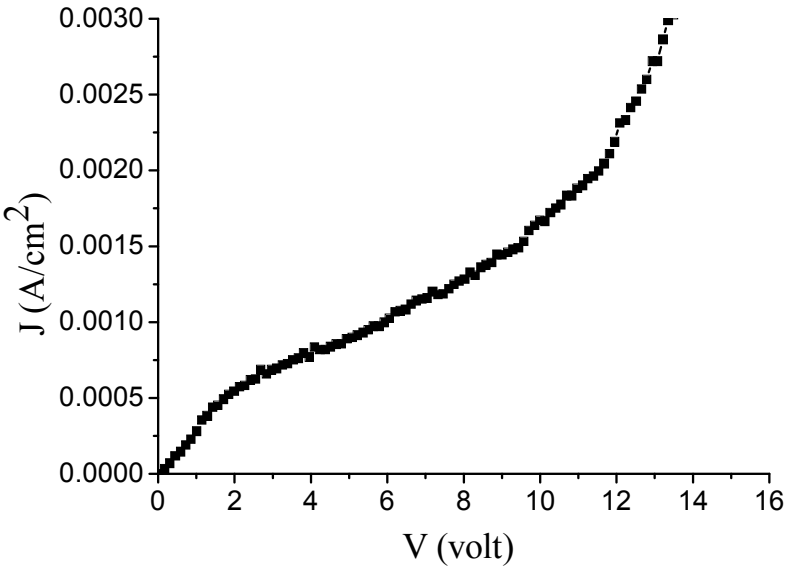

(a)

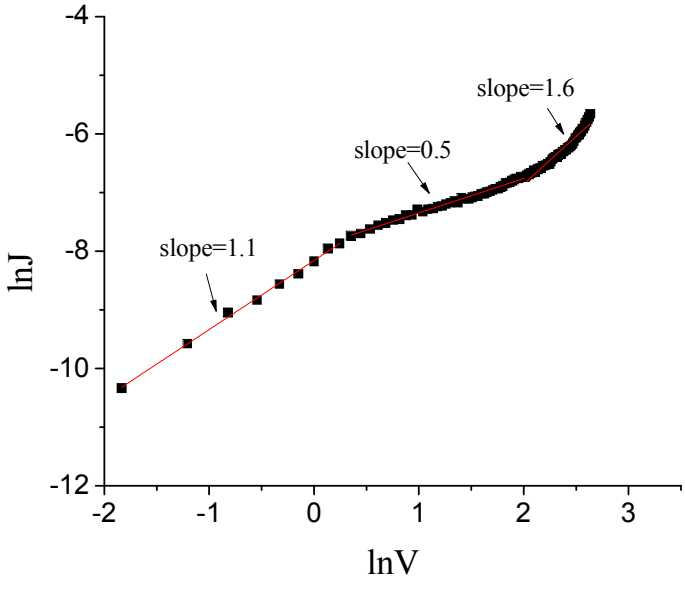

(b)

Figure 4.11 Two characteristics curves of ITO/44.3nm PVK/50nm crystal violet /InGa device, (a) current density- voltage characteristics and, (b) lnJ-lnV characteristics.

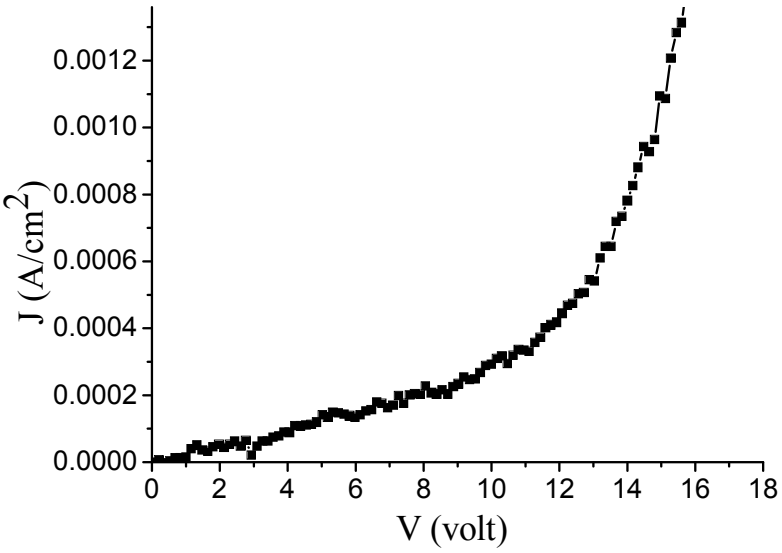

(a)

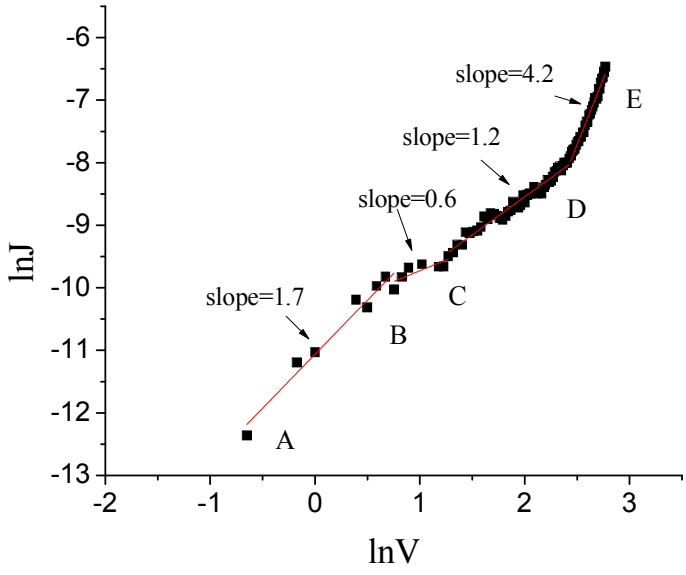

(a)

Figure 4.12 Two characteristics curves of ITO/94.48nm PVK/50nm crystal violet /InGa device, (a) current density- voltage characteristics and, (b) lnJ-lnV characteristics.

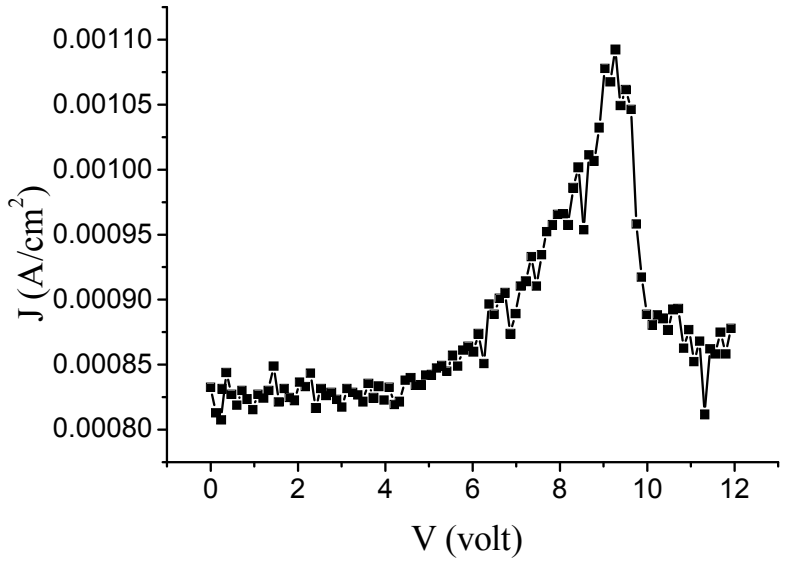

(a)

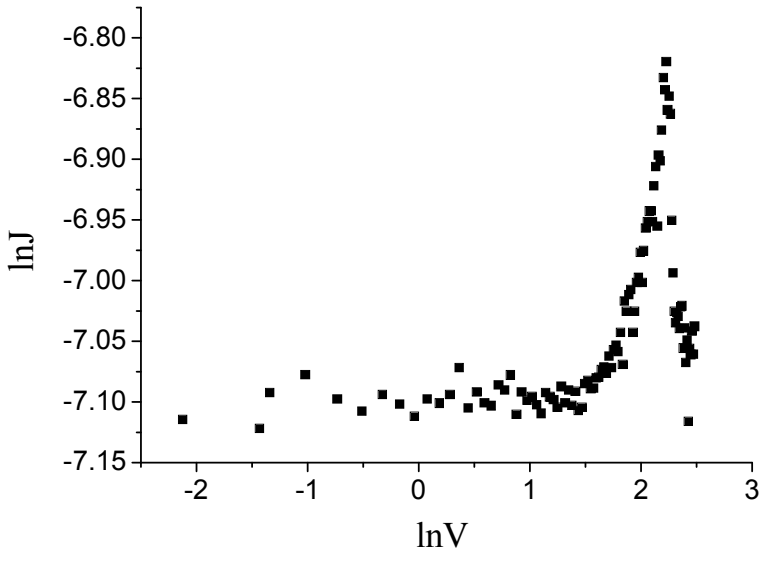

(b)

Figure 4.13 Two characteristics curves of ITO/198nm PVK/50nm crystal violet /InGa device, (a) current density- voltage characteristics and, (b) lnJ-lnV characteristics.

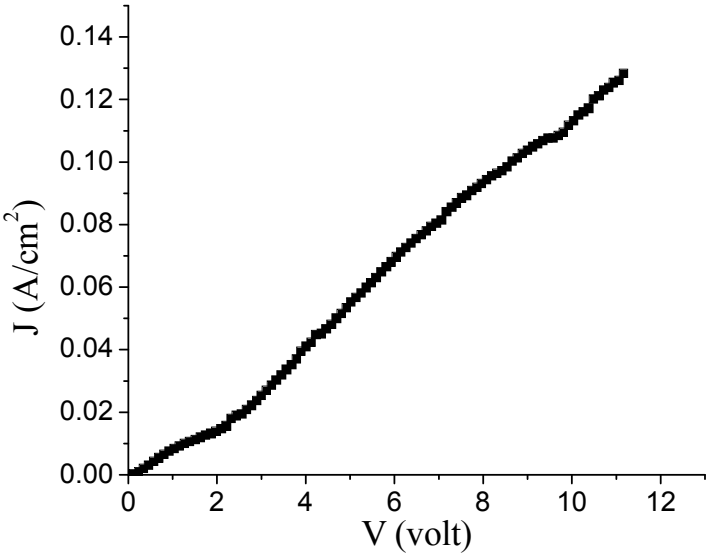

(a)

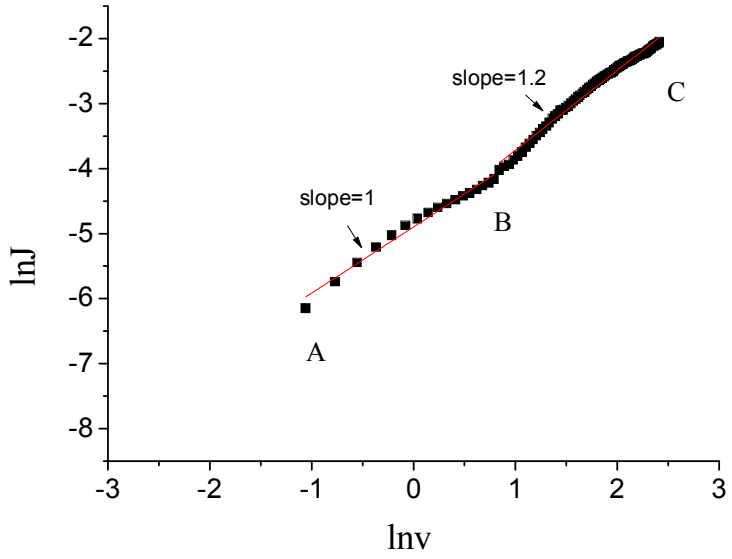

(b)

Figure 4.14 Two characteristics curves of ITO/35.33nm PVK/50nm Bromophenol blue /InGa device, (a) current density- voltage characteristics and, (b) lnJ-lnV characteristics.

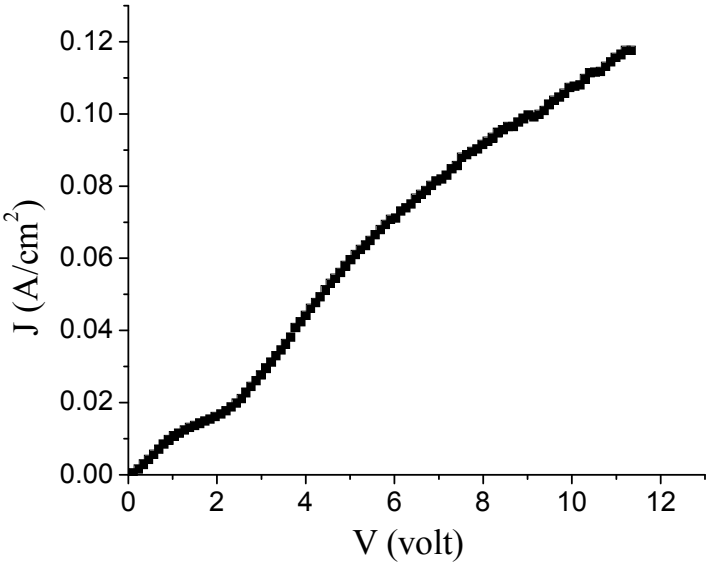

(a)

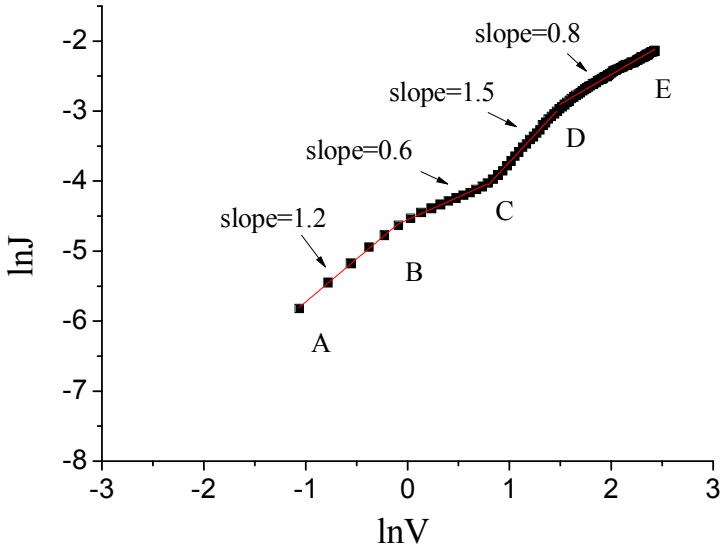

(b)

Figure 4.15 Two characteristics curves of ITO/44.3nm PVK/50nm Bromophenol blue /InGa device, (a) current density- voltage characteristics and, (b) lnJ-lnV characteristics.

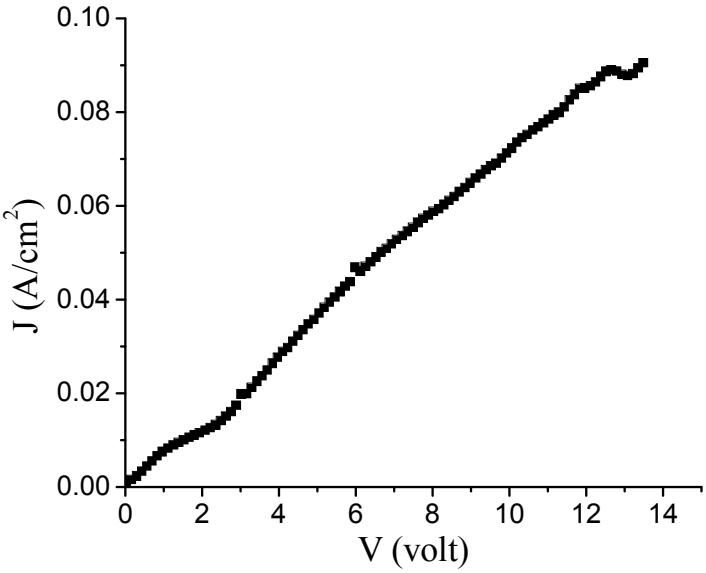

(a)

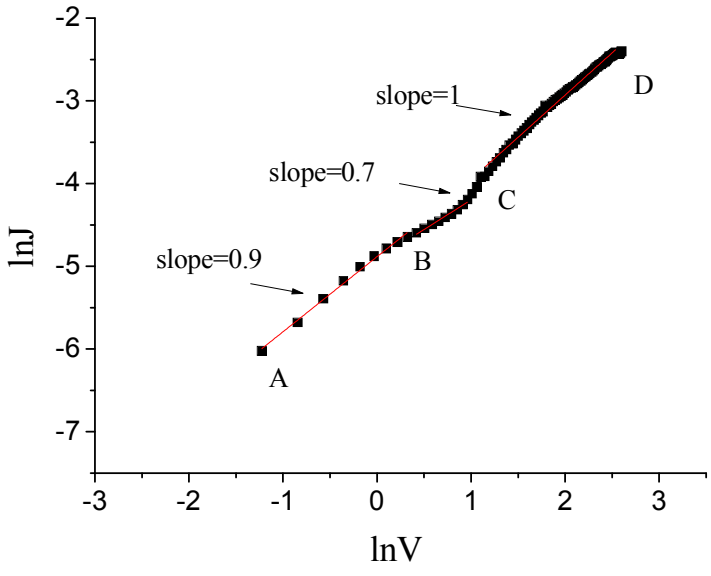

(b)

Figure 4.16 Two characteristics curves of ITO/94.48nm PVK/50nm Bromophenol blue /InGa device, (a) current density- voltage characteristics and, (b) lnJ-lnV characteristics.

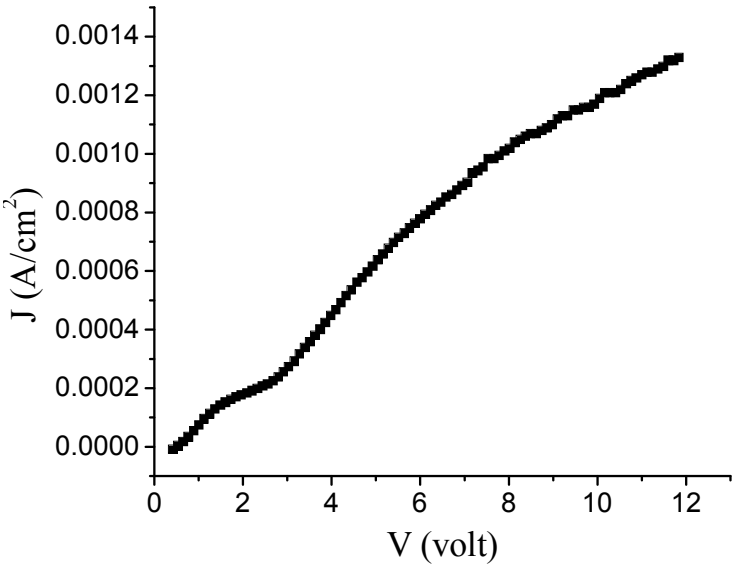

(a)

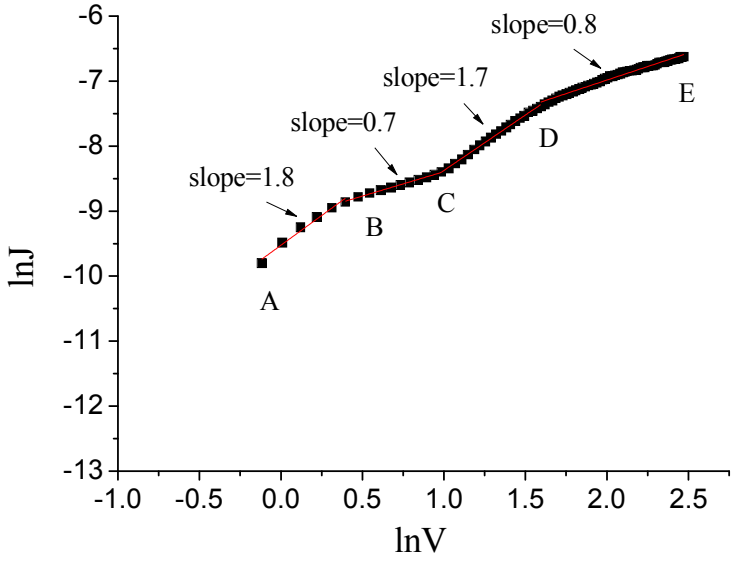

(b)

Figure 4.17 Two characteristics curves of ITO/198nm PVK/50nm Bromophenol blue /InGa device, (a) current density- voltage characteristics and, (b) lnJ-lnV characteristics.

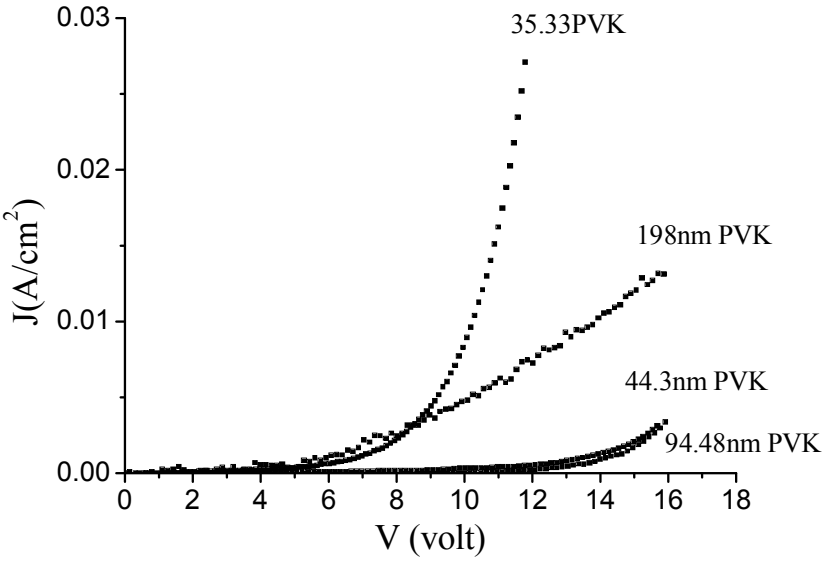

Figure 4.18 J-V curves of all samples of ITO/PVK/50nm Rhodamine B/InGa.

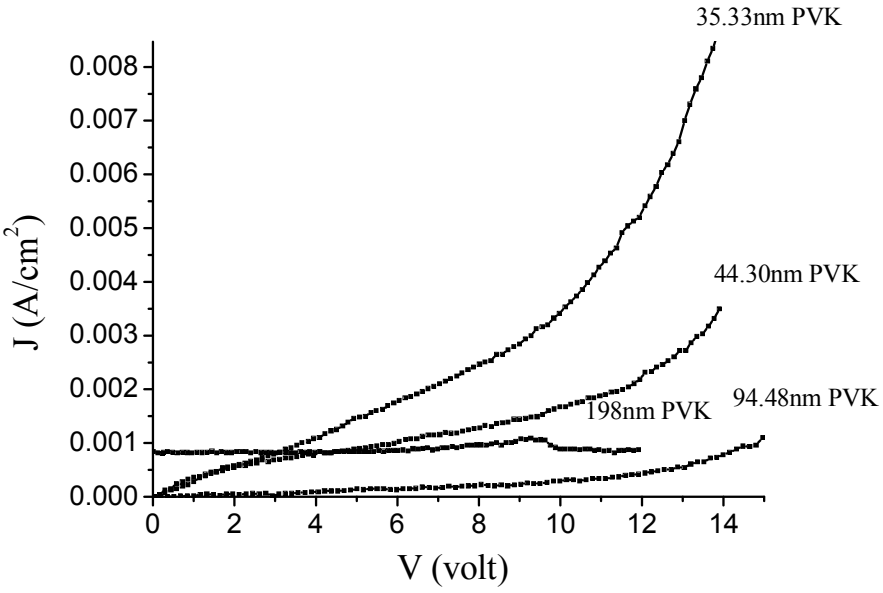

Figure 4.19 J-V curves of all samples of ITO/PVK/50nm crystal violet/InGa.

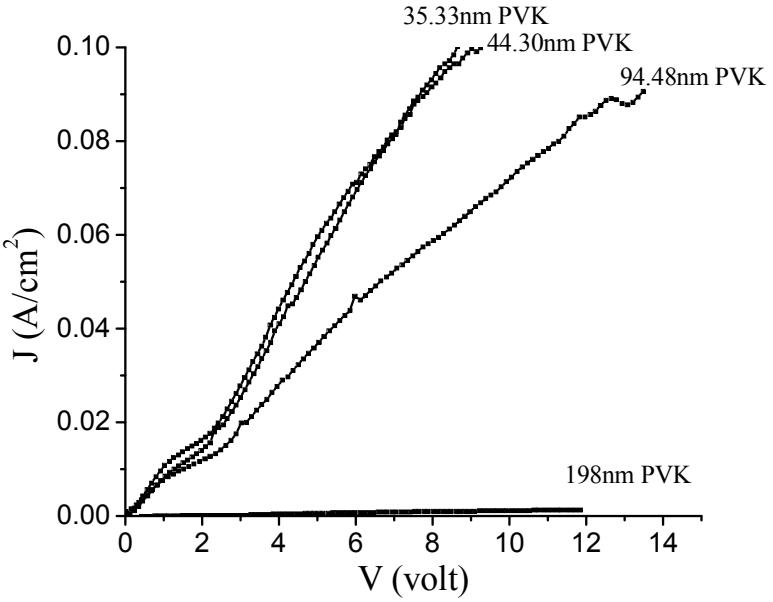

Figure 4.20 J-V curves of all samples of ITO/PVK/50nm Bromophenol blue/InGa.

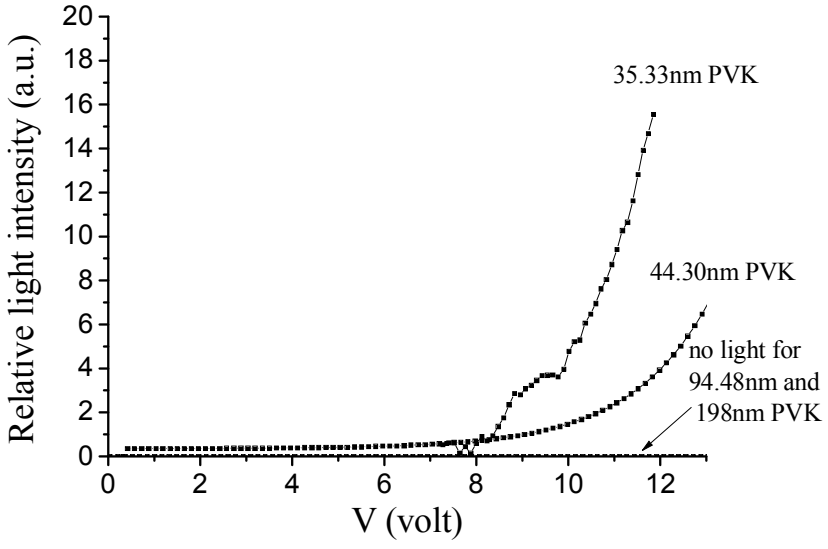

Figure 4.21 Relative light intensity-voltage characteristics of ITO/PVK/50nm Rhodamine B/InGa.

4.5.1 Current Density-Voltage Characteristic Curves

The J-V characteristic curves show nonlinearity for all groups except the group G3 where the four samples show semi-linear J-V characteristic curves. The J-V characteristics show an exponential increase of current with the applied voltage, which is similar to a typical diode characteristic curve. Under forward bias, the current density increases slowly with increasing voltage. At a certain voltage, the threshold voltage (Vth), the current density increases sharply.

The thershold voltage is a significant parameter characterizing the operation of organic light emitting diode (OLED). It is the voltage at which the OLED begings to emit light [5]. The threshold voltage can be estimated by estimated by the relative light intensity-voltage characteristics curve. These values are tabulated in table (4.4). The J-V relationship is increased exponentially for $G_1$and G_2 groups that is slow increase of current density at low applied voltages and sharp increase of current density at high applied voltage. For G_3 samples the sharp increase of current density at low applied voltage was observed which may refer to leakage current which is linearly dependent on the applied voltage. The leakage current is due to the movement of the free charge carriers of InGa inside the device toward the ITO electrode. To study the effect of increasing the thickness of the PVK layer, the J-V curves of all samples of group G_1 are shown together in Fig. 4.18 whereas for all samples of group G_2 in Fig. 4.19 and for all samples of group G_3 in Fig. 4.20. These figures show that, as the thickness increases the sample exhibit more resistance to the current flow through it and the current density decreases for the same voltage. Morever, the threshold voltage increases with increasing the thickness of the PVK layer.

Table 4.4: Experimental values of threshold voltage for G_1S_1 and G_2S_2.

sample	G_1S_1	G_1S_2
V_{th}	8 volt	10 volt

4.5.2 Relative Light Intensity with the Driving Voltage

Electroluminescence have been observed only in two samples (G_1S_1 and G_1S_2) of the first group (G_1). The variation of electroluminescence with the applied DC voltage is shown in Figs. 4.6 (c) and 4.7 (c) for the two samples. The two figures show clearly that no electroluminescence can be detected at low applied voltage. The samples start

emitting light when the V_{th} is reached and the luminunce increase gradually when the applied voltage exceeds V_{th}. Also the V_{th} for J-V characteristic is the same for relative light intensity with the applied voltage. The V_{th} for sample ITO/37nm PVK/50nm Rhodamine B /InGa is about 8 volt, and for ITO/50nm PVK/50nm Rhodamine B /InGa is about 10 volt, that is because the thickness of former is smaller than the latter sample. The light intensity decreases with increasing the thickness and no light is detected for thick PVK layer.

4.5.3 Relative Light Intensity with Increasing Current

Fig. 4.6 (d) and fig. 4.7 (d) illustrate the characteristic curves of electroluminescence versus current. The curves show linear relationships between electroluminescence and the current.

4.5.4 Energy Band Diagram

Figure 4.22 show the energy band diagram of the ITO/PVK/Rhodamine B/ InGa sample, and the information about the work function of the electrodes, and HOMO, LUMO of PVK and Rhodamine B. [5,29,30,33]

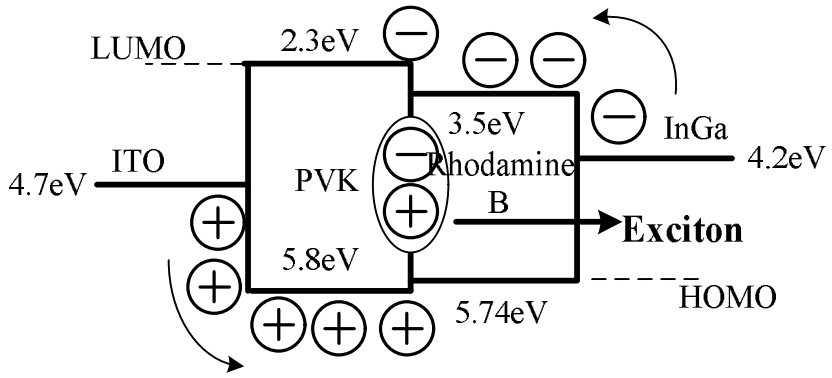

Figure 4.22: Mechanism of electroluminescence of a ITO/PVK /Rhodamine B/InGa device.

4.5.5 Conduction Mechanism

Fig. 4.6 (b) through fig. 4.17 (b) show the dependence of the current density J on the voltage V in the natural logarithmic scale. These curves exhibit non-linear relationship and divided it in two to four regions as AB, BC, CD and DE These different regions have different slopes which referred that the J-V relation (in the natural logarithmic scale) in type $J \propto V^s$ where s is the slope of the curve.

Table 4.5 Experimental values of slope for each region of lnJ-lnV characteristic curves.

sample	AB	BC	CD	DE
G_1S_1	2	1.2	3	5.7
G_1S_2	1	0.3	1	2.6
G_1S_3	1.6	3.2	8.8	-
G_1S_4	1.5	0.5	2.4	-
G_2S_1	1.3	2.8	-	-
G_2S_2	1.01	0.5	1.6	-
G_2S_3	1.7	0.6	1.2	4.2
G_2S_4	-	-	-	-
G_3S_1	1	1.2	-	-
G_3S_2	1.2	0.6	1.5	0.8
G_3S_3	0.9	0.7	1	
G_3S_4	1.8	0.7	1.7	-0.8

The region where the slope of lnJ-lnV curves is equal about 1, the region is be to said ohmic and the conduction. At the region where the slope equal 2, the conduction is SCL mechanism [5, 15, 21].

CHAPTER FIVE
SINGLE LAYER DEVICE

5.1 Introduction

This chapter presents the experimental technique of the devices with the structure ITO/blend of PVK and a dye /InGa. Dyes with different concentrations were used with PVK as ablend to form a film on ITO coates glass sheets. J-V characteristics curves, lnJ-lnV curves and the relative of light intensity versus voltage and current have been presented. Finally the conduction mechanisms will be discussed.

5.2 Sample Structure

The second set of samples is composed of ITO/ blend of PVK and a dye/InGa as shown in Fig. 5.1. Three dyes were used: crystal violet, Bromophenol blue and Fluorescein. Table 5.1 shows molecular formula, melting point, and molecular structure of Fluorescein. The PVK was doped with each dye to form a blend of polymer and dye. Table 5.2 lists the details of all samples.

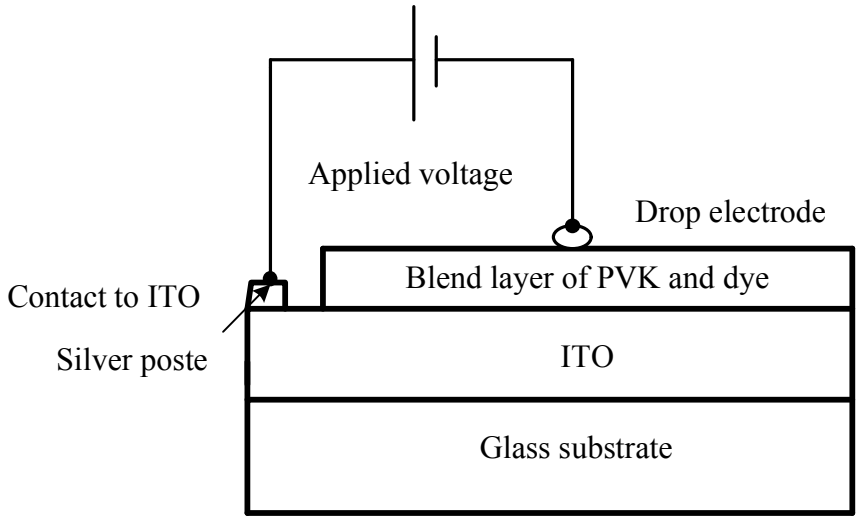

Figure (5.1): Schematic drawing of a single layer sample.

Table 5.1 Molecular formula, melting point, and molecular structure of Crystal violet, Fluorescein and Bromophenol blue.

Dyes	Molecular formula	Melting point	Molecular structures
Crystal violet	$C_{25}N_3H_{30}Cl$	205 °C	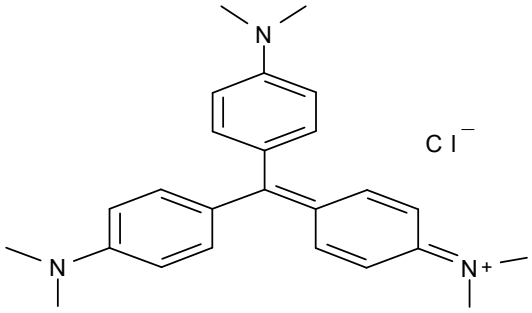
Fluorescein	C20H12O5	314-316 °C	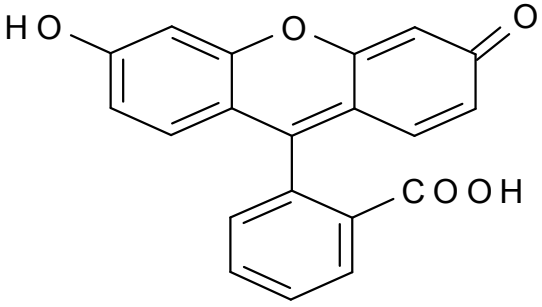
Bromophenol blue	$C_{19}H_{10}Br_4O_5S$	272 - 273 °C	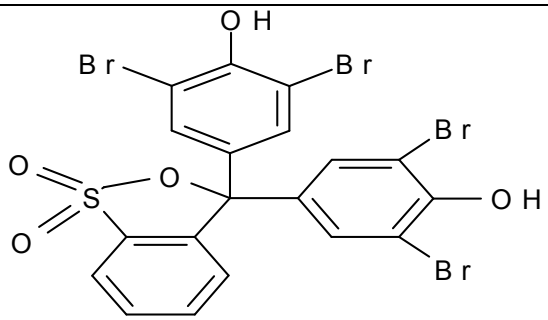

Table 5.2 The structure of PVK-dye blend device.

Group No.	Structure	Sample No.	Dye solution	Polymer solution	Dye concentration (by weight)
G_0	ITO/ PVK /InGa	S_0	-	15mg PVK+1ml toul+5ml THF	0%
G_4	ITO/blend of PVK and crystal	G_4S_1	1ml THF+0.15mg crystal violet	15mg PVK+1ml toul+4ml THF	1%
		G_4S_2	1ml THF+0.30mg		2%

	violet/InGa		crystal violet		
		G_4S_3	1ml THF+0.45mg crystal violet		3%
		G_4S_4	1ml THF+0.60mg crystal violet		4%
		G_4S_5	1ml THF+0.75mg crystal violet		5%
G_5	ITO/blend of PVK and Fluorescein /InGa	G_5S_1	1ml chloroform+0.15mg Fluorescein		1%
		G_5S_2	1ml chloroform+0.30mg Fluorescein		2%
		G_5S_3	1ml chloroform+0.45mg Fluorescein		3%
		G_5S_4	1ml chloroform+0.60mg Fluorescein		4%
		G_5S_5	1ml chloroform+0.75mg Fluorescein		5%
G_6	ITO/blend of PVK and Bromophenol blue/ InGa	G_6S_1	1ml THF+0.15mg Bromophenol blue	15mg PVK+1ml toul+4ml THF	1%
		G_6S_2	1ml THF+0.30mg Bromophenol blue		2%
		G_6S_3	1ml THF+0.45mg Bromophenol blue		3%
		G_6S_4	1ml THF+0.60mg Bromophenol blue		4%
		G_6S_5	1ml THF+0.75mg Bromophenol blue		5%

5.3 Experimental Procedure

PVK powder with an average molecular weight of 11×10^5 was weighted using a sensitive electrical balance (ESJ182-4) with a resolution of 10^{-4} gm. The PVK was the dissolved in a proper amount of mixed solvents of toluene and tetrahydrofuran THF as indicated in table 5.2. A homogenous solution was then obtained. A solution of a dye and THF or chloroform with different concentrations were then added to the PVK solution to get the blend solution and deposited on the ITO substrate to form thin layer with thickness 44nm. Table 5.2 shows the amount of solvents and dyes used to make three groups of devices with different dye concentrations.

5.4 Results and Discussions

In this chapter, the expremintal results obtained for all fabricated devices are presented. These results include the current-voltage characteristics, current-voltage relation in logarithmic scale, and relative light intensity with the applied voltage and the current. Sixteen samples have been studied. The InGa electrode was negatively biased whereas the transparent electrode ITO was positivley biased. All samples are biased over the the range of voltages from 0 to 16 volt. Electrical measurment were carried out at room teperature. The drivin voltage and the resulting current were obtained and measured using NI USB-6251 data acquisition card interfaced with a laptop. The relative intensity was measured using a photodiode. The output of the photodiode was amlified then collected by the same data acquisition card.

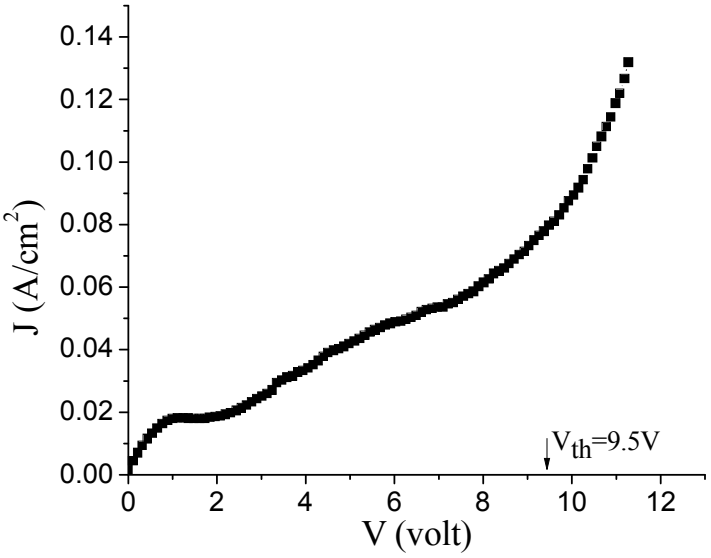
J (A/cm^2)
V (volt)
V_{th}=9.5V
0.14
0.12
0.10
0.08
0.06
0.04
0.02
0.00
0
2
4
6
8
10
12

(a)

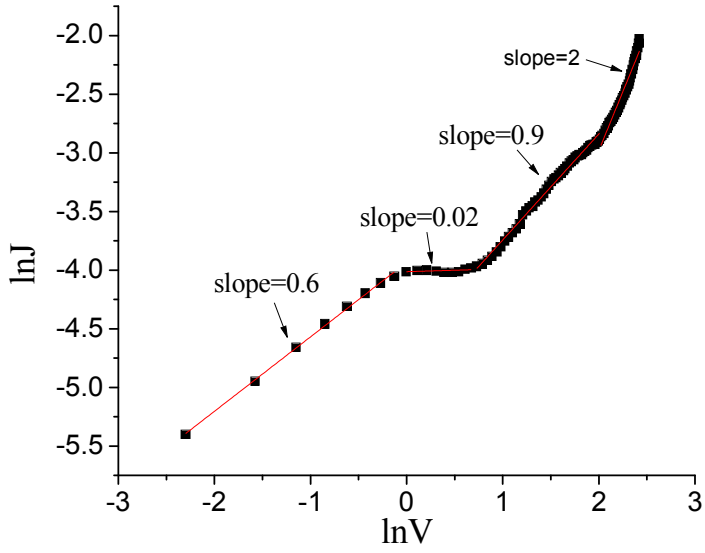
lnJ
lnV
slope=2
slope=0.9
slope=0.02
slope=0.6
-2.0
-2.5
-3.0
-3.5
-4.0
-4.5
-5.0
-5.5
-3
-2
-1
0
1
2
3

(b)

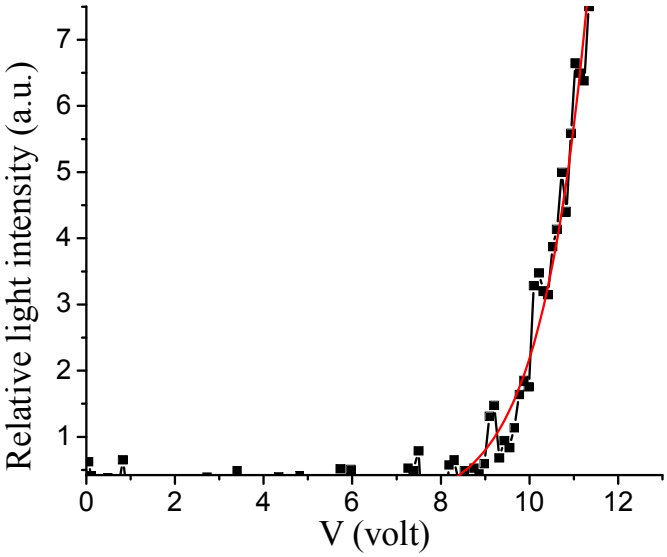

(c)

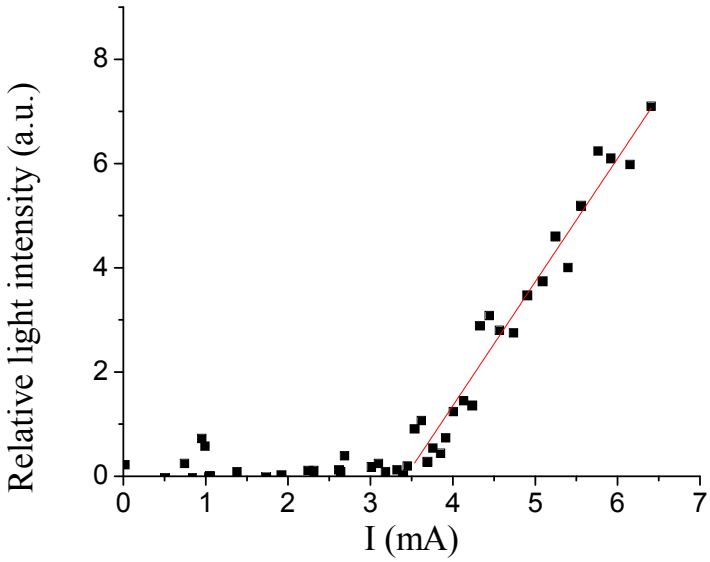

(d)

Figure 5.2 Four characteristics curves of ITO/44nm PVK /InGa device, (a) current density- voltage characteristics, (b) lnJ-lnV characteristics, (c) relative light intensity-voltage characteristics and, (d) relative light intensity-current characteristics.

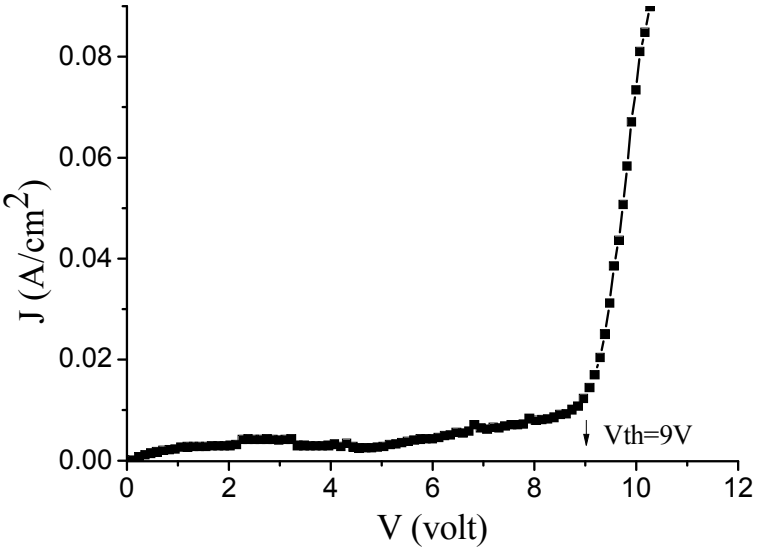
0.08
0.06
0.04
0.02
0.00
J (A/cm2)
0
2
4
6
8
10
12
V (volt)
Vth=9V

(a)

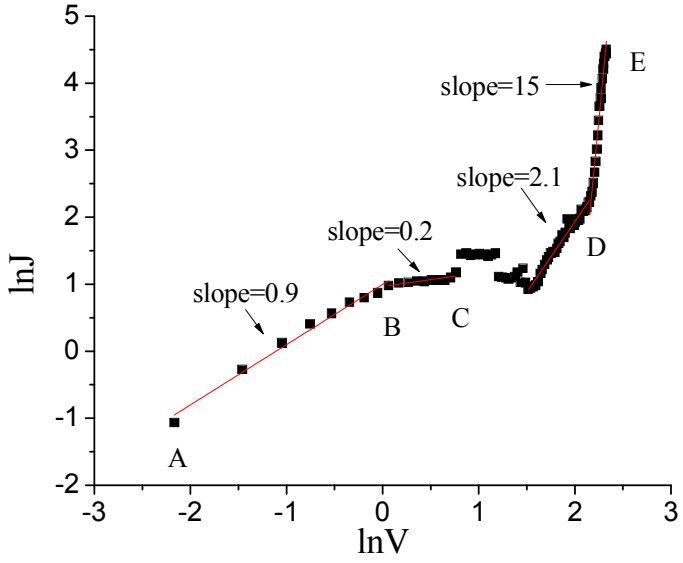
5
4
3
2
1
0
-1
-2
lnJ
-3
-2
-1
0
1
2
3
lnV
slope=15
E
slope=2.1
D
slope=0.2
slope=0.9
A
B
C

(b)

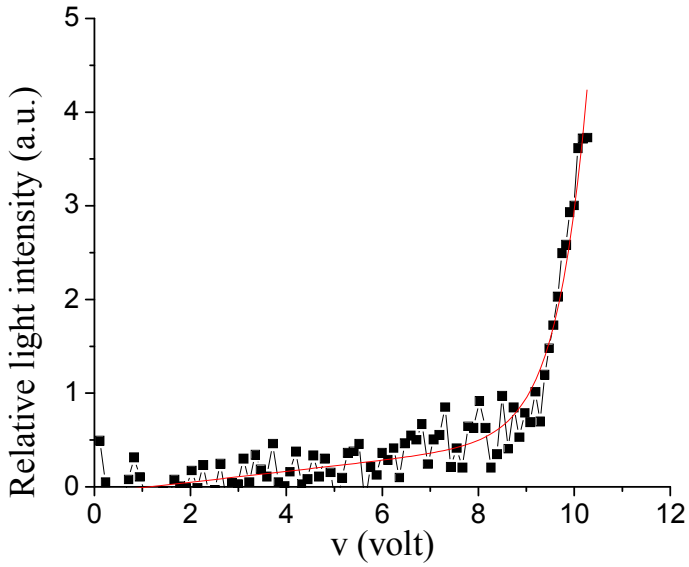

(c)

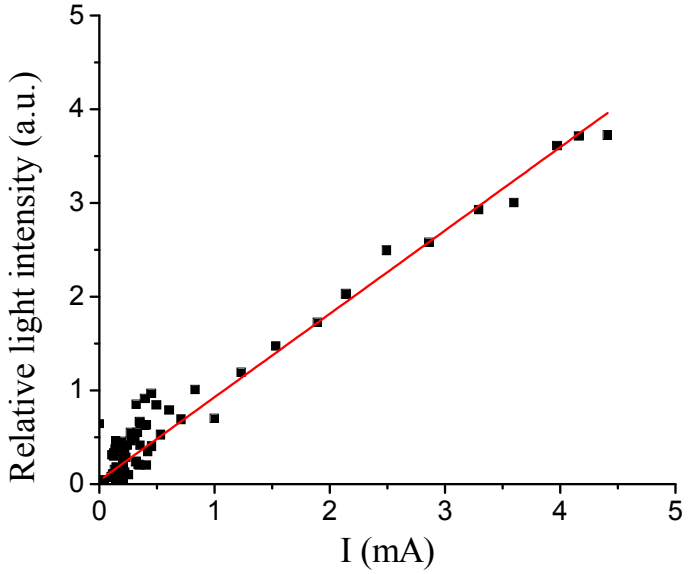

(d)

Figure 5.3 Four characteristics curves of G_4S_1 (1% crystal violet-PVK blend), (a) current density-voltage characteristics, (b) lnJ-lnV characteristics, (c) relative light intensity-voltage characteristics and, (d) relative light intensity-current characteristics.

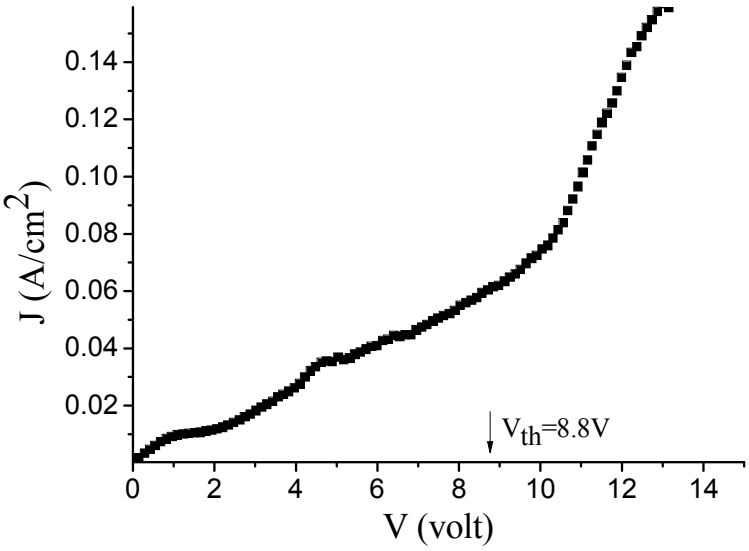
J (A/cm2)
0.14
0.12
0.10
0.08
0.06
0.04
0.02
Vth=8.8V
0
2
4
6
8
10
12
14
V (volt)

(a)

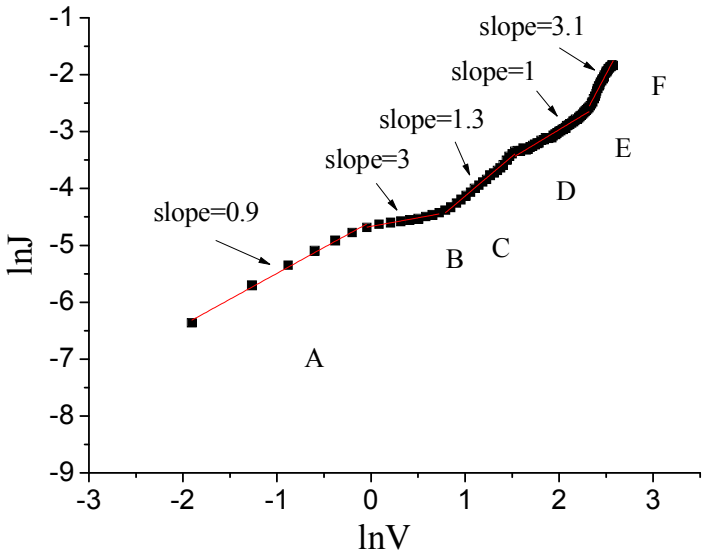
lnJ
-1
-2
-3
-4
-5
-6
-7
-8
-9
slope=3.1
slope=1
slope=1.3
slope=3
slope=0.9
A
B
C
D
E
F
-3
-2
-1
0
1
2
3
lnV

(b)

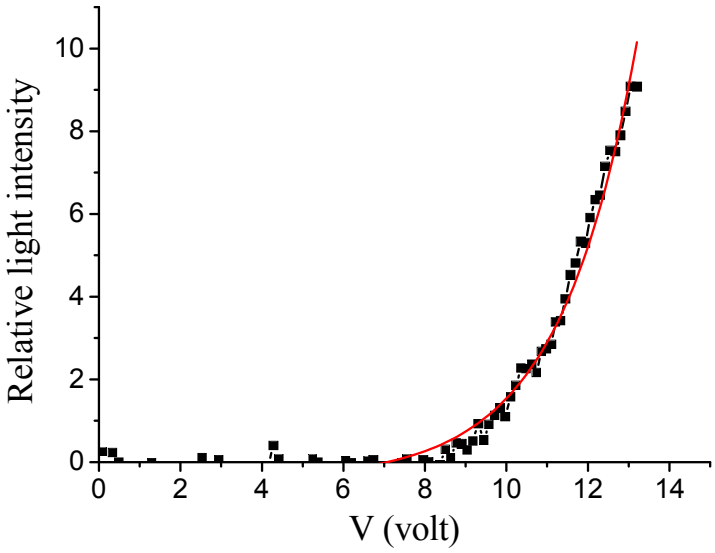

(c)

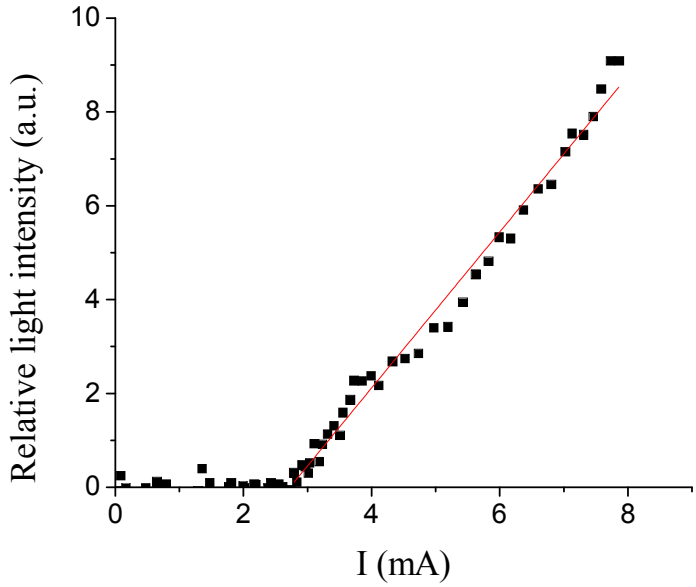

(d)

Figure 5.4 Four characteristics curves of G_4S_2 (2% crystal violet-PVK blend), (a) current density-voltage characteristics, (b) lnJ-lnV characteristics, (c) relative light intensity-voltage characteristics and, (d) relative light intensity-current characteristics.

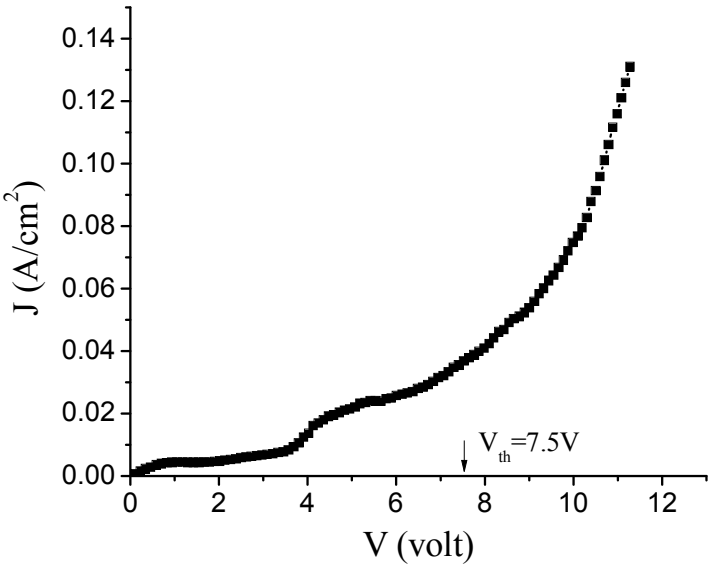
J (A/cm^2)
V (volt)
V$_{th}$=7.5V
0.14
0.12
0.10
0.08
0.06
0.04
0.02
0.00
0
2
4
6
8
10
12

(a)

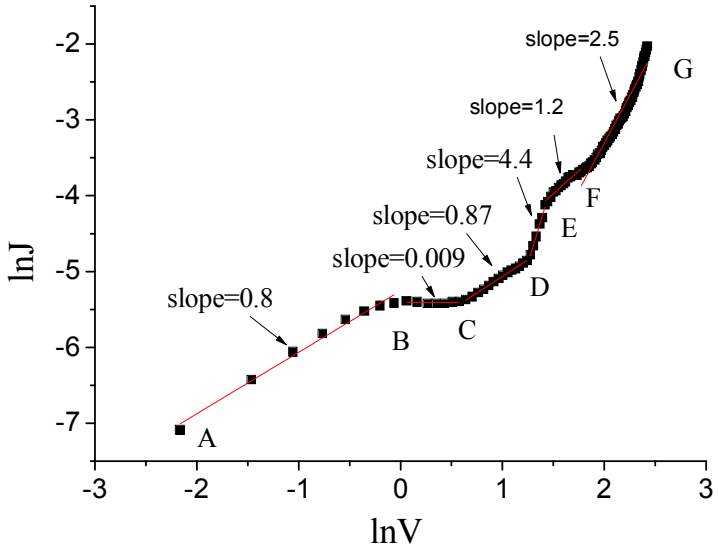
lnJ
lnV
slope=0.8
slope=0.009
slope=0.87
slope=4.4
slope=1.2
slope=2.5
A
B
C
D
E
F
G
-2
-3
-4
-5
-6
-7
-3
-2
-1
0
1
2
3

(b)

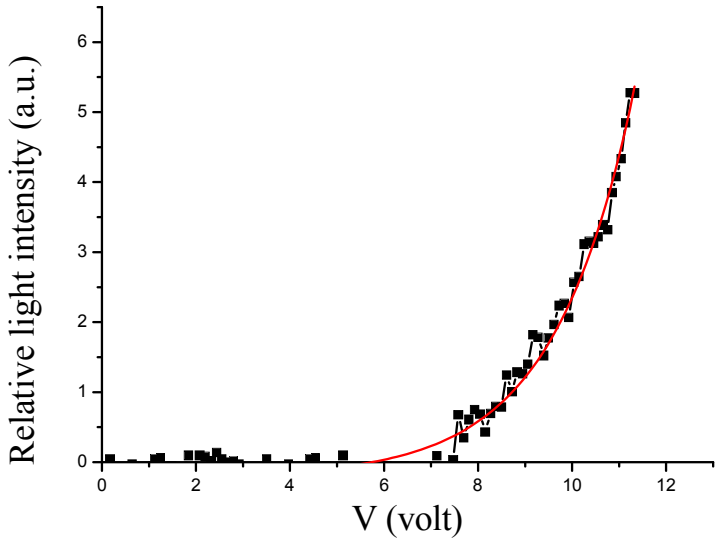

(c)

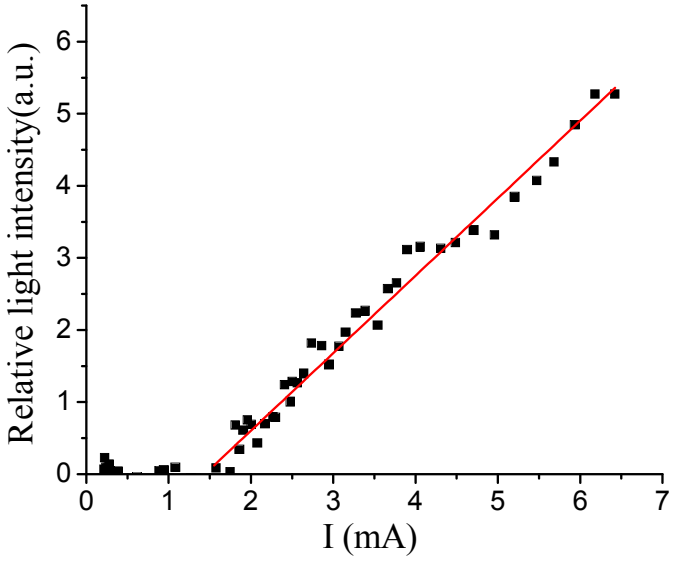

(d)

Figure 5.5 Four characteristics curves of G_4S_3 (3%vrystal violet-PVK blend), (a) current density-voltage characteristics, (b) lnJ-lnV characteristics, (c) relative light intensity-voltage characteristics and, (d) relative light intensity-current characteristics.

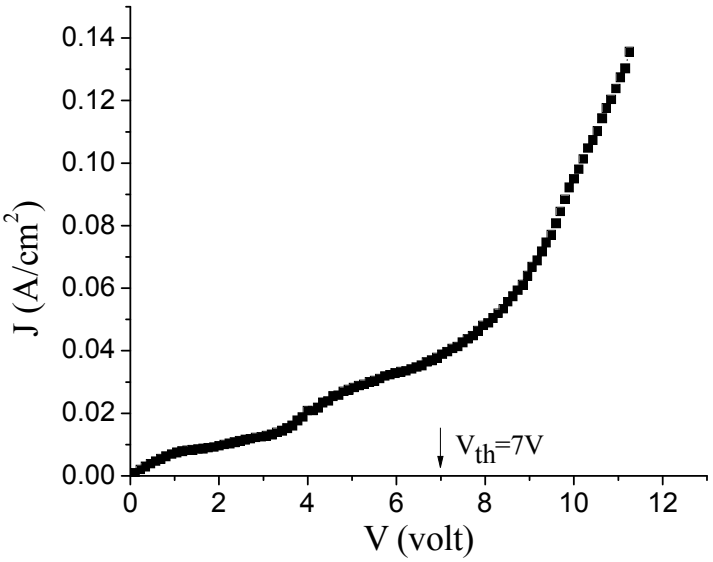
0.14
0.12
0.10
0.08
0.06
0.04
0.02
0.00
J (A/cm2)
Vth=7V
0
2
4
6
8
10
12
V (volt)

(a)

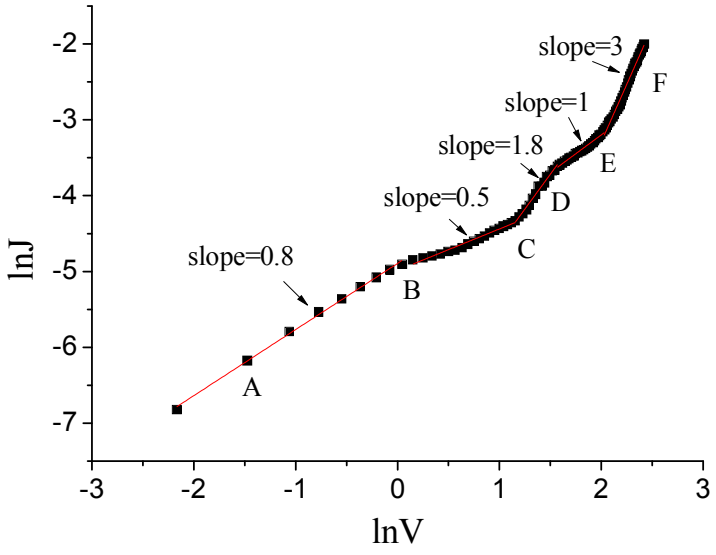
-2
-3
-4
-5
-6
-7
lnJ
slope=3
F
slope=1
slope=1.8
E
D
slope=0.5
C
slope=0.8
B
A
-3
-2
-1
0
1
2
3
lnV

(b)

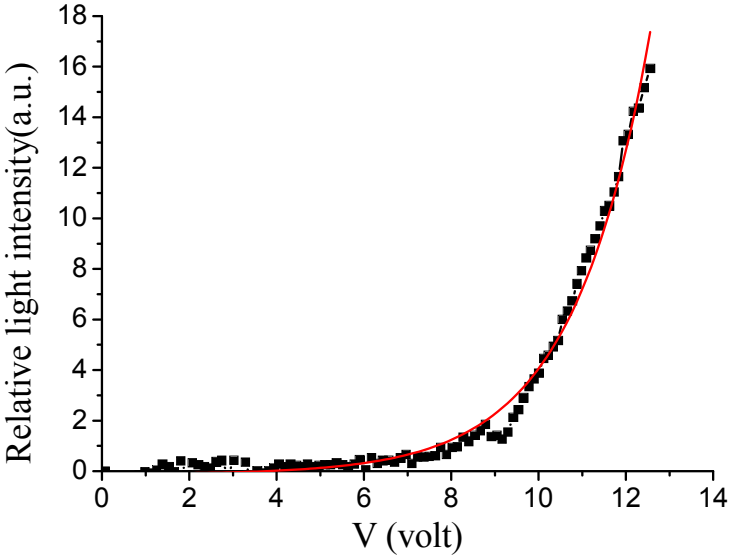

(c)

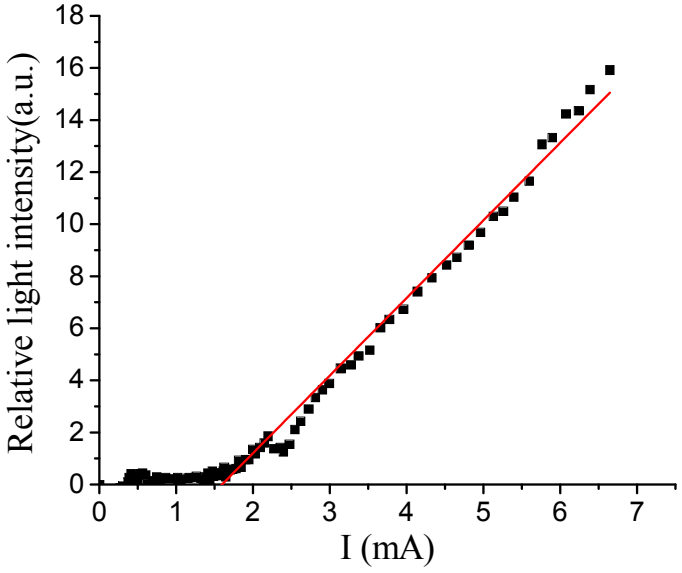

(d)

Figure 5.6 Four characteristics curves of G_4S_4 (4% crystal violet-PVK blend), (a) current density-voltage characteristics, (b) lnJ-lnV characteristics (c) relative light intensity-voltage characteristics and, (d) relative light intensity-current characteristics.

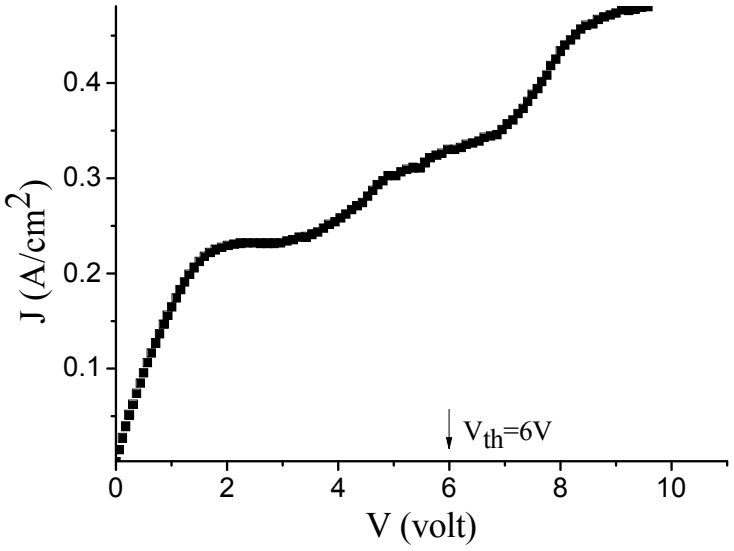
J (A/cm2)
V (volt)
Vth=6V
0.1
0.2
0.3
0.4
0
2
4
6
8
10

(a)

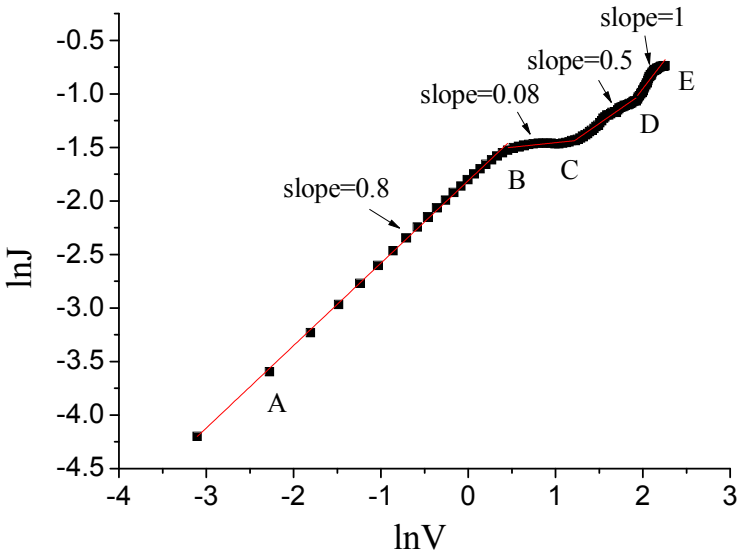
lnJ
lnV
slope=0.8
slope=0.08
slope=0.5
slope=1
A
B
C
D
E
-0.5
-1.0
-1.5
-2.0
-2.5
-3.0
-3.5
-4.0
-4.5
-4
-3
-2
-1
0
1
2
3

(b)

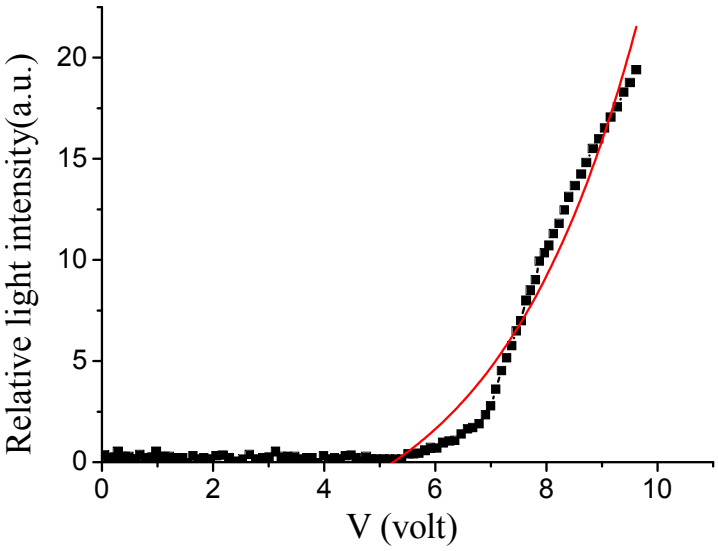

(c)

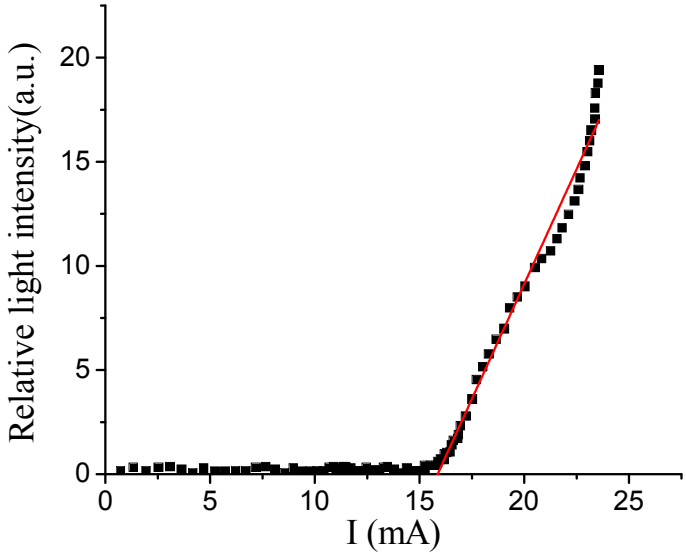

(d)

Figure 5.7 Four characteristics curves of G_4S_5 (5% crystal violet-PVK blend), (a) current density-voltage characteristics, (b) lnJ-lnV characteristics, (c) relative light intensity-voltage characteristics and, (d) relative light intensity-current characteristics.

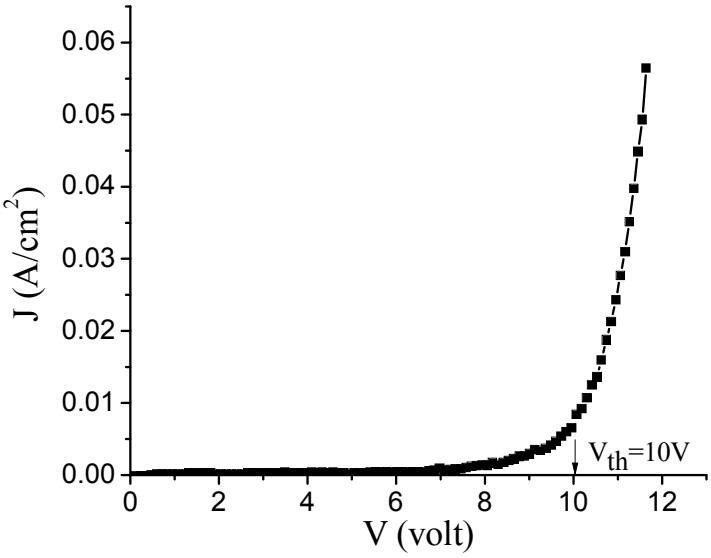
J (A/cm^2)
V (volt)
V_{th}=10V
0.06
0.05
0.04
0.03
0.02
0.01
0.00
0
2
4
6
8
10
12

(a)

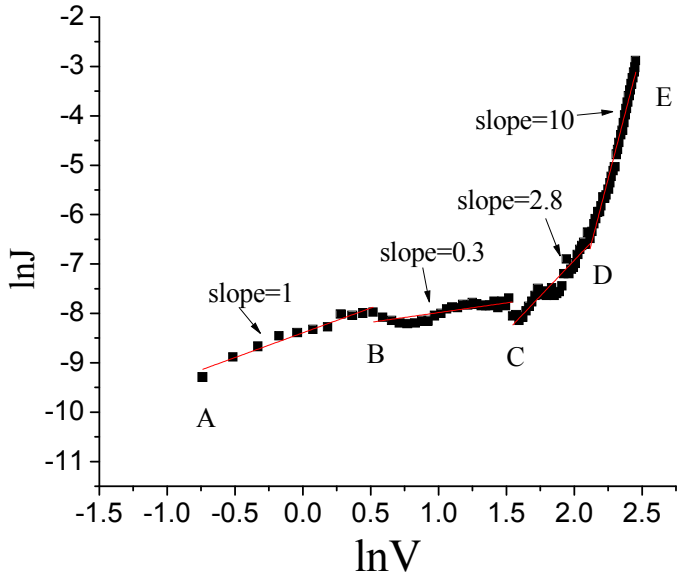
lnJ
lnV
slope=1
slope=0.3
slope=2.8
slope=10
A
B
C
D
E
-2
-3
-4
-5
-6
-7
-8
-9
-10
-11
-1.5
-1.0
-0.5
0.0
0.5
1.0
1.5
2.0
2.5

(b)

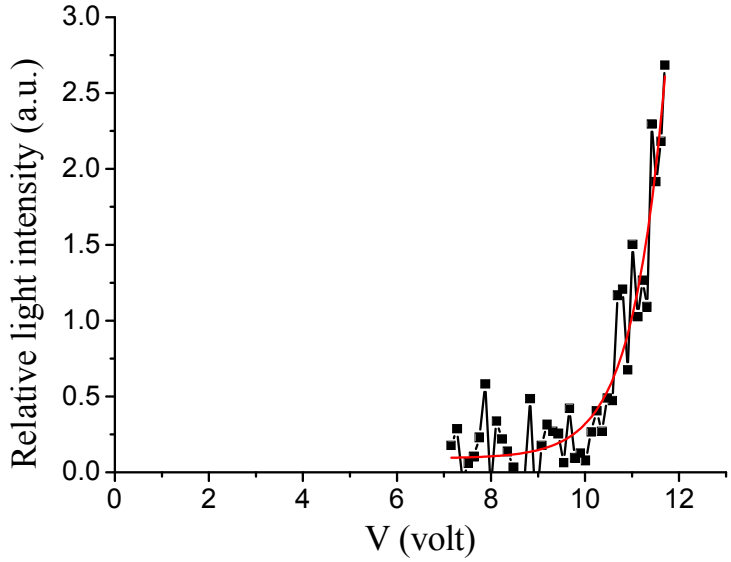

(c)

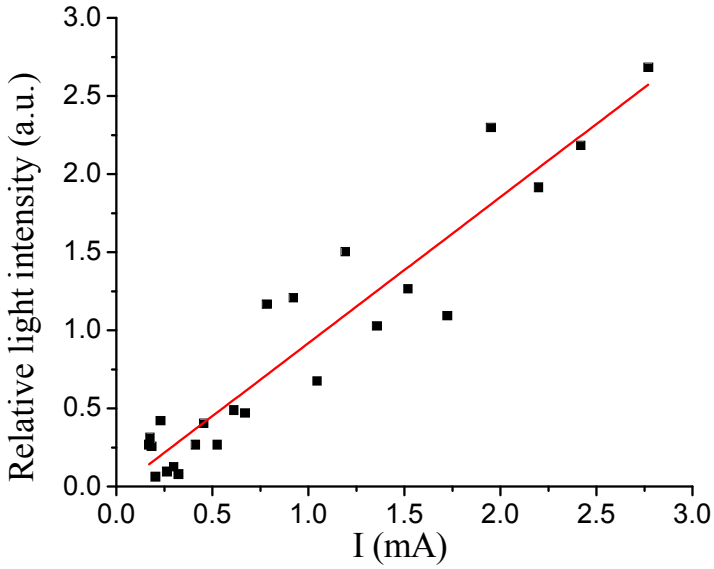

(d)

Figure 5.8 Four characteristics curves of G_5S_1 (1% Fluorescein-PVK blend), (a) current density-voltage characteristics, (b) lnJ-lnV characteristics, (c) relative light intensity-voltage characteristics and, (d) relative light intensity-current characteristics.

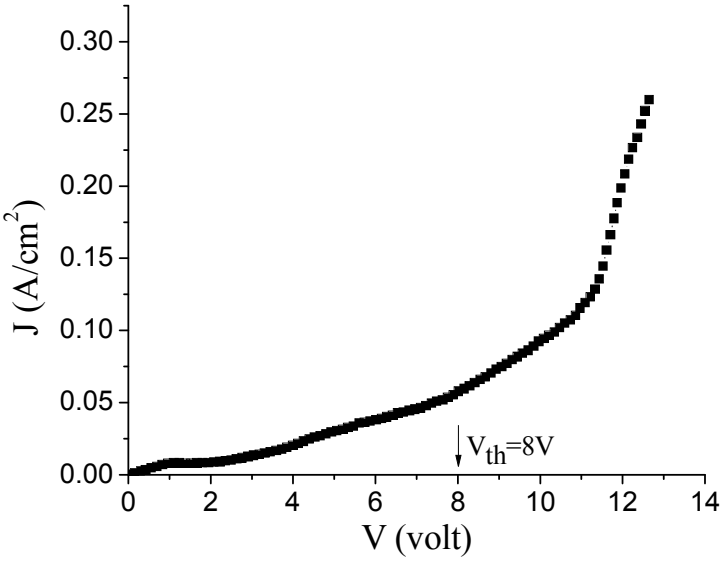
0.30
0.25
0.20
0.15
0.10
0.05
0.00
J (A/cm2)
0
2
4
6
8
10
12
14
V (volt)
Vth=8V

(a)

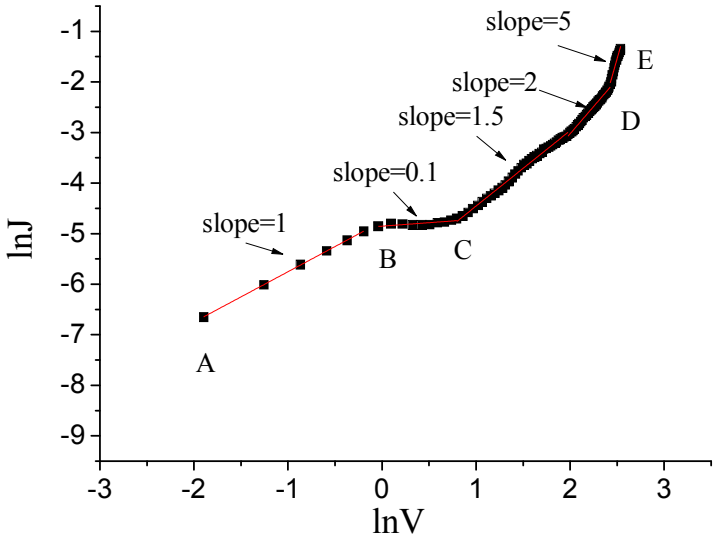
-1
-2
-3
-4
-5
-6
-7
-8
-9
lnJ
-3
-2
-1
0
1
2
3
lnV
slope=5
E
slope=2
D
slope=1.5
slope=0.1
slope=1
A
B
C

(b)

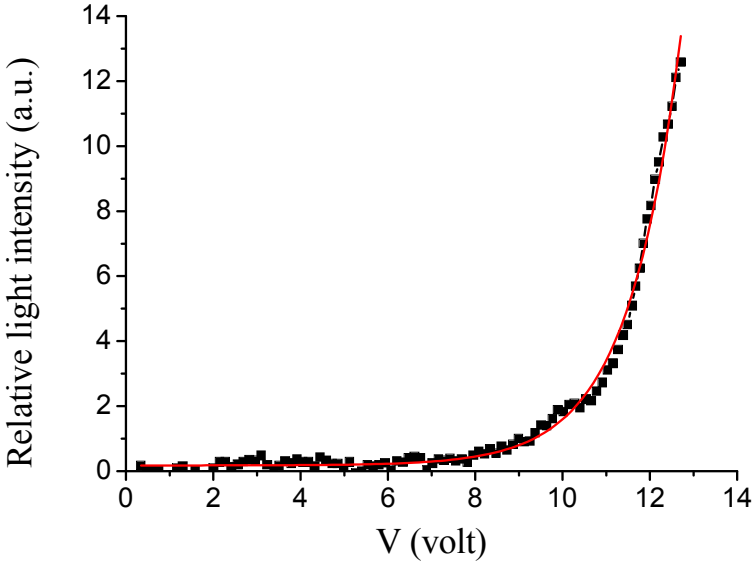

(d)

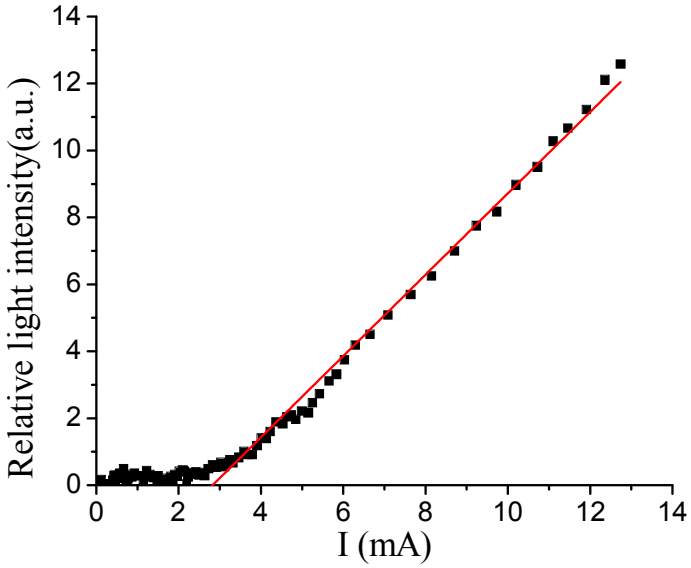

(d)

Figure 5.9 Four characteristics curves of G_5S_2 (2%Fluorescein-PVK blend), (a) current density- voltage characteristics, (b) lnJ-lnV characteristics, (c) relative light intensity-voltage characteristics and, (d) relative light intensity-current characteristics.

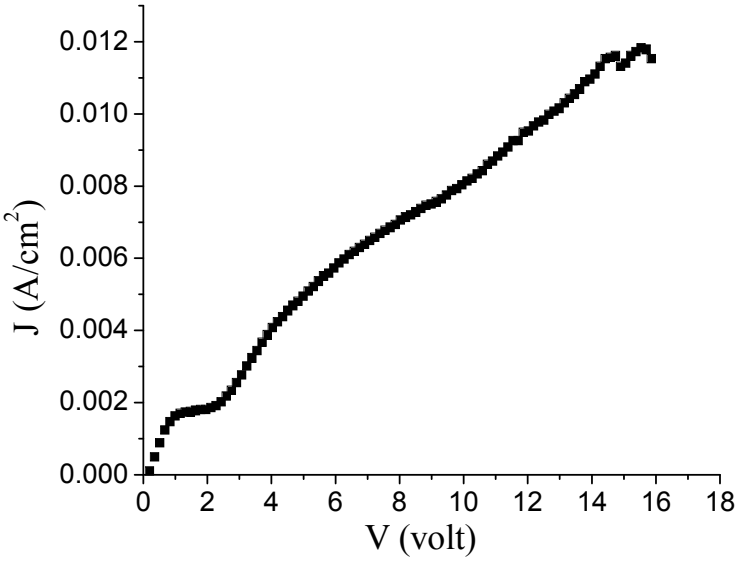

(a)

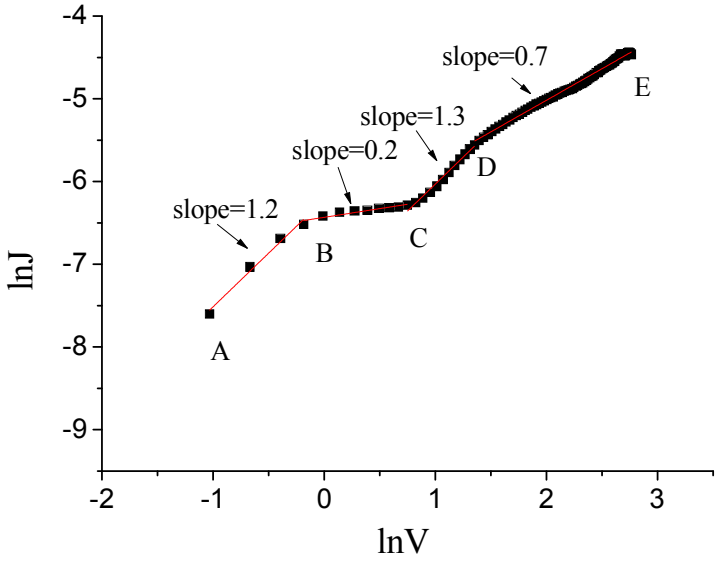

(b)

Figure 5.10 Two characteristics curves of G_5S_3, (3%Fluorescein-PVK blend), (a) current density-voltage characteristics, (b) lnJ-lnV characteristics.

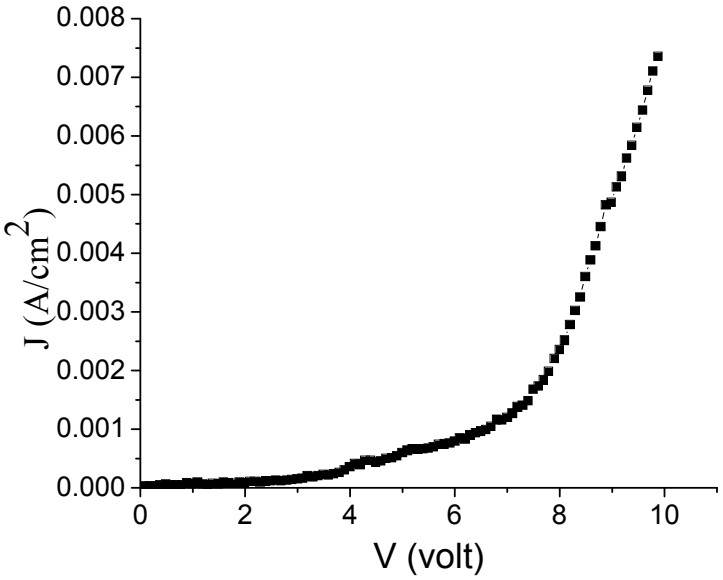

(a)

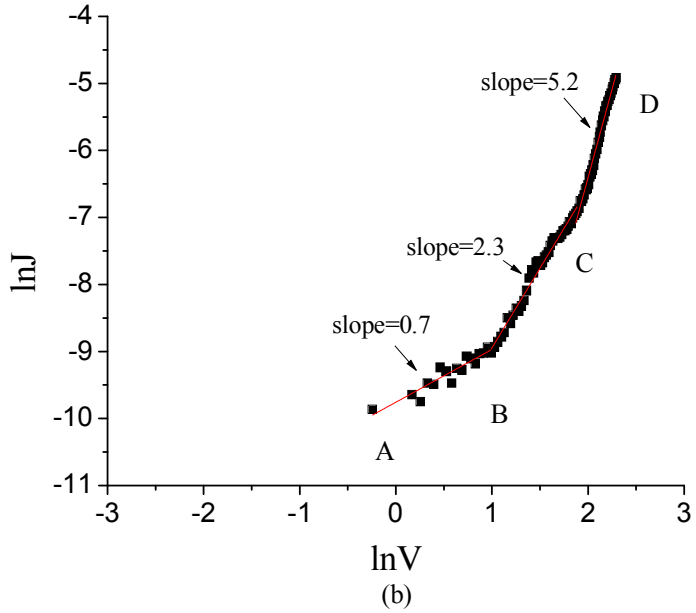

(b)

Figure 5.11 Two characteristics curves of G_5S_4 (4%Fluorescein-PVK blend), (a) current density-voltage characteristics, (b) lnJ-lnV characteristics.

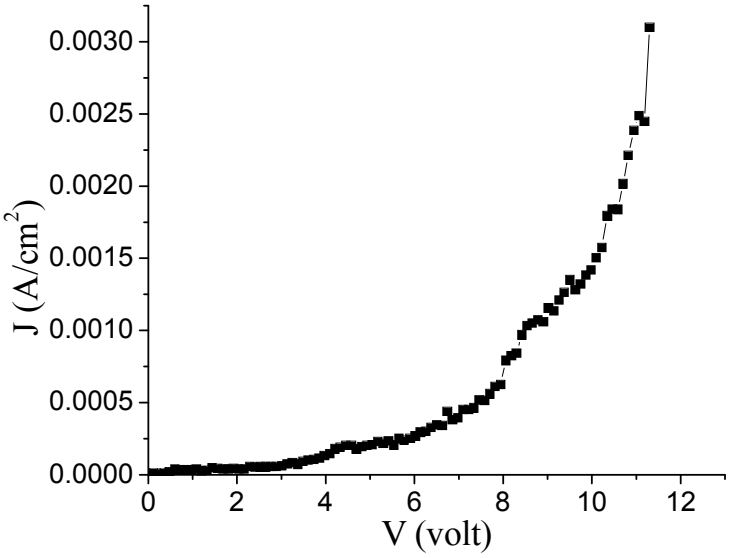

(a)

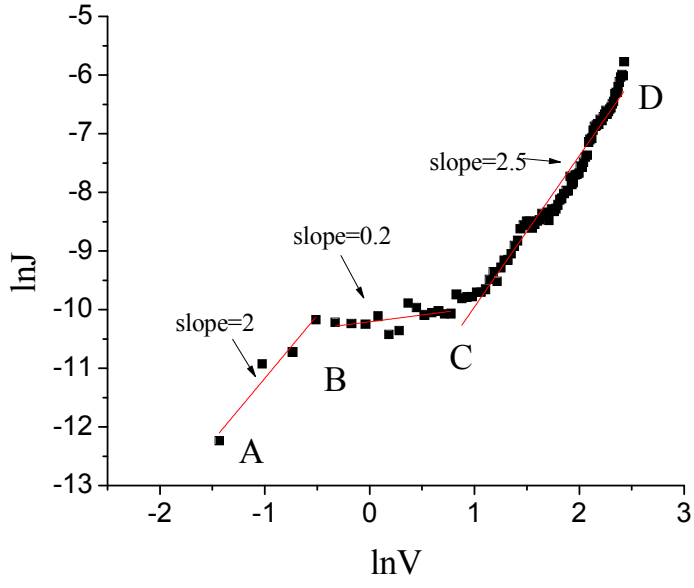

(b)

Figure 5.12 Two characteristics curves of G_5S_5 (5%Fluorescein-PVK blend), (a) current density-voltage characteristics, lnJ-lnV characteristics.

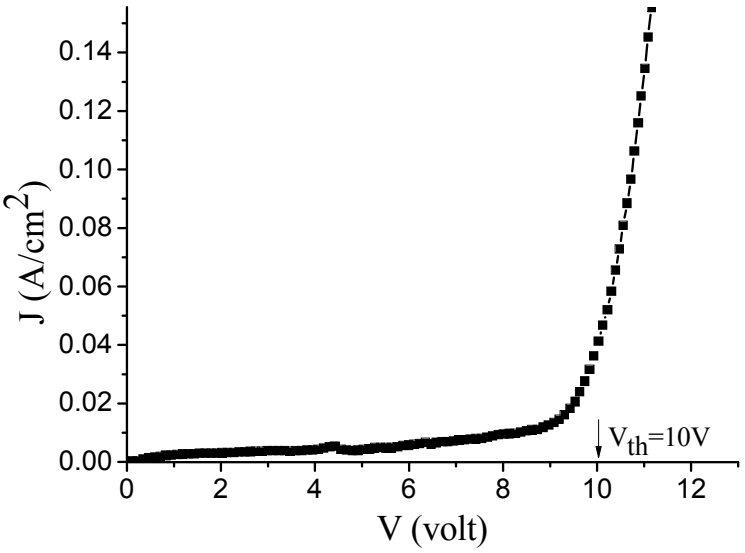
J (A/cm2)
V (volt)
Vth=10V
0.00
0.02
0.04
0.06
0.08
0.10
0.12
0.14
0
2
4
6
8
10
12

(a)

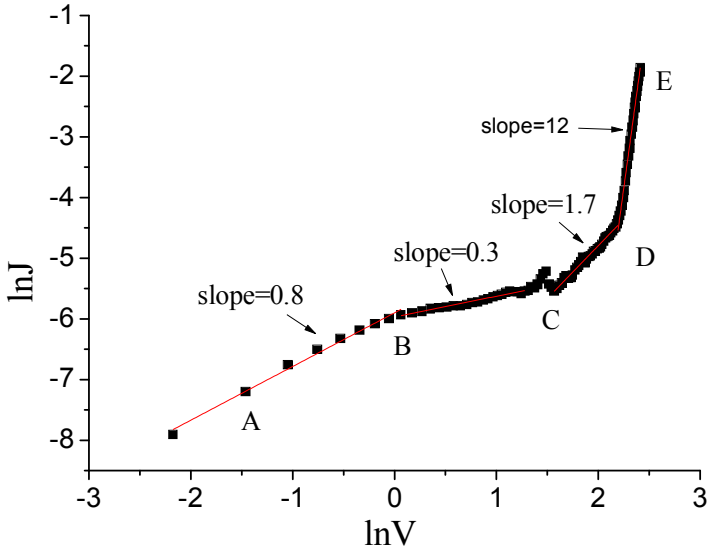
lnJ
lnV
slope=0.8
slope=0.3
slope=1.7
slope=12
A
B
C
D
E
-1
-2
-3
-4
-5
-6
-7
-8
-3
-2
-1
0
1
2
3

(b)

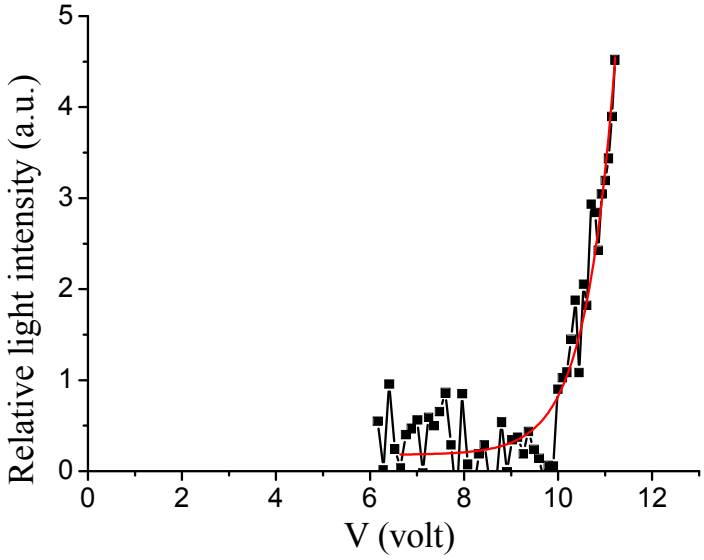

(c)

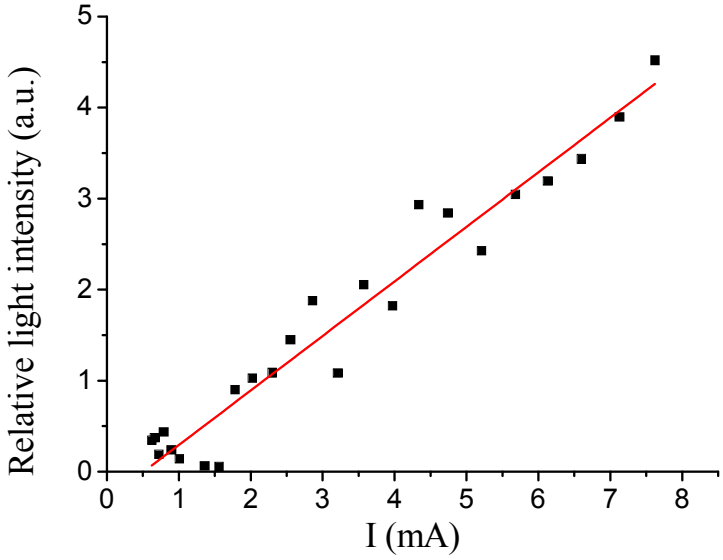

(d)

Figure 5.13 Four characteristics curves of G_6S_1 (1%Bromophenol blue-PVK blend) , (a) current density- voltage characteristics, (b) lnJ-lnV characteristics, (c) relative light intensity-voltage characteristics and, (d) relative light intensity-current characteristics.

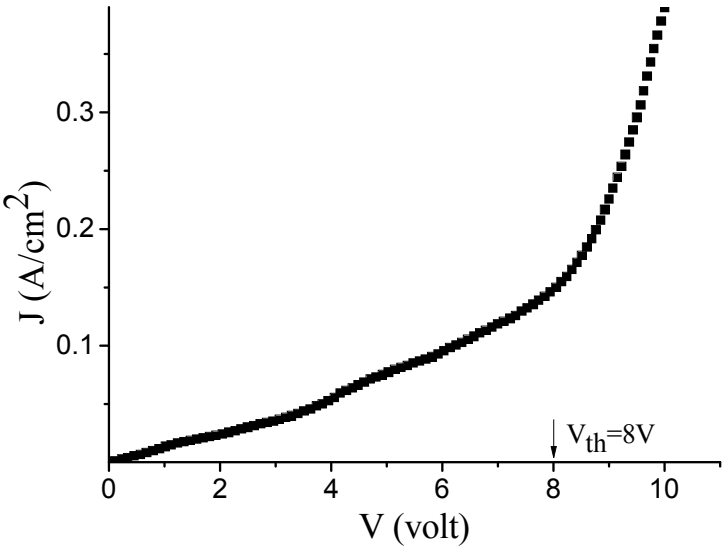
J (A/cm2)
0.3
0.2
0.1
Vth=8V
0
2
4
6
8
10
V (volt)

(a)

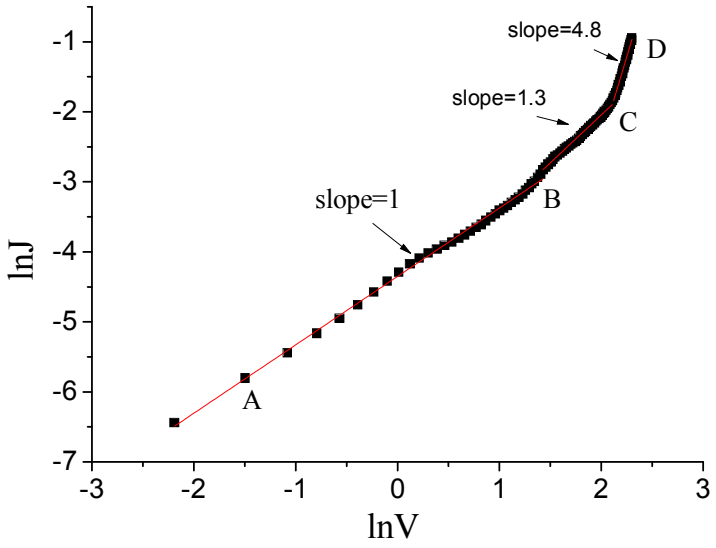
lnJ
-1
-2
-3
-4
-5
-6
-7
slope=4.8
D
slope=1.3
C
slope=1
B
A
-3
-2
-1
0
1
2
3
lnV

(b)

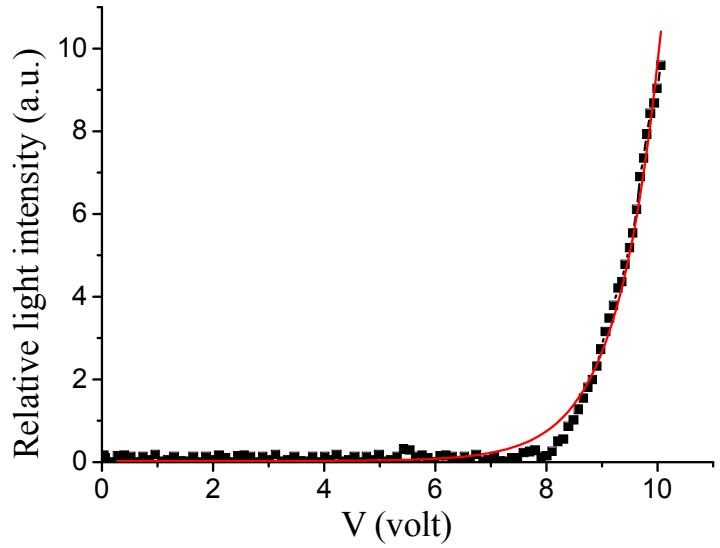

(c)

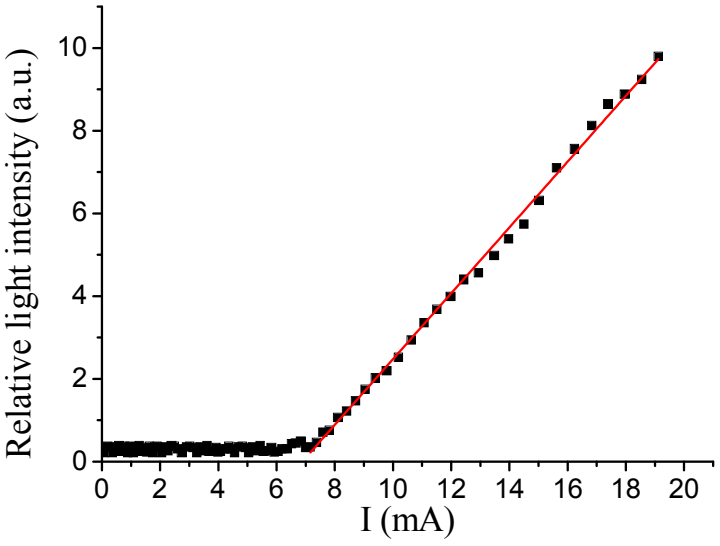

(d)

Figure 5.14 Four characteristics curves of G_6S_2 (2%Bromophenol blue-PVK blend), (a) current density-voltage characteristics, (b) lnJ-lnV characteristics, (c) relative light intensity-voltage characteristics and, (d) relative light intensity-current characteristics.

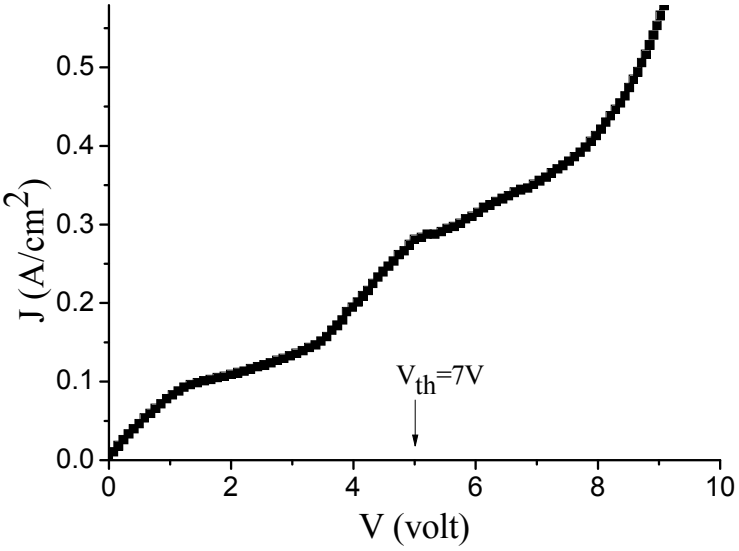
J (A/cm2)
V (volt)
Vth=7V
0.0
0.1
0.2
0.3
0.4
0.5
0
2
4
6
8
10

(a)

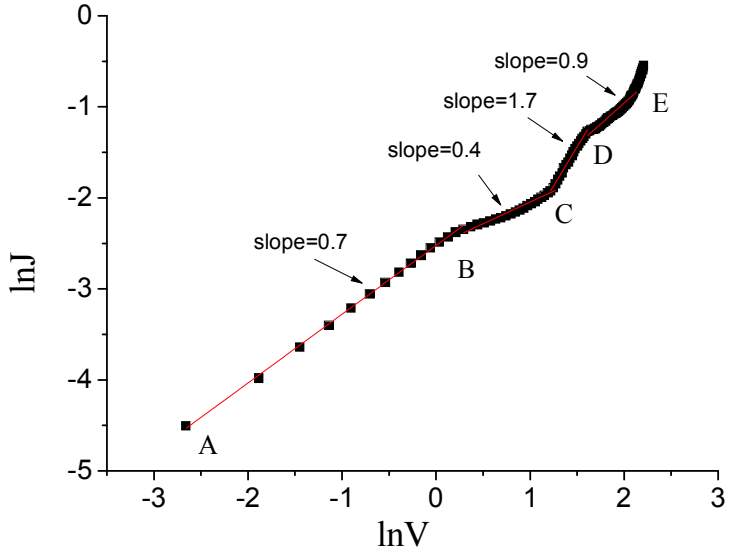
lnJ
lnV
slope=0.9
slope=1.7
slope=0.4
slope=0.7
A
B
C
D
E
0
-1
-2
-3
-4
-5
-3
-2
-1
0
1
2
3

(b)

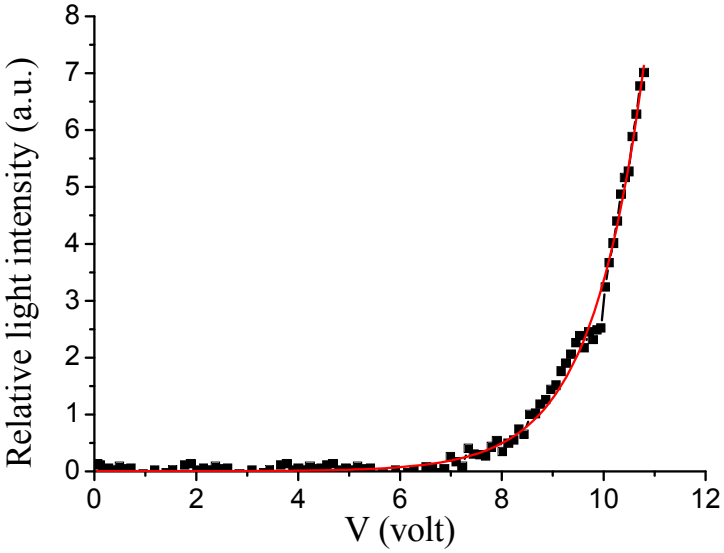

(c)

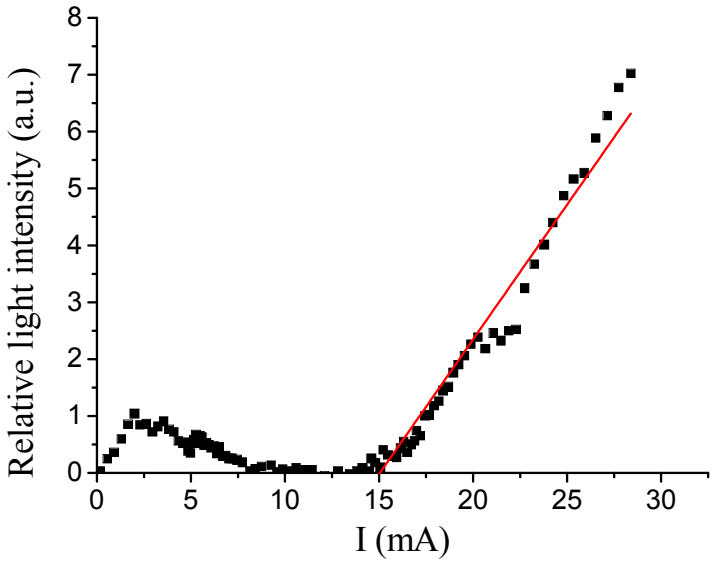

(d)

Figure 5.15 Four characteristics curves of G_6S_3 3%Bromophenol blue-PVK blend), (a) current density-voltage characteristics, (b) lnJ-lnV characteristics, (c) relative light intensity-voltage characteristics, (d) relative light intensity-current characteristics.

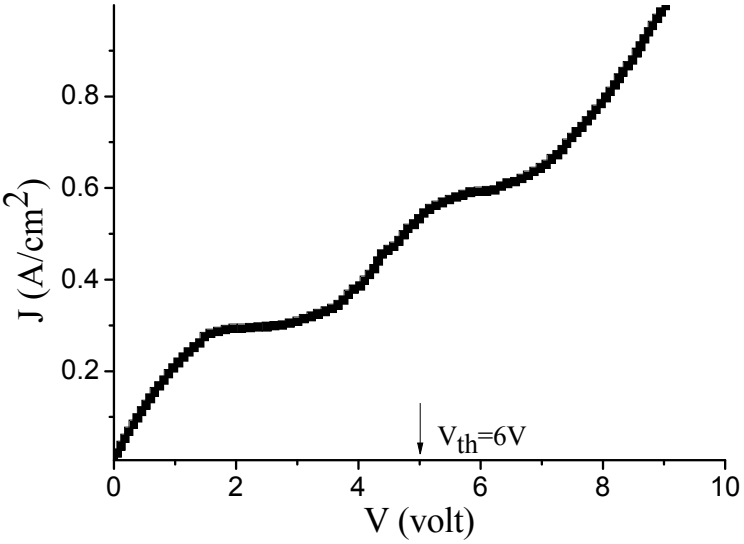
J (A/cm2)
0.8
0.6
0.4
0.2
Vth=6V
0
2
4
6
8
10
V (volt)

(a)

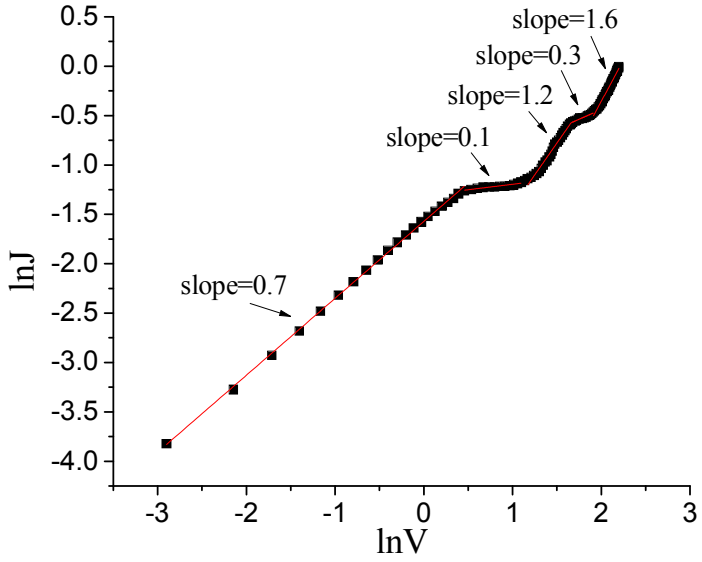
slope=1.6
slope=0.3
slope=1.2
slope=0.1
slope=0.7
lnJ
0.5
0.0
-0.5
-1.0
-1.5
-2.0
-2.5
-3.0
-3.5
-4.0
-3
-2
-1
0
1
2
3
lnV

(b)

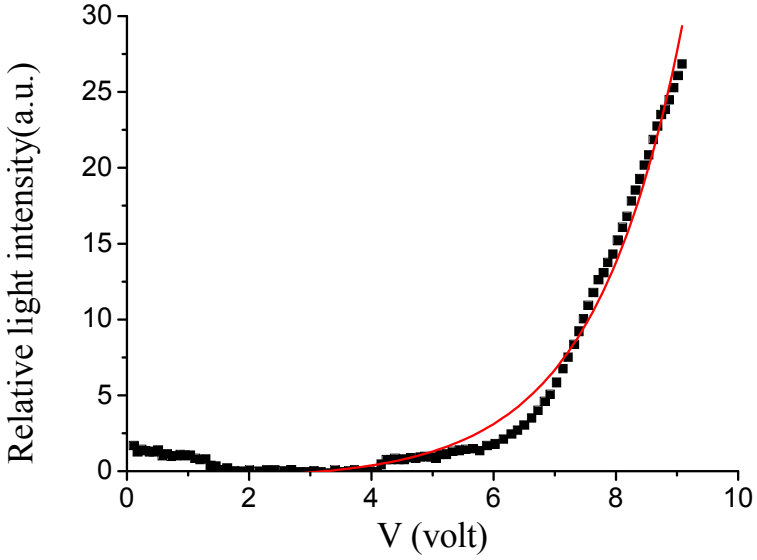

(c)

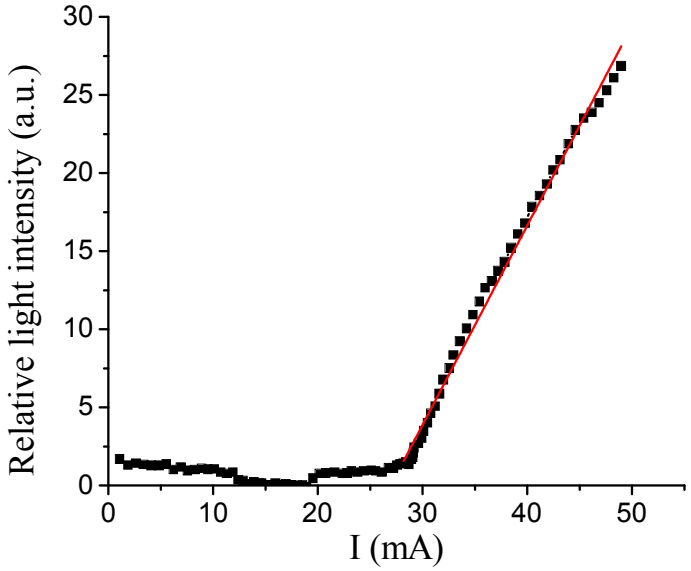

(d)

Figure 5.16 Four characteristics curves of G_6S_4 (4%Bromophenol blue-PVK blend), (a) current density-voltage characteristics, (b) lnJ-lnV characteristics, (c) relative light intensity-voltage characteristics, and (d) relative light intensity-current characteristics.

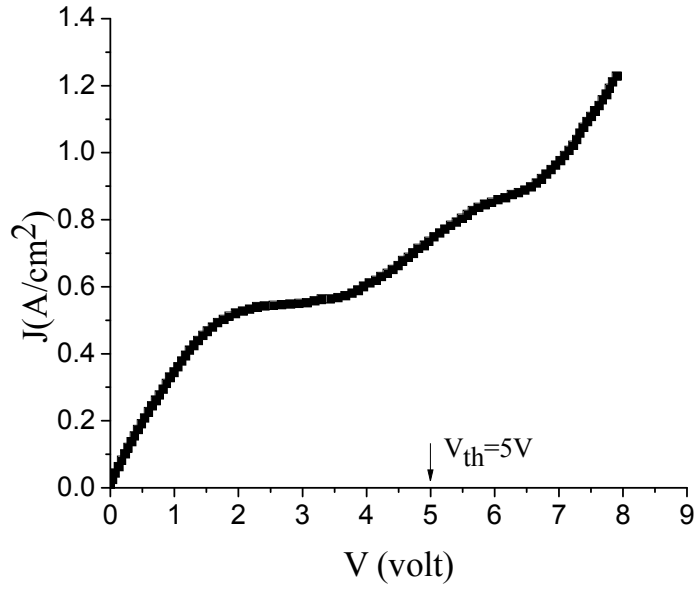
J(A/cm2)
V (volt)
Vth=5V
1.4
1.2
1.0
0.8
0.6
0.4
0.2
0.0
0
1
2
3
4
5
6
7
8
9

(a)

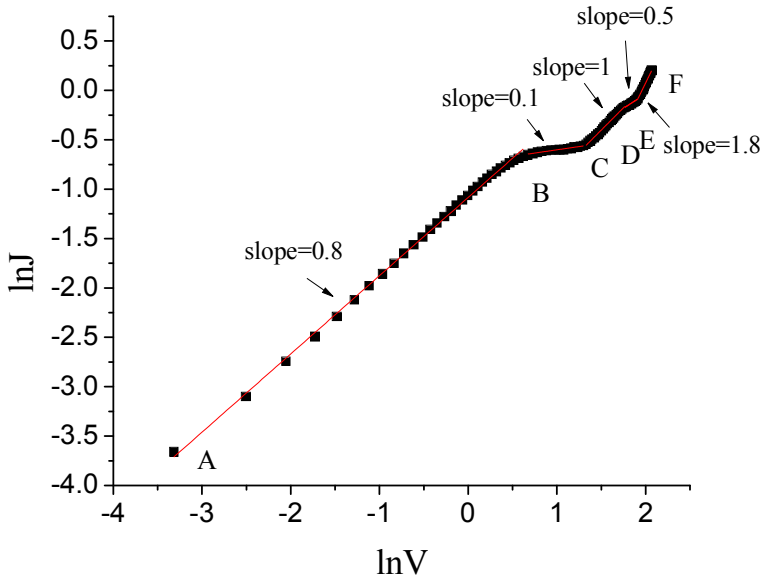
lnJ
lnV
slope=0.8
slope=0.1
slope=1
slope=0.5
slope=1.8
A
B
C
D
E
F
0.5
0.0
-0.5
-1.0
-1.5
-2.0
-2.5
-3.0
-3.5
-4.0
-4
-3
-2
-1
0
1
2

(b)

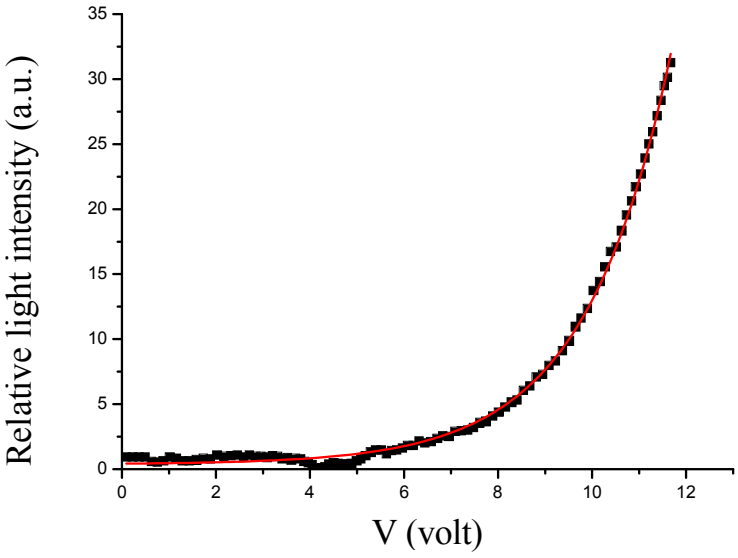

(c)

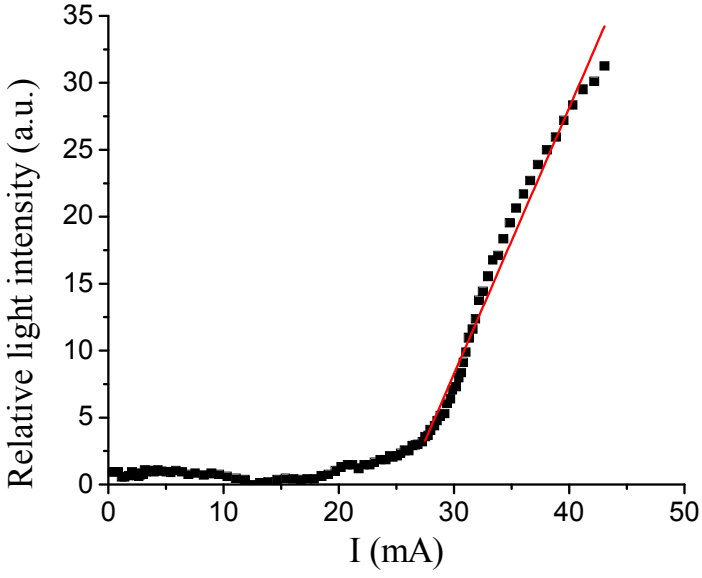

(d)

Figure 5.17 Four characteristics curves of G_6S_5 (5%Bromophenol blue-PVK blend), (a) current density-voltage characteristics, (b) current lnJ-lnV characteristics, (c) relative light intensity-voltage characteristics and, (d) relative light intensity-current characteristics.

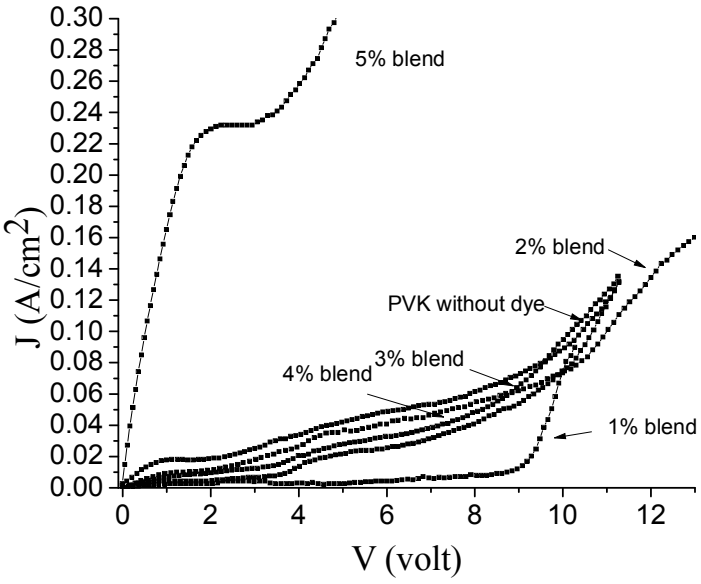

(a)

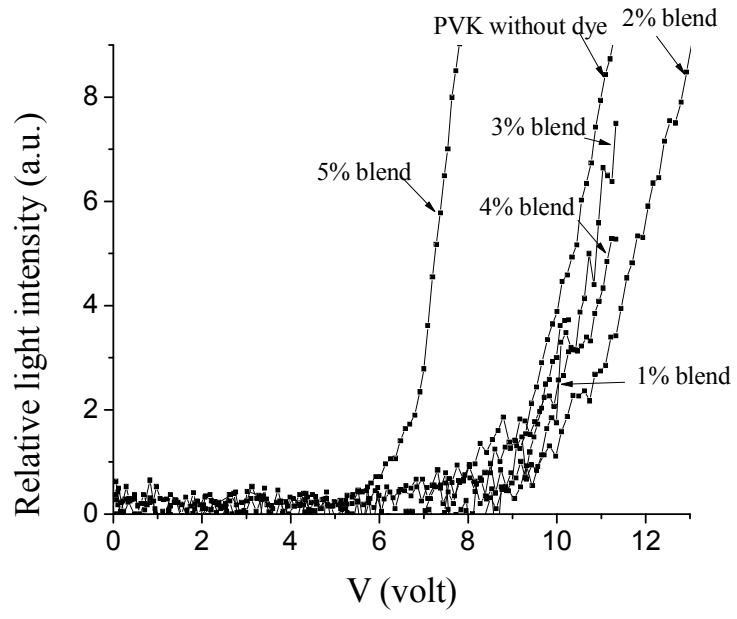

(b)

Figure 4.18 Two characteristics curves of of ITO/1%, 2%, 3%, 4%, and 5%crystal violet-PVK blend /InGa, (a) current density- voltage characteristics and, (b) relative light intensity-voltage characteristics.

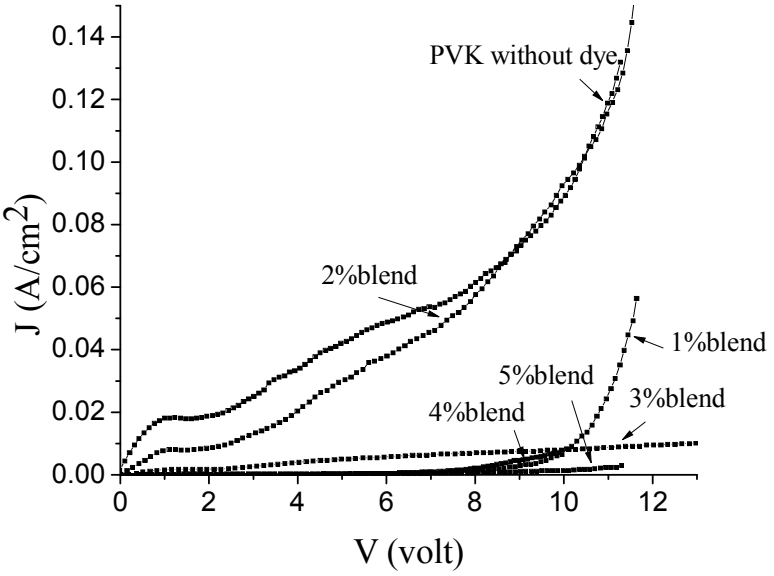

(a)

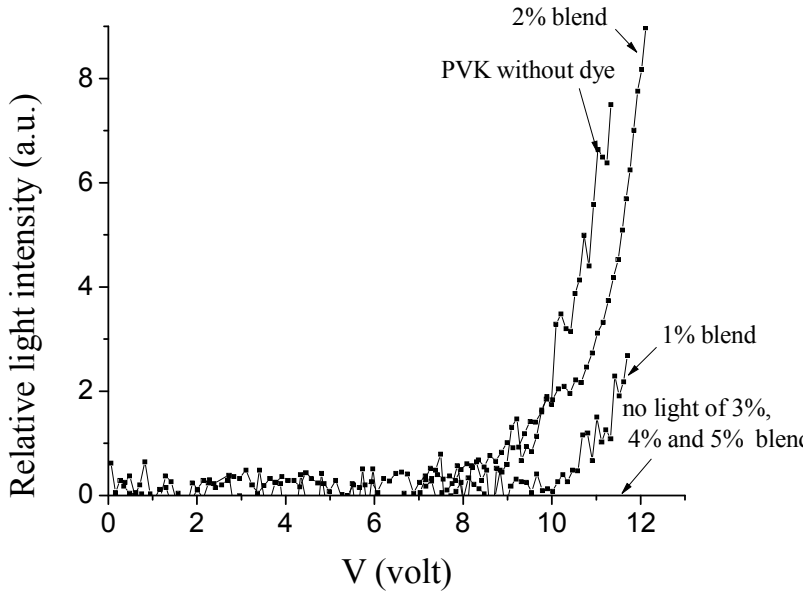

(b)

Figure 4.19 Two characteristics curves of of ITO/1%, 2%, 3%, 4%, and 5% Fluorescein -PVK blend /InGa, (a) current density- voltage characteristics and, (b) relative light intensity-voltage characteristics.

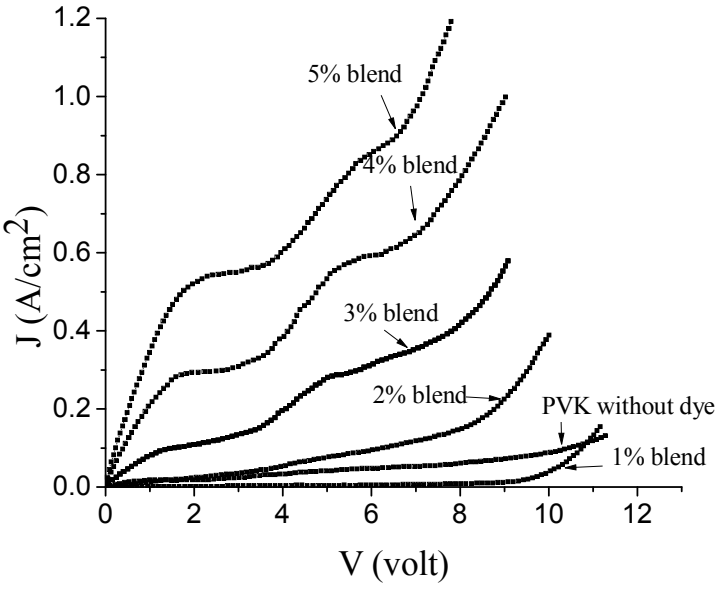

(a)

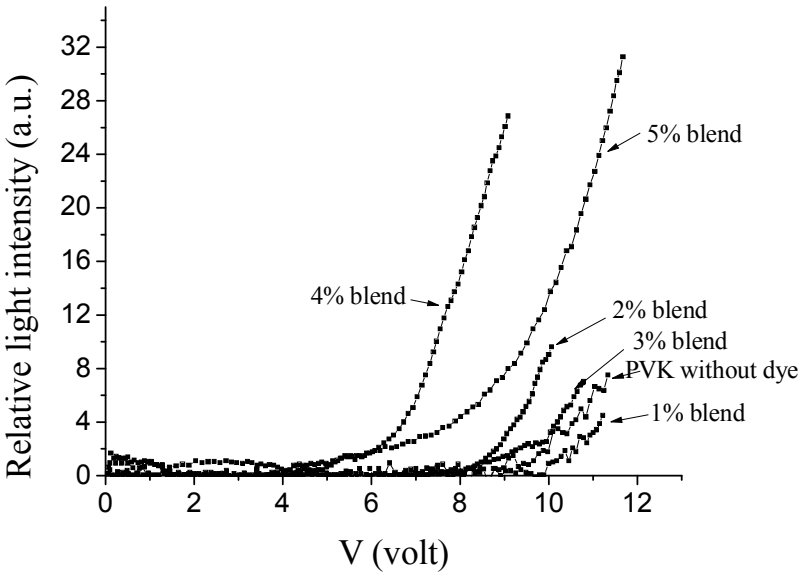

(b)

Figure 4.20 Two characteristics curves of of ITO/1%, 2%, 3%, 4%, and 5% Bromophenol blue -PVK blend /InGa, (a) current density- voltage characteristics and, (b) relative light intensity-voltage characteristics.

5.4.1 Current Density-Voltage Characteristic Curves

All samples were connected in forward bias where the InGa electrode was negatively biased and the transparent electrode ITO was positively biased. The current passing through the samples is due to the injection of charges from the metalic electrodes. The J-V characteristic curves show nonlinearity for all samples. The J-V characteristics show an exponential increase of current with the applied voltage in G_4S_1, G_5S_1, G_5S_4, G_4S_5, and G_6S_1 which is similar to a typical diode characteristic curve. Under forward bias of low voltage the current density increases slowly with increasing voltage. At certain higher voltage (threshold voltage V_{th})the current density increases sharply. The J-V relationship increases exponentially for G_4S_1, G_5S_1, G_5S_4, G_4S_5 and G_6S_1 samples that is slow increase of current density at low applied voltage and sharp increase of current density at high applied voltage.

For other samples it can be seen that the sharp increase of current density at low applied voltage which may be attriputed to leakage current which is linearly dependent on the applied voltage. The leakage current may be attributed due to the movment charge carriers from blend process toward the ITO electrode [5]. Most of samples show an increa in the the current density and a decrease in the threshold voltage when increasing the concentration of the dye. As mentioned in chapter four, the threshold voltage of a device is a crucial parameters in the field of OLEDs. It can be estimated by the relative light intensity-voltage characteristics curve. The value of V_{th} for all samples have been detremined and tabulated in table 5.3, where the V_{th} for PVK without blend is 9.5volt.

Table 5.3 The threshold voltages for a single layer device.

Blend PVK and crystal violet (G4)	Vth volt	Blend PVK and Fluorescein (G5)	Vth volt	Blend PVK and Bromophenol blue (G6)	V_{th} volt
G_4S_1	9	G_5S_1	10	G_6S_1	10
G_4S_2	8.8	G_5S_2	8	G_6S_2	8
G_4S_3	7.5	G_5S_3	-	G_6S_3	7
G_4S_4	7	G_5S_4	-	G_6S_4	6
G_4S_5	6	G_5S_5	-	G_6S_5	5

5.4.2 Relative Light Intensity with Driving Voltage

Electroluminescenc (EL) was detected in thirteen samples. Only G_5S_3, G_5S_4, and G_5S_5 are observed to give no EL. The variations of the EL with applied voltage are shown in Figs. 5.3 (c) to Fig. 5.16 (c). At low forward bias voltage there is no EL. The luminescent samples start emitting light at the threshold voltage. EL increases rapidly with increaseing the forward bias voltage when the applied voltage exceeds V_{th}.

5.4.3 Relative Light Intensity with Current

Fig. 5.2 (d) through fig. 5.14 (d) illustrate the characteristic curves of EL versus current. Samples G_5S_3, G_5S_4 and G_5S_5 do not produce electroluminescence. The curves show linear relationships between the intensity of emitting light with the current.

4.4.4 Conduction Mechanisms

Fig. 5.2 (b) through Fig. 5.16 (b) show the dependence of the natural log of current density J on the natural log of the voltage V. These curves exhibit nonlinear relationship and can be divided into four to five regions as AB, BC, CD, DE, and EF. These different regions have different slopes which indicate that the J-V relation (in the natural logarithmic scale) have the form $J \propto V^s$ where s is the slope of the curve. At low voltages the lnJ-lnV characteristic curves show the slopes for region AB is equal to about 1. That means this region follows the Ohm's law given by Eq. (2.14) and the conduction mechanism is ohmic. This is the case for all samples. As the voltage increases the ohmic conduction breakdown occurs and the slope equal to be about 0.009 to 2.3 in the region BC, indicate that the charge carriers injected from electrodes inside the samples are so large that create an electric field almost cancel the electric field from the electrodes. As the voltage increases more, the slope is nearly equal to about 2 in the region CD for some samples as shown in table 5.4. In this case the region obeys Child's law given by Eq. (2.21) and the conduction becomes space charge limited SCL. As the voltage increases, the three above conduction mechanisms are repeated, that means the occurance of the SCL conduction mechanism breakdown and the emergence of another dominating conduction mechanism in which the slope can reach to 4 and 5.

Table 5.4 Experimental values of slope for each region of lnJ-lnV characteristic curves.

sample	AB	BC	CD	DE	EF
G_0S_0	0.6	0.02	0.9	2	
G_4S_1	0.9	0.2	2.1	15	
G_4S_2	0.9	0.3	1.3	1	3.1
G_4S_3	0.8	0.009	0.87	4.4	1.2
G_4S_4	0.8	0.5	1.8	1	3
G_4S_5	0.8	0.08	0.5	1	
G_5S_1	1	0.3	2.8	10	
G_5S_2	1	0.1	1.5	2	5
G_5S_3	1.2	0.2	1.3	0.7	
G_5S_4	0.7	2.3	5.2		
G_5S_5	2	0.2	2.5		
G_6S_1	0.8	0.3	1.7	12	
G_6S_2	1	1.3	4.8		
G_6S_3	0.7	0.4	1.7	0.9	
G_6S_4	0.7	0.1	1.2	0.3	1.6
G_6S_5	0.8	0.1	1	0.5	1.8

The repetition of conduction mechanisms is attributed to the following:

After domination for a voltage interval, SCL collapses and turns to Ohmic conduction mechanism in which a slight increase of the current of V is observed. This can be attributes to the presence of traps inside the blend of PVK film. When the SCL dominates, the current is observed to increase sharply with V (high slope to J-V curve is found). Then sharp increas is due to filled traps. At acertain value of V the trapped electron gain energy that is sufficient to get free from its trap and this is proccess is called Frenkel-pool emission. Any increas in V after this process increases the injection of the charge carrier but some of these carrier are trapped and this explain the breakdown of SCL conduction mechanism. Finally, it is worth to mention that in region where the slope reaches 4-5 after SCl conduction regions, all the traps are completely filled. Figure 5.21 shows the energy band diagram for the polymer at neutral and different doping.

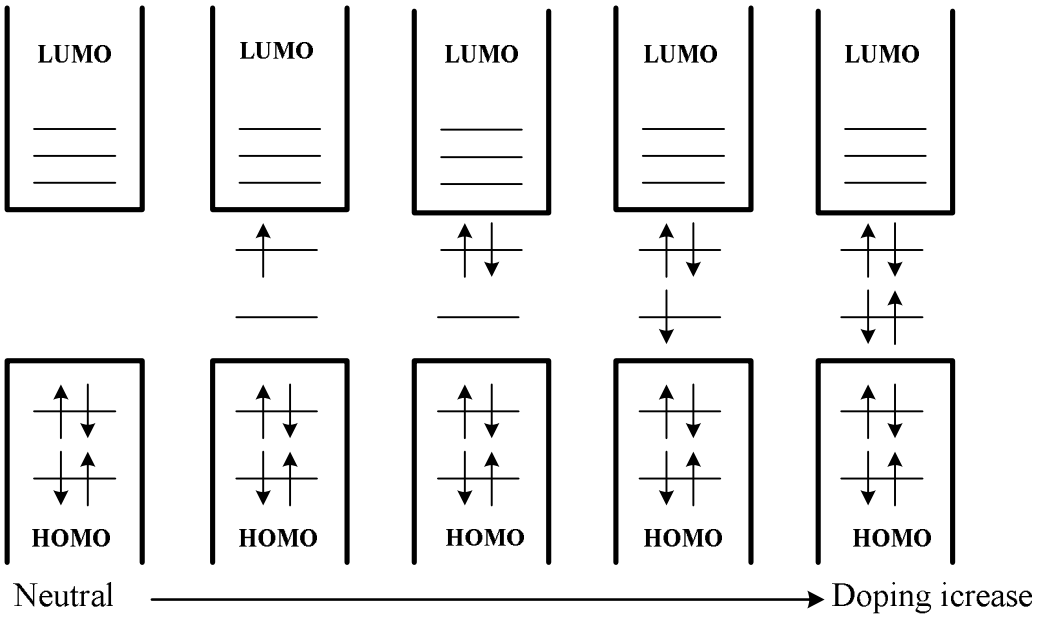

Figure 5.21 The energy band diagram for the polymer at neutral and different doping.

As shown in Fig. 5.3 to Fig. 5.16, as doping increases the threshold voltage decreases. This can be attributed to the existence of impurity levels (electrons or holes) in the energy gap. When the electronic wave function of impurity state overlap, an electron bound to one impurity state can tunnel to an unoccupied impurity state. This tunneling process between impurity sites is referred to as impurity conduction [15].

.

.

CONCLUSIONS

In this work, twelve double layer samples with different dyes and sixteen samples of single layer blended devices with different dye concentrations have been studied. The J-V characteristics curves, lnJ-lnV curves and the relative of light intensity versus voltage and current have been presented at room temperature.

In the double layer devices, the J-V curves show an exponential increase of current with the applied voltage for ITO/PVK with different thickness/50nm Rhodamine B /InGa and ITO/PVK with different thickness/ 50nm crystal violet/InGa groups, that is slow increase of current density at low applied voltages and sharp increase of current density at high applied voltage which is similar to a typical diode characteristics. For ITO/PVK with different thickness/50nm Bromophenol blue/ InGa samples the sharp increase of current density at low applied voltage was observed which may refer to leakage current. The group ITO/PVK with different thickness/50nm Bromophenol blue/ InGa shows semi-linear J-V characteristic curves.

Two samples ITO/35.33nm PVK/Rhodamine B/InGa and ITO/44.3nm PVK/Rhodamine B/InGa are found to work as organic light emitting diodes (OLEDs). The threshold voltage is found to be 8 and 10 volt respectively.

In single layer devices, the J-V relationship is exponentially increasing for ITO/ PVK and 1%crystal violet blend/InGa, ITO/ PVK and 5%crystal violet blend/InGa, ITO/ PVK and 1%Fluorescein blend/ InGa, ITO/ PVK and 4%Fluorescein blend/ InGa, and ITO/ PVK and 1%Bromophenol blue blend/ InGa samples. For the other samples the sharp increase of current density at low applied voltage may refer to leakage current. All single layer samples work as OLED devices except the samples ITO/PVK and 3%Fluorescein blend/ InGa, ITO/PVK and 4%Fluorescein blend/ InGa, and ITO/PVK and 5%Fluorescein blend/ InGa. The smallest value of threshold voltage V_{th} was 5volt in ITO/ PVK and 5%Bromophenol blue blend/ InGa sample and the largest value was 10 volt in ITO/ PVK and 1%Fluorescein blend/ InGa sample.

At low voltages, the lnJ-lnV characteristic curves show slopes equal to about 1. This means that the conduction mechanism is ohmic, and obeys the relation

$$J_{ohm} = qn\mu\frac{V}{d}$$

At higher applied voltage, it was found that the current depends quadratically on the voltage in most samples and the slope of lnJ-lnV characteristic curves equal to about 2 This indicates that the conduction mechanism is SCLC which obeys the following relation

$$J = \frac{9}{8}\mu k \varepsilon_0 \frac{V^2}{d^3}$$

Moreover, as the voltage increased there was a repetition in the conduction mechanisms.

REFERNCES

[1] M. Chanda, Introduction to polymer science and chemistry: a problem solving approach, CRC Press, Boca Raton FL, 2006.

[2] F. Billmeyer, Textbook of Polymer Science, 3rd edition, John Wiley & Sons Inc., New York, 1984.

[3] M. Tuttle, "A brief Introduction to Polymeric Materials", University of Washington, Seattle, 1999.

[4] A. Shenoy, Rheology of Filled Polymer Systems, Kluwer Academic Publishers, Boston, 1999.

[5] H. Musleh, "Investigation of the Effect of Various Dyes on OLEDs Electroluminescence", Master of Science Thesis, Islamic Universtiy of Gaza, Gaza, 2009.

[6] W. Tabaza, "Some Electrical Properties of Doped Poly(9–vinylcarbazole)", Master of Science Thesis, Islamic Universtiy of Gaza, Gaza, 2005.

[7]A. El Tayyan, "A study of Electrical and Photoelectrical Conductivities of Poly(9-vinylcarbazole)", Ph.D. Thesis, university of khartoum, khartoum, 1998.

[8] L. Sperling, Introduction to Physical Polymer Science, 4th edition, John Wiley an Sons Inc., New Jersey, 2006.

[9] D. Bower, An Introduction to Polymer Physics, Cam- bridge, U.K., 2002.

[10] A. Nardes, "On the conductivity of PEDOT:PSS thin Films", Technische Universiteit Eindhoven, Brazil 2007.

[11] S. Kumar, " Electrical and Optical Properties of Plasma Polymerized Films", Ph.D. Thesis, Mahatma Gandhi University, India, 1997.

[12] W. Schnabel, Polymers and Light Fundamentals and Technical Applications, Wiley-Vch Verlag Gmbh & Co. Kgaa, Weinheim, 2007.

[13] B. Hamadani, "Electronic Charge Injection and Transport in Organic Field-Effect transistors", Ph.D. Thesis, Rice Universty, Texas, 2007.

[14] J. Roesler, H, Harders, and M. Baeker, Mechanical Behaviour of Engineering Materials: Metal, Ceramics, Polymers and Composites, Springer-Verlag Berlin Heidelberg 2007.

[15] K. Kao, Dielectric phenomina in solids: with emphasis on physical concepts of electronic processes, Elsevier Academic Press, California, 2004.

[16] S. Kailas, "Material Science, Indian Institute of Science", Indian Institute of Science, Bangalore, 2001.
[17] T. Anderson and S. Roth," Conducting Polymers: Electrical Transport and Current Applications", Braz. J Phys., 24, 746-754, 1994.
[18] W. Silveira, "Microscopic View of Charge Injection in a Model Organic Semiconductor", Ph.D. Thesis, Cornell University, 2005.
[19] S. Sze and Kwok Ng, Physics of Semiconductor Devices, 3rd ed. John Wiley & Sons, Inc., Hoboken, New Jersey, 2007.
[20] B. Choudhury, "Organic light emitting devices (OLEDs) and Structurally integrated photoluminescence based chemical and biological sensors excited by OLEDs", Ph.D. Thesis, Iowa State University, Iowa, 2005.
[21] Z. Chiguvare, J. Parisi, and V. Dyakonov, "Current limiting mechanisms in indium-tin-oxideÕpoly3-hexylthiopheneÕ aluminum thin film devices", Appl. Phys., 94, 2440-2448, 2003.
[22] S. Bashar, "Study of Indium Tin Oxide (ITO) for Novel Optoelectronic Devices", Ph.D. Thesis, University of London, London, 1998.
[23] W. ZHU, "Organic Thin Film Transistor", Master of Engineering Thesis, Mcgill University, Montreal, 2003.
[24] M. Vissenberg "Opto-Electronic Properties of Disordered Organic Semiconductors", Aan de University, 1999.
[25] X. Deng, "Light-Emitting Devices with Conjugated Polymers", Int. J. Mol. Sci, 12, 1575-1549, 2011.
[26] N. Tessler, "Organic Semiconductors and Devices", Technion institute, Haifa, 1999.
[27] Peumans, Bulovic, and Forrest," Exciton Diffusion", Appl. Phys., 76, 38- 48, 2000.
[28] C. Chiang, "Nano Structure and Novel Charging Materials of the Small Molecule Based OLED Devices", Masters thesis, Durham University, 2007
[29] M. Dickey, R. Chiechi, R. Larsen, E. Weiss, D. Weitz, and G. Whitesides, " Eutectic Gallium-Indium (EGaIn): A Liquid Metal Alloy for the Formation of Stable Structures in Microchannels", Adv. Funct. Mater., 18, 1097–1104, 2008.
[30] R. Chiechi, E. Weiss, M. Dickey, and G. Whitesides, "Eutectic Gallium–Indium (EGaIn): A Moldable Liquid Metal for Electrical Characterization of Self-Assembled Monolayers",Angew. Chem. Int. Ed., 47, 142 –144, 2008.

[31] S.. Taya and T. El-Agez, "Design of a spectroscopic ellipsometer by synchronous rotation of the polarizer and analyzer in opposite directions", Sensors and Actuators A: Phys., (in submission).

[32] A. Al-kanoo, "Characterization of different samples using rotating polarizer and analyzer ellipsometer with fixed compensator", Master of Science Thesis, Islamic Universtiy of Gaza, 2012.

[33] P. Ruankham, C. kung, N. Mangkorntong, P. Mangkorntong and S. Choopun, " Photoelectrochemical Characteristic of ZnO Dye-sensitized Solar Cell with Platinum Nanoparticle as a Counterelectrode", CMU. J.Nat.Sci.,7, 177-183, 2008.